

The Pennsylvania State University
The Graduate School

**OPTIMAL PERSISTENT MONITORING USING COORDINATED
SOARING**

A Thesis in
Aerospace Engineering
by
Dmitriy Makovkin

© 2014 Dmitriy Makovkin

Submitted in Partial Fulfillment
of the Requirements
for the Degree of

Master of Science

May 2014

The thesis of Dmitriy Makovkin was reviewed and approved* by the following:

Jacob W. Langelaan
Associate Professor of Aerospace Engineering
Thesis Advisor

Joseph F. Horn
Associate Professor of Aerospace Engineering

George A. Lesieutre
Professor of Aerospace Engineering
Head of the Department of Aerospace Engineering

*Signatures are on file in the Graduate School.

Abstract

Coordinated soaring by a flock of small unmanned aerial vehicles (SUAVs) provides a means of conserving fuel while performing aerial tasks. The ability to exploit thermal columns in the atmospheric boundary layer allows SUAVs to remain airborne without expending any onboard sources of energy, i.e., soaring flight. This thesis presents an analysis of the cruising phase during coordinated soaring where a flock of SUAVs relies on thermal exploitation to maximize endurance for monitoring-type missions.

A maneuver is investigated that involves each SUAV repeating a round-trip between a thermal and a monitoring/surveillance target so as to maintain continuous monitoring of the target. The focus is on minimizing the number of agents required to maintain continuous, persistent monitoring of the target for a set of atmospheric conditions (thermal strength and distance between the thermal and monitoring target) and on maximizing a free parameter (time or distance) when the number of agents is specified.

It will be shown that the optimal cruising speed for maximizing the endurance of monitoring-type missions varies between the best L/D speed and the MacCready speed and depends on the “aggregate thermal strength” of a given cycle, or equivalently, the ratio of the time that one SUAV spends away from the target to the time that it spends at the target. An examination of multiple-thermal exploitation is also presented, followed by an evaluation of the flight simulations supporting the single-thermal results.

Table of Contents

List of Figures	vii
List of Tables	ix
List of Symbols	x
Acknowledgments	xiii
Chapter 1	
Introduction	1
1.1 Motivation	2
1.2 The Problem	3
1.3 Related Work	4
1.3.1 Increasing Endurance with Thermal Exploitation	5
1.3.2 Miscellaneous	6
1.4 Contributions	6
1.5 Reader's Guide	7
Chapter 2	
The Persistent Monitoring Problem	9
2.1 Cooperative Soaring	9
2.2 Persistent Monitoring	11
2.3 Minimizing the Resources in a Cycle	14
2.4 MacCready Speed	15
2.5 Summary	20
Chapter 3	
Governing Equations for Persistent Monitoring	21

3.1	Single-Agent Single-Thermal	21
3.1.1	Maximizing the Working Altitude	23
3.1.2	Optimal Airspeeds	24
3.2	Single-Agent Multiple-Thermal	28
3.2.1	Optimal Airspeeds	30
3.2.2	Inter-Thermal Cruising	31
3.3	Optimizing Multiple Agents by Maximizing a Free Parameter	32
3.3.1	Free Time	33
3.3.2	Free Distance	35
3.3.3	Aggregate Thermal	37
3.4	Multiple-Thermal Exploitation	40
3.5	Transitional Altitude Changes	44
3.6	A Comment on Assumptions	46
3.7	Summary	48
Chapter 4		
	Simulation Results	51
4.1	Simulation Setup	52
4.2	Initial Simulation Results for the ASW-27B	53
4.3	ASW-27B Simulations with Transitional Altitude Changes	61
4.4	SB-XC Simulations with a Modified Departure Controller	61
4.5	ASW-27B Simulations with a Modified Departure Controller	67
4.6	Summary	69
Chapter 5		
	Conclusion	71
5.1	Summary of Contributions	71
5.2	Recommendations for Future Work	74
5.2.1	Increased Complexity in Simulations	74
5.2.2	Multiple-Thermal Exploitation	74
5.2.3	Novel Thermalling Controller	74
5.2.4	Departure and Arrival Controllers	75
Appendix A		
	Vehicle Properties	76
Appendix B		
	Supplementary Material	78
B.1	Exploitation During Dissipation	78
B.2	Accounting for the Area of Sink Around a Thermal	81

B.3 Novel Thermalling Controller Equations	82
B.4 Effect of Transitional Altitude Changes	84
References	89

List of Figures

1.1	Thermal exploitation by a soaring SUAV [1].	2
1.2	Silent Wings persistent monitoring scenario.	3
1.3	Glider launches.	5
2.1	General cooperative soaring scenario with monitoring, exploration, and thermalling jobs available for each cooperating agent.	10
2.2	The cooperative persistent monitoring cycle, consisting of only the monitoring and thermalling jobs.	12
2.3	The MacCready speed takes an agent from point a (an arbitrary altitude) to point b (the top of the second thermal) the fastest.	15
2.4	MacCready speed vs. thermal climb rate for the ASW-27B (left y-axis, solid blue) and the SB-XC (right y-axis, dashed green).	17
2.5	MacCready speed for the SB-XC with an expected thermal climb rate of 1m/s adjusted for a headwind of 5m/s.	18
2.6	Number of agents required for single-thermal exploitation with the ASW-27B for $\Delta h = 700\text{m}$ and a monitoring sink rate of 0.52m/s.	19
3.1	The cooperative persistent monitoring cycle.	22
3.2	Optimal cruising airspeed for single-agent scenarios with the ASW-27B glider, $s_s = 0.52\text{m/s}$	27
3.3	Number of agents required for single-thermal exploitation cruising at the optimal v for the ASW-27B, $s_s = 0.52\text{m/s}$	29
3.4	The t_{free} gained from cruising at v_{opt} instead of $v_{L/D}$, $\Delta h = 700\text{m}$, $s_s = 0.52\text{m/s}$	36
3.5	The d_{free} gained from cruising at v_{opt} instead of $v_{L/D}$, $\Delta h = 700\text{m}$, $s_s = 0.52\text{m/s}$	36
3.6	The polar maps of multiple-thermal exploitation for $\Delta h = 350\text{m}$, $s_s = 0.52\text{m/s}$, $T_1 = 1.5\text{m/s}$, and $T_2 = 3\text{m/s}$	42
3.7	The polar maps of multiple-thermal exploitation for $\Delta h = 200\text{m}$, $T_1 = 1\text{m/s}$, and $T_2 = 4.5\text{m/s}$ and the corresponding d_3 annotated along the 90° line.	43

4.1	Silent Wings simulation flight paths during single-thermal exploitation with an ASW-27B glider.	52
4.2	Polar fits for the ASW-27B and the SB-XC.	54
4.3	Simulation plot of the scenario $\Delta h = 350\text{m}$, $d = 1\text{km}$, and $T = 4\text{m/s}$, whose theoretical aggregate thermal strength is 2.14m/s	55
4.4	Simulation flight path for run 1 of case 3 with v_c	56
4.5	Simulation flight path for run 1 of case 3 for v_c divided into the individual N_1 through N_4	59
4.6	Simulation flight path for run 3 of case 2 for $v_{L/D}$ with the superposition of N_1 through N_4	60
4.7	Silent Wings SB-XC screenshot.	63
B.1	A comparison of the estimated, transitionally-derived, and novel thermalling controller-derived cruising airspeeds for the ASW-27B.	85
B.2	A comparison of the estimated, transitionally-derived, and novel thermalling controller-derived cruising airspeeds for the SB-XC.	86
B.3	The number of required agents with the estimated, transitionally-derived, and novel thermalling controller-derived, and best L/D cruising airspeeds for the ASW-27B.	87
B.4	The number of required agents with the estimated, transitionally-derived, and novel thermalling controller-derived, and best L/D cruising airspeeds for the SB-XC.	88

List of Tables

3.1	The additional maximum allowable distance between M and T provided by v_{opt} as opposed to $v_{L/D}$ given $\Delta h = 700\text{m}$ and $s_s = 0.52\text{m/s}$.	29
3.2	The operating range for v_{opt} in terms of d given six thermal climb rates (m/s) for the ASW-27B, with $\Delta h = 700\text{m}$ and $s_s = 0.52\text{m/s}$.	34
4.1	The case descriptions of the four different scenarios tested in simulation.	57
4.2	This table lists the number of agents required in 24 simulations.	57
4.3	Case descriptions for the simulation results with transitional altitude changes included in the airspeed calculation.	62
4.4	Simulation results with transitional altitude changes included in the airspeed calculation.	62
4.5	Case descriptions for the initial SB-XC simulations with a modified departure controller.	65
4.6	Initial SB-XC simulations with a modified departure controller.	65
4.7	Case descriptions for the SB-XC simulation results with a modified departure controller and δh_T compensation.	66
4.8	SB-XC simulations with a modified departure controller and δh_T compensation.	66
4.9	Case descriptions for the ASW-27B simulation results with a modified departure controller and δh_T compensation.	68
4.10	ASW-27B simulations with a modified departure controller and δh_T compensation.	68
A.1	Properties of the Schleicher ASW-27B glider [2].	76
A.2	Properties of the RnR Products SB-XC glider [3].	77

List of Symbols

L/D	Lift-to-drag ratio, p. iii
E	Exploration job, p. 10
M, S	Monitoring job, p. 11
T_i	Thermalling job i , p. 11
T_i	Climb rate in T_i , p. 12
t_c	Total cruising duration, p. 16
t_t	Total thermalling duration, p. 16
d_i	Length of leg i , p. 16
v_i	Cruising airspeed during leg i , p. 16
s_i	Cruising sink rate during leg i , p. 16
Δh	Working altitude at T , p. 16
a, b, c	Coefficients for the quadratic fit of a sink polar, p. 16
v_{MC}	MacCready airspeed, p. 16
s_{am}	Sink rate of an air mass, p. 17
$v_{L/D}$	Best L/D airspeed, p. 17
s_{\min}	Minimum sink rate of an aircraft, p. 17
v_{\min}	Cruising airspeed for s_{\min} , p. 17

N	Number of agents required for net zero-altitude-loss continuous monitoring, p. 18
s_s	Monitoring sink rate of an aircraft, p. 18
t_{tm}	Transient maneuver duration, p. 22
t_m	Monitoring duration, p. 22
v_{ground}	Ground speed, p. 24
v_{air}	Airspeed, p. 24
A, B	Auxiliary variables for the optimal airspeed equations, p. 25
t_{ci}	Cruising duration of leg i , p. 26
t_{away}	Time spent away from M, p. 26
$s_{L/D}$	Sink rate at $v_{L/D}$, p. 28
v_c	Optimal airspeed for single-agent M cycles, p. 30
d_c	Combined length of the first and final cruise legs in multiple-thermal exploitation, p. 30
t_{free}	Free loitering time in multiple-agent cycles, p. 33
d_{free}	Free exploration distance in multiple-agent cycles, p. 33
L	Loitering job atop a thermal, p. 33
$\lceil N \rceil$	Integer number of agents required for net zero-altitude-loss continuous monitoring, p. 33
v_{opt}	Optimal airspeed for multiple-agent M cycles, p. 34
v_{free}	Airspeed of an aircraft during free exploration, p. 35
s_{free}	Sink rate of an aircraft during free exploration, p. 35
s_c	Sink rate at v_c , p. 38
g	Acceleration due to gravity, p. 45
$\delta h_{\bar{j}}$	Transitional altitude change atop job j , p. 45

δh_j	Transitional altitude change at the bottom of job j , p. 45
\bar{N}	Corrected N accounting for transition T → M, p. 58
v_{ci}	Optimal airspeed for leg i with transitional changes in altitude included, p. 62
$\delta h_{\underline{T}}$	Arrival altitude loss due to the area of sink surrounding a thermal, p. 67
T_d	Dissipating climb rate function, p. 79
h_d	Optimal departure altitude in a dissipating thermal, p. 79
m	Thermal linear decay slope, p. 80
N_0	Initial amplitude of an exponential decay model, p. 80
λ	Exponential decay rate of a dissipating thermal, p. 80

Acknowledgments

Many thanks are due to Ola Røer Thorsen of the Silent Wings team for the time spent helping set up the fixed thermal in the Silent Wings soaring simulator. Thank you to Nathan Depenbusch for creating the interface between Simulink and Silent Wings. Thank you to Shawn Daugherty for creating the Silent Wings SB-XC model. And a deep thank you to Professor Jack Langelaan for accepting me into his lab group and providing me with the guidance and motivation necessary for completing this work.

This research was funded by the Office of Naval Research under Grant N000141110656.

Chapter **1**

Introduction

THIS thesis presents an analysis of the relationship between atmospheric conditions and the number of soaring small unmanned aerial vehicles (SUAVs) required to ensure persistent monitoring of a ground target. The focus is on minimizing the number of SUAVs required for a persistent monitoring cycle by investigating the optimal cruising airspeeds. This research was motivated by a combination of the limited onboard fuel capacity of SUAVs and the lack of intuition regarding single and multiple-thermal exploitation for both single-agent and multiple-agent scenarios.

To begin understanding the system, the persistent monitoring cycle is limited to only consist of the monitoring and thermalling jobs, with the assumption that the exploration job is being completed by a third party, i.e., the strengths and locations of nearby thermals are already known. This assumption places the focus on the cruising phase during the cycle and not on the auxiliary tasks required for success.

This thesis: (a) derives the closed-form equations for the optimal cruising airspeeds during different persistent monitoring scenarios, (b) introduces the novel concept of the “aggregate-thermal,” (c) presents a short analysis of multiple-thermal exploitation, and (d) presents flight simulator results demonstrating the significance and accuracy of the theoretical conclusions.

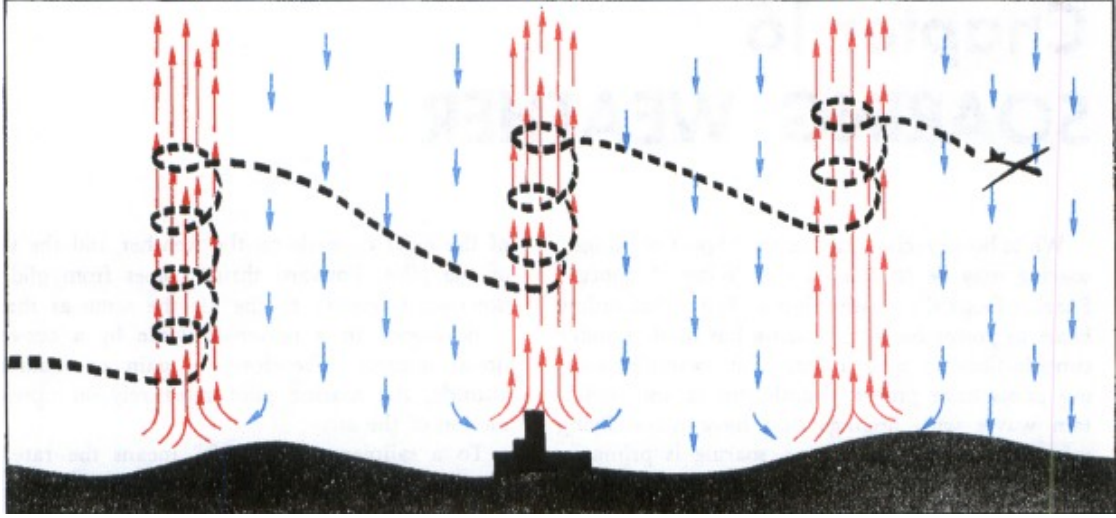


Figure 1.1. Thermal exploitation by a soaring SUAV [1].

1.1 Motivation

Small unmanned aerial vehicles excel at tasks unsuitable for their larger counterparts. Their small size, low cost, and ability to cooperate autonomously with other SUAVs have generated interest in many diverse applications including forest fire monitoring, severe weather monitoring, load transport, and stationary high-altitude monitoring platforms [4–10]. However, their practicality and implementability are hindered by their limited onboard propulsion energy, limiting range and endurance.

Luckily, it has been shown that thermal exploitation can significantly increase SUAV endurance. Since John Wharington first proposed the idea of autonomous thermal soaring SUAVs [11, 12], there has been a lot of research on improving thermal centering controllers, path planners, and the balance between exploration and exploitation of the thermal field [13–19]. One area yet to be investigated is the cruising stage during monitoring-type missions where a SUAV travels repeatedly between a thermal column and a monitoring target. Here, this topic is explored with a focus on maximizing airborne time, i.e., endurance, for missions requiring continuous uninterrupted monitoring of a ground target.

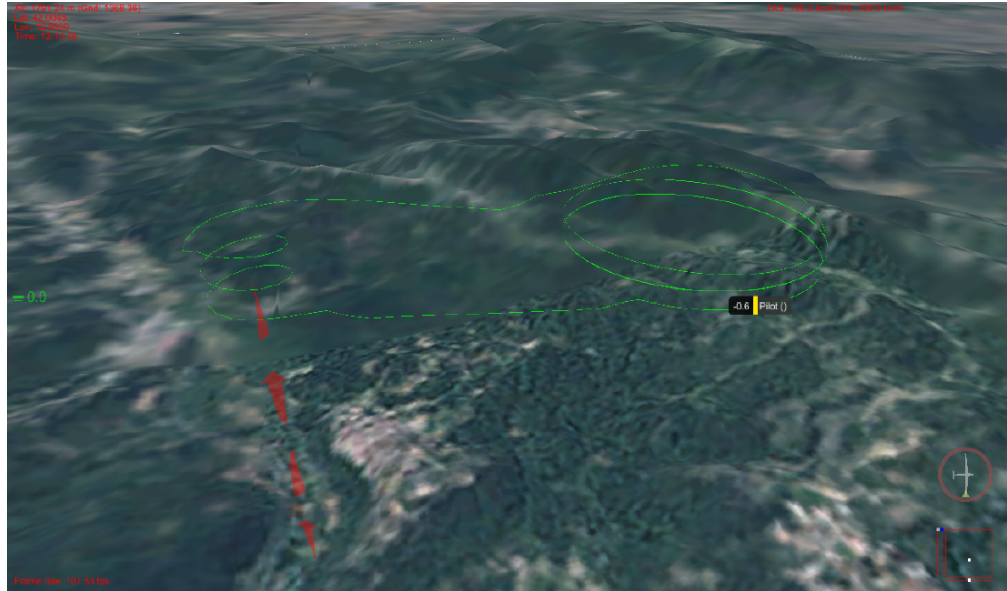


Figure 1.2. Silent Wings persistent monitoring scenario.

1.2 The Problem

Persistent monitoring soaring scenarios confine the aircraft to a specific region of a few square kilometers around a monitoring target. When a flock of SUAVs is used in conjunction with thermal lift, one aircraft is assigned to monitor the target while the other aircraft explore and exploit the surrounding thermals, creating a map of thermal lift while maintaining altitude.

In this thesis, the exploration stage is disregarded and it is assumed that the strengths and locations of thermals are known. This results in a scenario where the aircraft are engaged in a cycle of monitoring a target, cruising to a thermal, exploiting a thermal, and cruising back to the target in a way that keeps at least one agent at the target at all times, resulting in continuous monitoring of the target. In the case of a persistent monitoring scenario where only one agent is available, the target must periodically be unoccupied and the agent can only attempt to minimize the time spent away from the target. And in the case of multiple-thermal exploitation, the agents exploit multiple thermals before arriving back at the monitoring target. These scenarios are constrained further by requiring each cycle to begin at a fixed altitude, thus, if the conditions were theoretically constant, the mission endurance would be infinite. The characteristic scenario and trajectory

are shown in Figure 1.2.

In this fashion, focus is placed on maximizing mission endurance by optimizing the cruising phase of continuous monitoring missions. It is important to note that the altitude and continuous monitoring constraints allow one to fully define the scenario and formulate governing equations; it will become clear that the results in this paper are not restricted to scenarios with these constraints. The subsequent analysis will address the following questions:

- **Which quantity is maximized when mission endurance is optimal?**

This question is not as simple as it seems. For instance, maximizing the time spent at the target will leave the agent at too low of an altitude to cruise to a thermal, whereas minimizing the number of agents in a monitoring cycle is not always optimal in multiple-agent scenarios.

- **What is the relationship between the optimal airspeed, the best L/D airspeed, and the MacCready airspeed?**

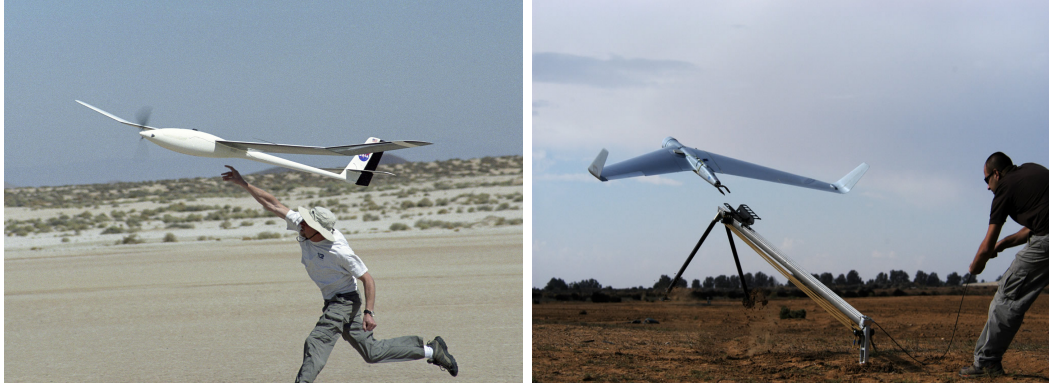
The fact that the optimal airspeed is neither the best L/D airspeed nor the MacCready airspeed (covered in Section 2.4) was a surprise at the onset of this research. Nevertheless, the three airspeeds are related to each other and, in particular, the relation to the MacCready speed gives rise to a novel quantity, here referred to as the “aggregate thermal.”

- **When is multiple-thermal exploitation beneficial to the cycle?**

Polar maps of regions where multiple-thermal exploitation is preferred over single-thermal exploitation will provide some understanding as to if and when such a risky cycle should be considered.

1.3 Related Work

This section will review some of the work that has either involved persistent monitoring or assisted in its development.



(a) Michael Allen launching his RnR Products SB-XC glider [22]. (b) Orbiter mini UAV system from Aeronautics Defense Systems [23].

Figure 1.3. Glider launches.

1.3.1 Increasing Endurance with Thermal Exploitation

Thermal columns, or “thermals” for short, are ascending masses of air that act as the primary convective units of the atmospheric boundary layer by equilibrating the temperature and pressure gradients between the ground and atmosphere [20]. Some typical defining characteristics of thermals include the following: diameters from less than 100 m to nearly 1000 m, heights of nearly 1500 m, vertical air currents ranging from 1 to 4 m/s, and lifespans between 5 and 30 minutes [21]. These values, however, depend strongly on time of day and season; thermal activity peaks between the hours of noon and sunset and the months of spring and summer when the ground can become significantly warmer than the surrounding air.

Previous studies have established the effectiveness of thermal exploitation for both single aircraft and coordinated aircraft scenarios. Allen presents two important facts derived from a UAV simulation with thermals calculated from meteorological data from Desert Rock, Nevada [24]. First, during summer and winter, thermals can provide a 12 and 6 hour increase in endurance, respectively, for an electric-powered SUAV with a nominal endurance of two hours. Second, “performance increase has a low sensitivity to many key simulation parameters including aircraft glide slope, number of updrafts, updraft lifetime, updraft velocity, and height-above-ground upper limit.” Depenbusch and Langelaan [25] demonstrate that, on average, with the goal of remaining airborne for as long as possible, a single SUAV doubles its endurance when keeping a memory of discovered thermal

locations, thermal strengths, and associated covariances. They also shows that, compared to a single SUAV using thermal mapping, a 23% average increase in endurance, defined as the soaring time until one SUAV reaches the ground, is provided by two coordinated SUAVs that explore the environment and share measurements with each other. Furthermore, four coordinated SUAVs experience a 98% average endurance increase over the two coordinated SUAVs.

1.3.2 Miscellaneous

Bethke et al. have examined persistent monitoring by a team of quad-rotors, where periodic recharge at known “filling stations” is performed as part of the mission [26–28]. Cutler et al. examine monitoring with a single UAV that exploits ridge lift, and develop a “seeability” metric as a means of quantifying video image quality during search and rescue missions [29]. Patel and Kroo show that, for SUAVs, pitch maneuvers can provide significant energy gains in turbulent air, thus extending mission endurance [30]. Pippin et al. tackle the multi-robot patrolling problem by periodically designating “shadower” agents that verify observations and update trust models of the “patrollers” [31]. Nigam et al. provide simulations of up to four UAVs that focus on optimal trajectories and coordinated ground coverage during persistent monitoring missions [32].

1.4 Contributions

The main contributions of this thesis are summarized below:

- **Governing equations for persistent monitoring scenarios**

Equations for the required number of agents in a cycle, the optimal airspeeds, and the free resources are derived for the persistent monitoring scenarios. The scenarios are divided into single-agent monitoring, multiple-agent monitoring, single-thermal exploitation, and multiple-thermal exploitation.

- **The definition of the aggregate thermal**

The aggregate thermal, which is essentially the rate at which energy is gained relative to a target location, is derived and its value as a metric in local

monitoring missions involving thermal exploitation is shown. It will also be evident how this aggregate rate can be applied to other fields where an energy source must be chosen among many to continue some mission objective.

- **Polar map visualization of multiple-thermal v.s. single-thermal exploitation**

Polar graphs will illustrate scenarios where multiple-thermal exploitation should be considered. These graphs will show the angular range that the two thermals must fall between in order to be beneficial to the cycle. The benefit will be meager in most scenarios but valuable in scenarios where an extra agent is barely needed.

- **Theory verification through Silent Wings soaring simulator**

Results from a high fidelity flight simulator are compared against the expected results from theory.

1.5 Reader's Guide

The remainder of this thesis is organized as follows:

- **Chapter 2: The Persistent Monitoring Problem** outlines the different persistent monitoring scenarios and covers the assumptions used in the later chapters. The chapter finishes with a note on integer optimization and a discussion of the MacCready speed and its suboptimality in persistent monitoring.
- **Chapter 3: Governing Equations for Persistent Monitoring** puts forth the governing equations for the number of agents required in a persistent monitoring cycle and the associated optimal airspeeds. This chapter includes a derivation and discussion of the aggregate thermal, as well as polar maps for multiple-thermal exploitation.
- **Chapter 4: Simulation Results** presents results from the Silent Wings soaring simulator. The simulated results are compared to the expected theoretical results and the accuracy of the theory is assessed.

- **Chapter 5: Conclusion** summarizes results and discusses areas of future work.

Chapter 2

The Persistent Monitoring Problem

THIS chapter outlines the persistent monitoring scenarios and introduces the theoretical background used throughout the thesis. First, the general cooperative soaring problem is presented and simplified into the persistent monitoring problem. Next, in Section 2.2, the persistent monitoring problem is simplified and the simplifying assumptions are reviewed. This is followed by a note on the difference between integer and non-integer optimization and its relevance to optimizing the persistent monitoring problem. The MacCready speed is introduced in Section 2.4 with a note on the fundamental difference between cooperative soaring and traditional cross-country soaring. A summary concludes the chapter.

2.1 Cooperative Soaring

As covered in section 1.3.1, thermal exploitation by a team of cooperating SUAVs is a theoretically effective way of extending mission endurance. The challenges appear when the cooperative soaring system is implemented outside of simulation.

One challenge is in outlining the job transitions and interactions. There are many possible tasks in cooperative soaring, mainly consisting of monitoring, local and global exploration, thermalling, communication relaying, loitering, and moderating. The timing and distribution of tasks are critical to mission endurance and all possible scenarios must be covered by the assignment algorithm or behavior controller. For example, which task should an agent be assigned if he has been lost due to a communications dropout? Should he continue his current task or

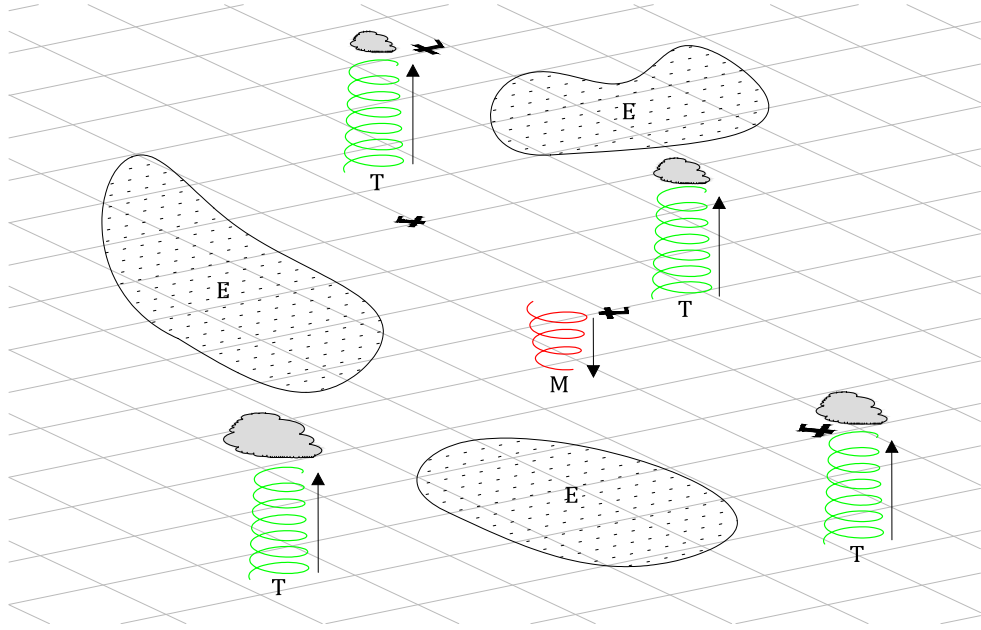


Figure 2.1. General cooperative soaring scenario with monitoring, exploration, and thermalling jobs available for each cooperating agent.

should he cruise toward another agent or the ground station to regain connection? Should the algorithm plan future task assignments without including this lost agent? Another consideration is in defining valid job transitions. Will an agent ever be assigned to an exploration job after completing a monitoring job without monitoring in between? Would it be beneficial to separate agents into monitoring cycles (alternating between monitoring and thermalling jobs) and exploration cycles (alternating between exploration and thermalling jobs) instead of allowing monitoring agents to exit the monitoring cycle? How long should the planning horizon be? Perhaps the least intuitive job in question is exploration. Which unexplored areas will yield the highest reward? How is this reward measured? Should the area be thoroughly or briefly explored?

The quantification of reward is another major challenge in implementing cooperative soaring missions. One possibility for quantifying the exploration reward is by calculating the associated risk of completing the exploration and choosing the minimum risk task [33]. A second possibility is to use reinforcement learning to find a relationship between environmental parameters, e.g., the percentage of unexplored area in the thermal map, the average thermal density in the thermal map,

average thermal strength, etc., and the total altitude gained by the system from the information provided by the exploration task. Another possibility is to avoid the approximation of a reward function altogether and instead use reinforcement learning to find a state-action policy dependent on the environmental parameters.

The takeaway message is that the general cooperative soaring system is very complex. To gain an understanding of the system requires a simplification that focuses on a smaller portion of the system. In this way, challenges are approached gradually and complexity is added incrementally until the entire system is understood. The reduced system in this thesis is one that is geared toward analyzing the theoretical optimal cruising airspeed between the monitoring target and the thermal and vice versa.

2.2 Persistent Monitoring

The reduced persistent monitoring system consists of only the monitoring and thermalling jobs. An example monitoring cycle, Figure 2.2(a), would begin at the top of the monitoring target, annotated by the “M”. An agent somehow arrives at the top of the target and from then on does not utilize any onboard sources of propulsion energy. The agent sinks at a constant rate and departs the target at an altitude that enables it to reach the thermal “T” at the fixed minimum allowable altitude. The agent then rises at a constant rate and departs the thermal upon reaching the top, the fixed inversion layer altitude, before arriving back at the monitoring target to repeat the cycle. If atmospheric conditions are constant, the agent would monitor the target indefinitely. If multiple agents are available, their actions are coordinated so that an agent is arriving at the monitoring target at the moment another agent is departing.

Multiple-thermal exploitation, Figure 2.2(b), is of interest because a flock may encounter many scenarios where exploiting a combination of thermals would reduce the number of agents required for a persistent monitoring cycle. Two interesting cases are the presence of one thermal on the path toward another and the utilization of a nearby thermal to reach a better thermal that would otherwise be too far given the working altitude. The reader must note that multiple-thermal exploitation is practical if and only if the climb rate in the first thermal is less than the climb rate

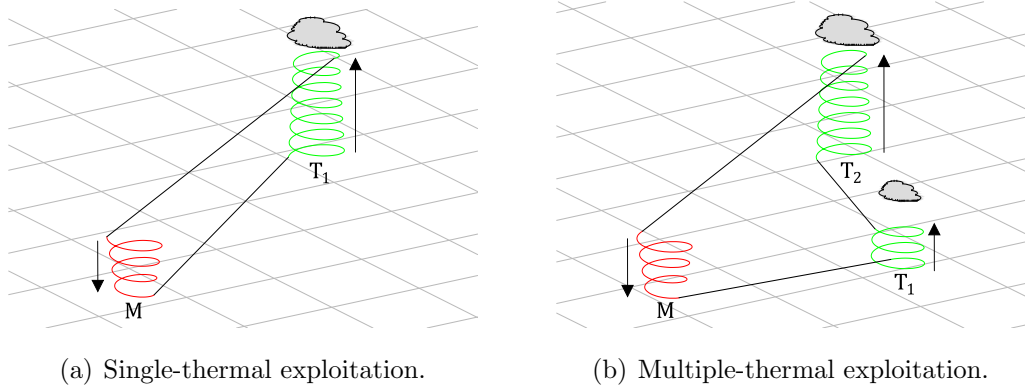


Figure 2.2. The cooperative persistent monitoring cycle, consisting of only the monitoring and thermalling jobs.

in the second thermal, $T_1 < T_2$, otherwise the second thermal would be avoided altogether. Thus, thermal T_1 must be treated strictly as a via point that enables an agent to leave the monitoring target at a later time with the intention of increasing monitoring time at the cost of increasing transit time. It follows that an agent arrives at thermal T_1 at the altitude floor and departs at the height needed for reaching thermal T_2 at the altitude floor. The stronger T_2 is then exploited over the full working altitude.

The persistent monitoring system requires a thermal map, i.e., the locations of nearby thermals, to be provided by a third party, whether it be from weather forecasting or a separate group of cooperating agents. A basic cooperative soaring implementation would divide a cooperating flock into monitoring agents and exploring agents because there is normally no reason for an exploring agent to *replace* a monitoring agent unless either the monitoring agent had mechanically failed, lost too much altitude to be recovered, or the exploring agent had found a thermal nearer to the monitoring target than the location of one of the monitoring agents. It would be more common for the monitoring cycle to *hire* an additional agent from the exploration cycle during instances where the nearest thermals are too far away for the monitoring agents at hand.

Therefore, the control schemes for the monitoring cycle and the exploration cycle may be perfected separately and combined by defining the conditions under which an agent from the exploration cycle would switch with an agent in the monitoring cycle or vice versa. Later, it will be shown that two or three agents are

capable of persistently monitoring a target for a wide range of practical thermal separations. Thus, an exploration cycle in reality would require about three or four monitoring agents, where at least one agent is designated as the moderator. The moderator is an agent that loiters atop the nearest thermal to the monitoring target and whose job is to enforce the persistent monitoring constraint of never leaving the target unoccupied. The moderator intercedes for a late-arriving agent in cycles that experience dissipating thermals, inaccurate thermal locations, regions of unexpected sinking air masses, or other manifestations of uncertainty. Note that the complexity of the system greatly increases when the target is not required to be constantly monitored. Without this constraint, the agents must decide on when and for how long the target should be abandoned.

The environmental assumptions for the system in this thesis are as follows:

1. Wind gusts are absent in the environment.
2. Thermalling climb rate and monitoring sink rate are constant with altitude.
3. The altitude floor and ceiling (inversion layer) are constant.
4. All agents have identical properties and capabilities.
5. Atmospheric conditions persist indefinitely.
6. The duration of transient maneuvers is negligible relative to the other phases of flight.
7. Changes in altitude during transient maneuvers are negligible for SUAVs.

The resulting system is one in which thermalling and monitoring dynamics are absent and atmospheric conditions are constant. One may think of thermalling and monitoring as taking an elevator up or down at a constant rate, respectively. Transient maneuvers refer to the actions needed for an agent to transition from one job to another, resulting in a change in altitude due to a change in airspeed. For example, an agent will lose altitude when departing the monitoring target if the cruising airspeed toward the thermal is greater than the monitoring airspeed; the agent must lose altitude (potential energy) to gain speed (kinetic energy). This altitude conversion will be canceled upon arriving at the monitoring target if the

cruising airspeed toward the thermal is equal to the cruising airspeed toward the target. In spite of this, it will later be shown that the total number of transitions in the monitoring cycle can produce a nonzero overall change in altitude, resulting in an asymmetric system. Thus, the seventh assumption will be relied upon until that discussion.

It is important to note that the assumptions allow one to fully define the scenario and formulate governing equations. As the thesis progresses, it will be shown how the results are not restricted to scenarios with these constraints and each assumption will eventually be lifted.

2.3 Minimizing the Resources in a Cycle

The various monitoring scenarios will be compared with each other by the quantification of the number of agents needed to achieve continuous or persistent monitoring in a given scenario. The optimal cruising airspeed, as well as the optimal airspeed held between thermals during multiple-thermal exploitation, can be found by differentiating this equation, where the resulting speed minimizes the number of agents required for a persistent monitoring cycle. Minimizing the number of agents is a way of minimizing the amount of resources required for a given cycle, thus maximizing the efficiency of the scenario. It will be shown that this is equivalent to minimizing the ratio of the amount of time an agent spends away from the monitoring target to the amount of time an agent spends at the monitoring target.

Minimizing this ratio is of interest in many types of scenarios involving one or more agents cruising between a thermal and some location requiring an extended presence. Instead of cruising between one monitoring target and one or more thermals, it may be necessary to alternate between multiple monitoring targets, perimeter monitoring for instance, or between exploration targets. The optimal airspeeds in these scenarios will take the same form because the objective is ultimately the same in each case: to gain altitude as quickly as possible without compromising the time spent at the target.

As the analysis proceeds, one will see why this approach does not apply to all scenarios. Specifically, minimizing the number of agents for a cycle is optimal for a

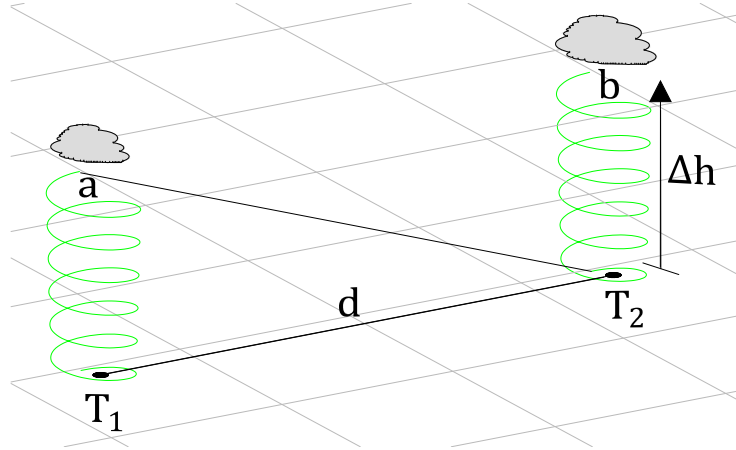


Figure 2.3. The MacCready speed takes an agent from point a (an arbitrary altitude) to point b (the top of the second thermal) the fastest.

system where only a single agent is available since this is equivalent to minimizing the ratio of time spent away to the time spent at the target. However, the system becomes fundamentally different when multiple agents are available: the monitoring cycle will always contain more than enough agents because there can only be an integer number of agents in reality. For example, a cycle requiring 2.5 agents in theory will need to employ 3 agents in reality. This fact requires the multiple-agent scenarios to be treated as integer optimization problems, where auxiliary quantities such as the loitering time and free exploration distance are used to represent the difference in resources between the integer and non-integer monitoring cycles.

2.4 MacCready Speed

The MacCready airspeed and its suboptimality in persistent monitoring and co-operative soaring scenarios must be discussed before moving on to the governing equations in the next chapter. The MacCready speed is the speed that takes a soaring aircraft from some arbitrary altitude to the top of the next thermal the fastest, illustrated in Figure 2.3. If the speed were slower, the aircraft would cruise for too long and would not make up that time in the thermal despite the smaller altitude loss during cruise. If the speed were faster, the aircraft would thermal for too long and would not regain that time despite the faster cruising time. It is for

this reason that cross-country glider pilots rely on the MacCready speed to minimize their flight times during races. Reichmann explains the MacCready speed by the following: “what we’re trying to find out is the best speed to use when flying toward a thermal of known strength in order to achieve the best cruise speed” [34].

The derivation of the MacCready speed is given below.

$$\begin{aligned} t &= t_c + t_t = \frac{d}{v} + \frac{\Delta h}{T_2} = \frac{d}{v} + s \frac{d}{v T_2} \\ &= \frac{d}{v} + (av^2 + bv + c) \frac{d}{v T_2} = \frac{d}{v} + \left(av + b + \frac{c}{v} \right) \frac{d}{T_2} \end{aligned} \quad (2.1)$$

where t_c and t_t are the cruising and thermalling durations, respectively. The distance between point a and b is given by d and the cruising airspeed is v , with an associated cruising sink rate of s . Δh is the height lost during the cruise and T_2 is the expected climb rate inside the thermal. The sink rate’s dependence on the cruising airspeed is included because the objective is to differentiate t with respect to v . For optimization calculations and controller design, this is expressed fairly well with a quadratic fit: $s = av^2 + bv + c$ [34]. The coefficients a and c are positive, whereas the coefficient b is negative since the sign convention in this thesis is to treat sink rates as positive quantities.

Differentiating Equation 2.1 with respect to v , setting to zero, and solving for v leads to

$$v = \sqrt{\frac{c + T_2}{a}} = v_{MC} \quad (2.2)$$

where the subscript MC is used to denote the MacCready speed. Note that the calculation of the MacCready speed depends only on the glider parameters and the estimate of the climb rate in the next encountered thermal; the speed to fly is independent of how far away the thermal is! One can see that it is in the best interest of the glider to fly faster when high thermal climb rates are expected, meaning that the altitude lost during a fast cruise will be recovered quickly by the high thermal climb rates during exploitation. Conversely, the glider flies slower on days with low expected thermal climb rates because the altitude lost during cruise would be recovered too slowly during exploitation. MacCready speeds for the Schleicher ASW-27B and the RnR Products SB-XC are shown in Figure 2.4.

If there is a constant air mass motion during the cruise, e.g., the gliders cruise

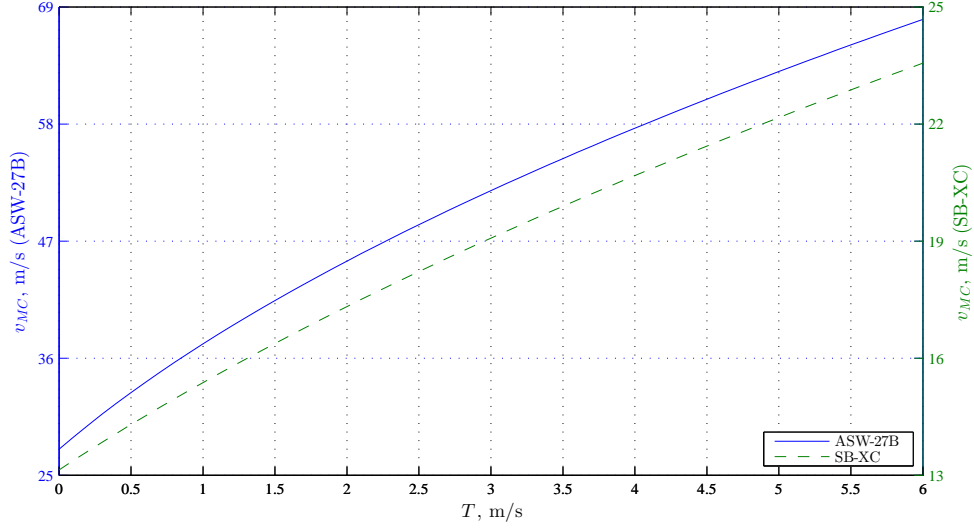


Figure 2.4. MacCready speed vs. thermal climb rate for the ASW-27B (left y-axis, solid blue) and the SB-XC (right y-axis, dashed green).

trajectory is through a sinking air mass, v_{MC} becomes

$$v_{MC} = \sqrt{\frac{c + T_2 + s_{am}}{a}} \quad (2.3)$$

where s_{am} is the sink rate of the air mass, again treated as positive down. Thus, it is in the best interest of the glider to fly faster through sinking air and slower through rising air, as expected. If $s_{am} = T_2$, the MacCready speed becomes the best L/D airspeed $v_{L/D} = \sqrt{c/a}$. This implies that if the speed of the air mass and the expected climb rate are zero, then the speed to fly is $v_{L/D}$. If $s_{am} = T_2 - s_{min}$, where s_{min} is the minimum sink rate of the glider, the MacCready speed becomes the airspeed for minimum sink $v_{min} = -b/2a$. This implies that if the speed of the air mass is zero and the expected thermal climb rate is equal to the minimum sink rate of the glider, then the speed to fly is the minimum sink airspeed of the glider. For head and tailwinds, the speed to fly is determined graphically (before flight) by drawing lines originating from different points along the airspeed axis and running tangent to the sink polar curve, illustrated in Figure 2.5 [34, 35]. In this figure, the origin is displaced up by 1m/s, right by 5m/s, and a line is then drawn tangent to the sink polar. The MacCready speed becomes the x-coordinate of the tangent point, approximately 17m/s. Note that the best L/D airspeed is found by drawing

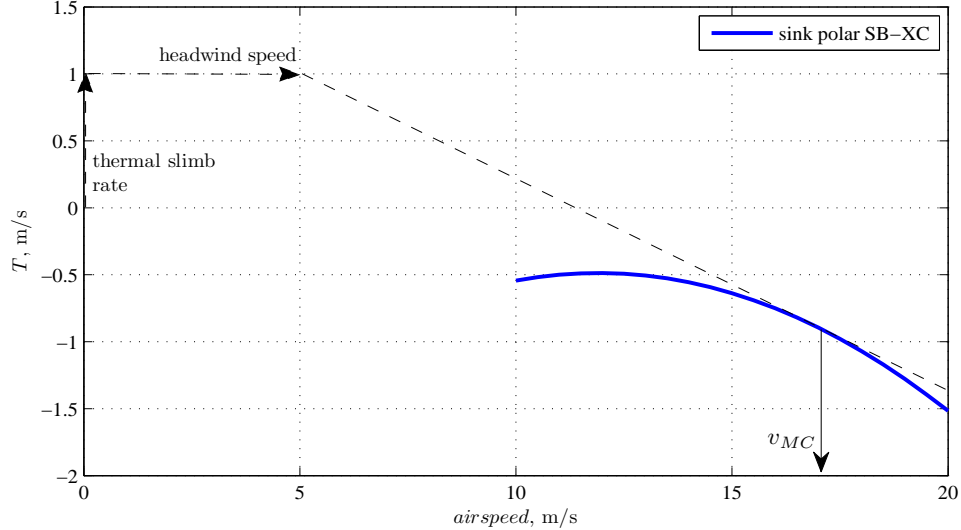


Figure 2.5. MacCready speed for the SB-XC with an expected thermal climb rate of 1m/s adjusted for a headwind of 5m/s.

the tangent line from the undisplaced origin. As a further reading, John Cochrane analyzes the inherent uncertainty in predicting thermal climb rates and the effect that this uncertainty has on cross-country speed [36].

Figure 2.6 shows the suboptimality of the MacCready speed in cooperative soaring missions, obtained from calculating the number of agents required for a cycle (Equation 3.2) under varying environmental conditions:

$$N = \frac{\frac{d}{v_1} + \frac{d}{v_2} + \frac{\Delta h}{T}}{s_s^{-1} \left(\Delta h - s_1 \frac{d}{v_1} - s_2 \frac{d}{v_2} \right)} + 1$$

which will be covered thoroughly in Chapter 3. Figure 2.6 can be interpreted in two ways: one, the number of agents required in a cycle for a thermal of a given climb rate and distance, or two, the maximum distance away a thermal can be for a given number of available agents. The graph on the left shows the case where the MacCready speed is used to cruise toward the thermal and the best L/D speed is used to cruise back to the monitoring target. The graph on the right shows the case where the best L/D speed is held for both cruise segments.

The MacCready speed is immediately dismissed as the optimal cruising speed because there are cases where weaker and farther thermals require the same number

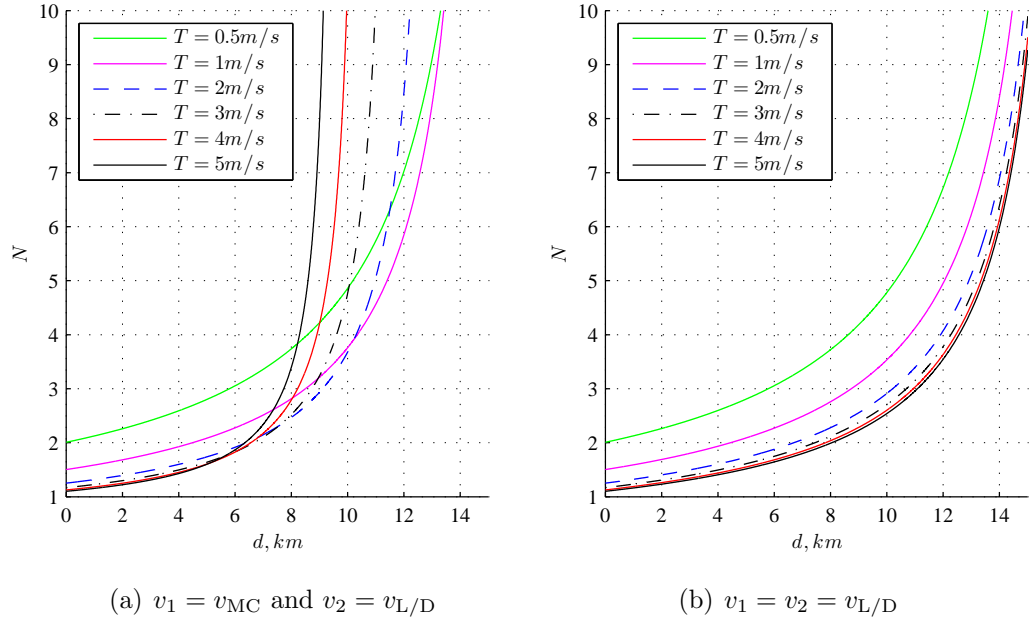


Figure 2.6. Number of agents required for single-thermal exploitation with the ASW-27B for $\Delta h = 700\text{m}$ and a monitoring sink rate of 0.52m/s .

of agents as stronger and nearer thermals. This effect is dominant in thermals that are greater than 6km away and is attributed to an inefficient exchange between an agent's altitude loss and cruising time for stronger thermals whose MacCready speeds are large. The larger altitude losses during cruise decrease the monitoring duration of the target because the agent must depart at a higher altitude so that he remains above the minimum allowable altitude upon arriving at the thermal. This is the fundamental difference between cooperative soaring and cross-country soaring: cross-country soaring does not take into account the effect that the cruising airspeed has on the starting location, whereas cooperative soaring aims to maximize the resources available at the starting location (monitoring target).

There is a subtlety that is not shown clearly in Figure 2.6: $v_{L/D}$ is not always more efficient than v_{MC} , particularly for distances less than 2km. This observation that the monitoring cycle was not optimized by the MacCready speed nor the best L/D speed sparked the progression of this research.

2.5 Summary

This chapter has outlined the different persistent monitoring scenarios, namely single-thermal, multiple-thermal, single-agent, and multiple-agent. The complex general cooperative soaring system was reduced to the persistent monitoring system, which is a minimal system that allows generalizations of cruising airspeeds to be made for the more complex system. For the time being, this system neglects thermalling and monitoring dynamics, assumes constant atmospheric conditions, and requires a third party to provide the locations of prospective thermals.

The difference between the resource optimization for single-agent scenarios and multiple-agent scenarios arises from the fact that multiple-agent scenarios will always have either a greater or equal amount of agents than what is theoretically required for the cycle, due to the integer number of agents required in real implementations. It becomes necessary to treat multiple-agent cycles as integer optimization problems where a free resource, e.g., loitering time or exploration distance, is optimized instead of the number of agents. This will become clearer in Section 3.3.

The chapter concluded with a discussion on the MacCready speed and its suboptimality in the persistent monitoring cycle. The suboptimality arises from an inefficient exchange between an agent's altitude loss and cruising time in the airspeed toward stronger thermals. This is expected because the MacCready speed is defined as a racing speed that minimizes the time for a glider to cruise from some arbitrary altitude to the top of a prospective thermal, irrespective of the distance between the two locations. Nevertheless, the subtle observation that, for small separations, the MacCready speed outperforms the best L/D speed meant that neither speed was optimal for the monitoring cycle, necessitating the formulation of the optimal cruising airspeed provided in the next chapter.

Chapter **3**

Governing Equations for Persistent Monitoring

THIS chapter covers the governing equations for the single-thermal, multiple-thermal, single-agent, and multiple-agent persistent monitoring cycles. The derivations will begin with the quantification of the number of agents required to ensure uninterrupted monitoring of the target. Optimal airspeeds are then found by differentiating the equations for the number of agents with respect to the cruising airspeeds. An optimal airspeed will exist for each cruise segment found in the monitoring cycles, which consist of target to thermal, thermal to target, and inter-thermal segments. Section 3.3.3 gives a derivation and discussion of the aggregate thermal, Section 3.4 provides insight on multiple-thermal exploitation with polar map visualizations, and Section 3.5 gives equations for the single-thermal single-agent cycle where transitional changes in altitude are accounted for. A comment on assumptions and a summary conclude the chapter.

3.1 Single-Agent Single-Thermal

The persistent monitoring cycles are reproduced here for convenience in Figure 3.1. Intuitively, the number of agents required for persistent monitoring is equal to the time required for one agent to complete the circuit divided by the time that one

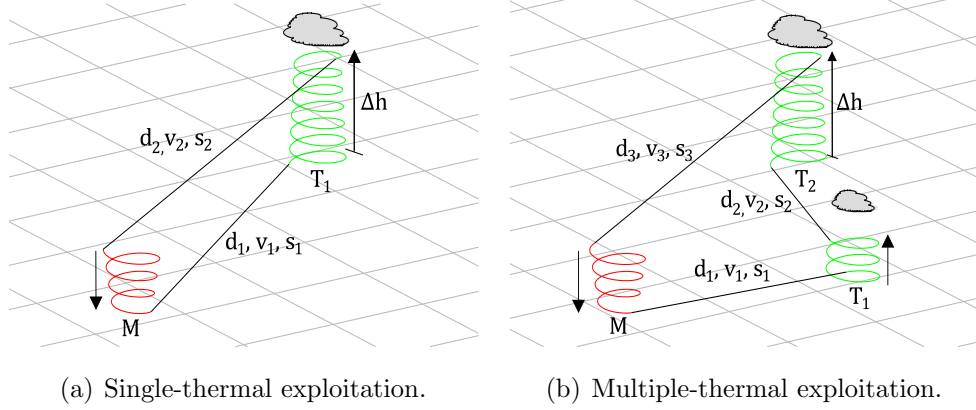


Figure 3.1. The cooperative persistent monitoring cycle.

agent spends monitoring the target:

$$N = \frac{t_c + t_t + t_{tm} + t_m}{t_m} \approx \frac{t_c + t_t}{t_m} + 1 \quad (3.1)$$

where t_c , t_t , t_m , and t_{tm} are the cruising, thermalling, monitoring, and transient maneuver durations, respectively. Recall that the duration of transient maneuvers will be neglected due to its insignificance when compared with t_c , t_t , and t_m .

Substituting the system parameters and applying the environmental assumptions discussed in Chapter 2 gives

$$N = \frac{\frac{d}{v_1} + \frac{d}{v_2} + \frac{\Delta h}{T}}{s_s^{-1} \left(\Delta h - s_1 \frac{d}{v_1} - s_2 \frac{d}{v_2} \right)} + 1 \quad (3.2)$$

with distance d , expected thermal climb rate T , working altitude Δh , monitoring sink rate s_s , the cruising airspeed and sink rate toward the thermal v_1 and s_1 , and the cruising airspeed and sink rate toward the monitoring target v_2 and s_2 . The working altitude is assumed to be constant and equal to the altitude ceiling minus the altitude floor for the agents. It is temporarily assumed that the two cruising paths are of the same distance d . The general case where the two cruising paths differ, for example, when an aircraft diverts to explore the surroundings or when multiple thermals are exploited, will be treated in Section 3.2.

To clarify Equation 3.2, the sum of the first two terms in the numerator represents the cruising duration of one agent for a given thermal with an expected

climb rate T and a distance d away from the target. The third term in the numerator of Equation 3.2 represents the time spent exploiting the thermal, t_t . It will be shown that minimizing N , i.e., maximizing efficiency, translates to exploiting the thermal over the entire working altitude Δh , i.e., not departing the thermal prior to reaching the altitude ceiling and not arriving at the thermal above the altitude floor. Lastly, the denominator of Equation 3.2 represents the time, t_m , spent monitoring the target at the aircraft's monitoring sink rate. The simplicity of t_t and t_m amounts to an elevator model of thermalling and monitoring: once an agent reaches either location, he sinks or rises at a constant rate until departing.

3.1.1 Maximizing the Working Altitude

To prove that the number of agents required for monitoring the target is minimized when Δh is maximized, start with the inequality $N_1 < N_2$, where N_1 represents a scenario with Δh_1 and N_2 represents an identical scenario but with Δh_2 such that $\Delta h_1 > \Delta h_2$. The goal is to reduce this inequality to show that $N_1 < N_2$ if and only if $\Delta h_1 > \Delta h_2$:

$$\frac{\frac{d}{v_1} + \frac{d}{v_2} + \frac{\Delta h_1}{T}}{s_s^{-1} \left(\Delta h_1 - s_1 \frac{d}{v_1} - s_2 \frac{d}{v_2} \right)} + 1 < \frac{\frac{d}{v_1} + \frac{d}{v_2} + \frac{\Delta h_2}{T}}{s_s^{-1} \left(\Delta h_2 - s_1 \frac{d}{v_1} - s_2 \frac{d}{v_2} \right)} + 1$$

Multiplying both sides by the product of the denominators, expanding, and canceling like terms results in

$$s_s \Delta h_2 d \left(\frac{1}{v_1} + \frac{1}{v_2} \right) - \frac{\Delta h_1 d}{T} \left(\frac{s_1}{v_1} + \frac{s_2}{v_2} \right) < s_s \Delta h_1 d \left(\frac{1}{v_1} + \frac{1}{v_2} \right) - \frac{\Delta h_2 d}{T} \left(\frac{s_1}{v_1} + \frac{s_2}{v_2} \right)$$

Collecting Δh_1 -terms on the right-hand side and Δh_2 -terms on the left-hand side gives

$$\Delta h_2 d \left[s_s \left(\frac{1}{v_1} + \frac{1}{v_2} \right) + \frac{1}{T} \left(\frac{s_1}{v_1} + \frac{s_2}{v_2} \right) \right] < \Delta h_1 d \left[s_s \left(\frac{1}{v_1} + \frac{1}{v_2} \right) + \frac{1}{T} \left(\frac{s_1}{v_1} + \frac{s_2}{v_2} \right) \right]$$

The terms in the square brackets are equal and the inequality reduces to the expected result

$$\Delta h_2 < \Delta h_1$$

Thus, given the environmental assumptions, maximizing the working altitude Δh will always minimize the required number of agents. In the case of persistent monitoring using a single thermal, optimal performance is obtained when agents exploit the full height of the thermal: a “partial recharge” will necessarily result in an increase in the number of agents. This, as discussed in Section 2.2, does not hold in multiple-thermal cycles where partial exploitation assists an agent in reaching a farther thermal.

3.1.2 Optimal Airspeeds

The optimal v_1 and v_2 can be found by differentiating Equation 3.2 with respect to v_1 and v_2 . To do this, the aircraft’s sink polar is expressed in terms of the cruising airspeed via a quadratic fit, as was done with the MacCready speed in Section 2.4. The flight path angle is assumed to be small, so that airspeed is equal to the ground speed (for typical gliders the flight path angle is approximately two degrees, which results in $v_{\text{air}}/v_{\text{ground}} = 1.0006$). The derivation for the optimal v_1 is as follows:

$$\begin{aligned} \frac{\partial N}{\partial v_1} &= \frac{\partial}{\partial v_1} \left[\frac{\frac{d}{v_1} + \frac{d}{v_2} + \frac{\Delta h}{T}}{s_s^{-1} \left(\Delta h - s_1 \frac{d}{v_1} - s_2 \frac{d}{v_2} \right)} + 1 \right] = \\ &\frac{\frac{\partial}{\partial v_1} \left(\frac{d}{v_1} + \frac{d}{v_2} + \frac{\Delta h}{T} \right)}{s_s^{-1} \left(\Delta h - s_1 \frac{d}{v_1} - s_2 \frac{d}{v_2} \right)} + \left(\frac{d}{v_1} + \frac{d}{v_2} + \frac{\Delta h}{T} \right) \frac{\partial}{\partial v_1} \left[s_s^{+1} \left(\Delta h - s_1 \frac{d}{v_1} - s_2 \frac{d}{v_2} \right)^{-1} \right] \end{aligned}$$

Evaluating the derivatives and approximating the s_1 in the partial derivative by the quadratic fit $av_1^2 + bv_1 + c$:

$$\frac{\partial N}{\partial v_1} = \frac{-d/v_1^2}{s_s^{-1} \left(\Delta h - s_1 \frac{d}{v_1} - s_2 \frac{d}{v_2} \right)} + \frac{\frac{d}{v_1} + \frac{d}{v_2} + \frac{\Delta h}{T}}{s_s^{-1} \left(\Delta h - s_1 \frac{d}{v_1} - s_2 \frac{d}{v_2} \right)^2} \frac{\partial}{\partial v_1} \left[av_1 + b + \frac{c}{v_1} \right] d$$

Evaluating the final derivative and setting to zero:

$$\frac{-d/v_1^2}{s_s^{-1} \left(\Delta h - s_1 \frac{d}{v_1} - s_2 \frac{d}{v_2} \right)} + \frac{\left(\frac{d}{v_1} + \frac{d}{v_2} + \frac{\Delta h}{T} \right) (a - c/v_1^2)d}{s_s^{-1} \left(\Delta h - s_1 \frac{d}{v_1} - s_2 \frac{d}{v_2} \right)^2} = 0$$

Multiplying both sides by the inverse of the first term:

$$1 - \frac{\left(\frac{d}{v_1} + \frac{d}{v_2} + \frac{\Delta h}{T}\right)(av_1^2 - c)}{\Delta h - s_1 \frac{d}{v_1} - s_2 \frac{d}{v_2}} = 0$$

Multiplying both sides by the denominator and expanding:

$$\Delta h - s_1 \frac{d}{v_1} - s_2 \frac{d}{v_2} - av_1 d - \frac{av_1^2 d}{v_2} - \frac{av_1^2 \Delta h}{T} + \frac{cd}{v_1} + c \left(\frac{d}{v_2} + \frac{\Delta h}{T} \right) = 0$$

Substituting the quadratic fit for the last remaining s_1 and expanding:

$$\Delta h - av_1 d - bd - d \frac{c}{v_1} - s_2 \frac{d}{v_2} - av_1 d - \frac{av_1^2 d}{v_2} - \frac{av_1^2 \Delta h}{T} + \frac{cd}{v_1} + c \left(\frac{d}{v_2} + \frac{\Delta h}{T} \right) = 0$$

Cancelling and collecting like terms:

$$\left(-\frac{ad}{v_2} - \frac{a\Delta h}{T} \right) v_1^2 - (2ad)v_1 + \left[\Delta h - d \left(\frac{s_2}{v_2} + b \right) + c \left(\frac{d}{v_2} + \frac{\Delta h}{T} \right) \right] = 0$$

Dividing by $-ad$:

$$\frac{1}{d} \left(\frac{d}{v_2} + \frac{\Delta h}{T} \right) v_1^2 + 2v_1 - \frac{1}{ad} \left[\Delta h - d \left(\frac{s_2}{v_2} + b \right) + c \left(\frac{d}{v_2} + \frac{\Delta h}{T} \right) \right] = 0$$

Invoking the auxiliary variables A_1 and B_1 for the leading coefficients leaves

$$A_1 v_1^2 + 2v_1 - B_1 = 0$$

and solving with the quadratic formula:

$$v_1 = \frac{-2 \pm \sqrt{2^2 + 4A_1 B_1}}{2A_1}$$

Finally, the positive root gives the optimal airspeed toward the thermal:

$$v_1 = \frac{-1 + \sqrt{1 + A_1 B_1}}{A_1} \quad (3.3)$$

where

$$A_1 = \frac{1}{d} \left(\frac{d}{v_2} + \frac{\Delta h}{T} \right) = \frac{1}{d} (t_{\text{away}} - t_{c1}) \quad (3.4)$$

$$B_1 = \frac{1}{ad} \left[\Delta h - d \left(\frac{s_2}{v_2} + b \right) + c(t_{\text{away}} - t_{c1}) \right] \quad (3.5)$$

Similarly, the equation for the optimal v_2 has an identical form due to the structure of Equation 3.2:

$$v_2 = \frac{-1 + \sqrt{1 + A_2 B_2}}{A_2} \quad (3.6)$$

where

$$A_2 = \frac{1}{d} \left(\frac{d}{v_1} + \frac{\Delta h}{T} \right) = \frac{1}{d} (t_{\text{away}} - t_{c2}) \quad (3.7)$$

$$B_2 = \frac{1}{ad} \left[\Delta h - d \left(\frac{s_1}{v_1} + b \right) + c(t_{\text{away}} - t_{c2}) \right] \quad (3.8)$$

The variables t_{c1} and t_{c2} were introduced to represent the two segments comprising t_c . The time spent away from the target is represented by t_{away} . The interdependence and identical form of v_1 and v_2 implies that $v_1 = v_2$. Indeed, after constructing the constrained optimization problem for Equation 3.2 using MATLAB's `fmincon` function, it was observed that given any set of environmental conditions, the optimal v_1 and v_2 were both equal to

$$v = \frac{-2 + \sqrt{4 + AB}}{A} \quad (3.9)$$

where

$$A = \frac{\Delta h}{Td} = \frac{1}{d} (t_{\text{away}} - t_c) \quad (3.10)$$

$$B = \frac{1}{ad} \left(\Delta h - 2bd + \frac{c\Delta h}{T} \right) = \frac{1}{ad} (\Delta h - 2bd) + A \frac{c}{a} \quad (3.11)$$

Figure 3.2 plots values of v (later renamed v_c) as a function of T and d with a working altitude of 700 and 350 meters for a Schleicher ASW-27 glider. The two graphs in the figure converge to the same values as d approaches zero and as

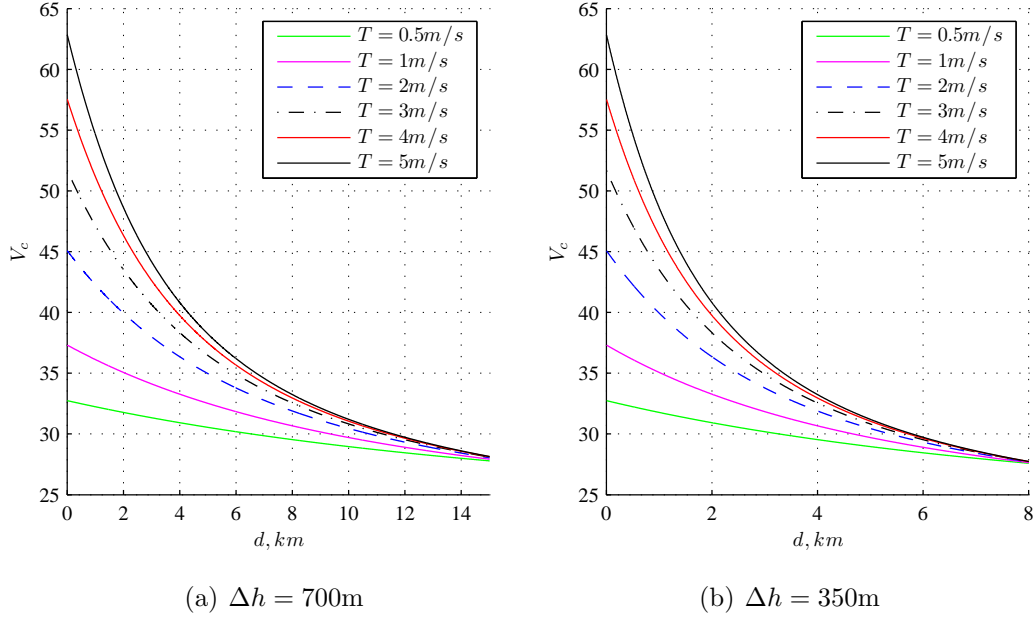


Figure 3.2. Optimal cruising airspeed for single-agent scenarios with the ASW-27B glider, $s_s = 0.52\text{m/s}$.

d approaches infinity. An alternative formulation in Section 3.3.1 will show that the limits of v are equal to the MacCready speeds as d approaches zero and the best L/D speed as d approaches infinity. The reader should note that the two graphs have different x -axis scales. Figure 3.3 plots the accompanying number of agents, also with respect to separation and thermal climb rate. There is a clear upper limit on d , beyond which persistent monitoring is unachievable no matter how many agents are available in the system.

At first glance, it appears that this equation must be solved iteratively because of the dependence on t_c . This, however, is not the case because t_c is included in t_{away} ; subtracting t_c eliminates the dependence on the two cruising segments. Symmetry within the cycle is expected because flying away from the target affects the cycle in the same way as flying toward the target. Both airspeeds affect the time spent at the target, where v_1 affects the departing altitude and v_2 affects the arriving altitude. Both airspeeds also affect the time spent away from the target with equal weight. Thus, the optimal v_1 that balances these two effects so as to minimize the N required for the system will equal the optimal v_2 . It is worthwhile to mention that B may be rewritten using the relations $v_{\text{L/D}} = \sqrt{c/a}$,

$v_{\min} = -b/2a$, $s_{L/D} = 2c + bv_{L/D}$, and $s_{\min} = bv_{\min}/2 + c$, where $v_{L/D}$ is the best L/D speed, v_{\min} is the speed at the minimum sink rate of the aircraft, and $s_{L/D}$ and s_{\min} are their corresponding sink rates [34].

Table 3.1 lists the gains in the maximum allowable distance from using the optimal airspeed as opposed to $v_{L/D}$ given a working altitude of 700m. Values within parenthesis represent the percentage gains in the maximum allowable distance with respect to the maximum allowable distance given by $v_{L/D}$. The first entry is not applicable because thermals with climb rates of 0.5m/s require three agents to complete a cycle regardless of their distance from the target. This is due to the minimum sink rate, which was assumed to be the sink rate during monitoring, being slightly larger than 0.5m/s. The calculation of d cannot be carried out directly by providing a value of N because the value of the optimal airspeed depends on d . Instead, the calculation of d for a certain number of agents was carried out by varying the distance from zero to sixteen kilometers in steps of five meters. The distance was recorded when the value of N reached an integer number.

Table 3.1 shows that if the optimal airspeed is ever to be used instead of the best L/D airspeed, it should be used in situations where $N \leq 2$, otherwise, the gains in distance do not justify the computational effort after considering the uncertainty of dynamic environments during real missions. It then becomes of interest to quantify the benefit of cruising at the optimal airspeed when $N \leq 2$. However, the method of calculating the maximum distance away a thermal can be does not apply for non-integer values of N , and calculating the difference in the number of agents required for a cycle is slightly non-intuitive. Instead, Equation 3.2 will be reformulated in Section 3.3 to account for a savings in time by considering exploration distance, d_{free} , and loitering time, t_{free} .

3.2 Single-Agent Multiple-Thermal

In the case of a two thermal persistent monitoring problem (Figure 3.1b) the number of agents required for persistent monitoring is

$$N = \frac{\frac{d_1}{v_1} + \frac{s_2 d_2}{v_2 T_1} + \frac{d_2}{v_2} + \frac{\Delta h}{T_2} + \frac{d_3}{v_3}}{s_s^{-1} \left(\Delta h - s_1 \frac{d_1}{v_1} - s_3 \frac{d_3}{v_3} \right)} + 1 \quad (3.12)$$

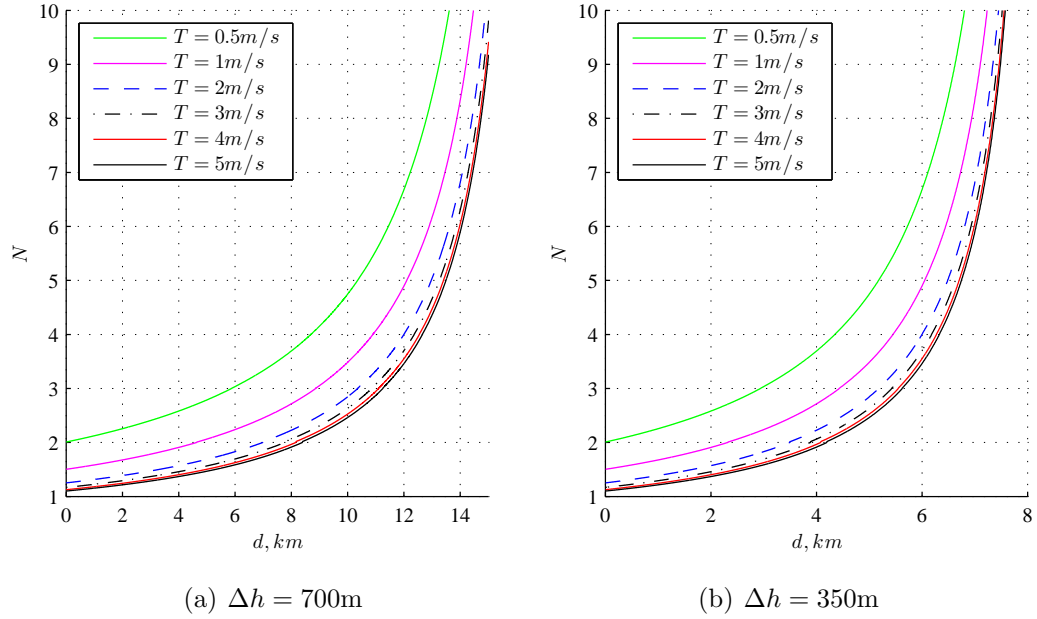


Figure 3.3. Number of agents required for single-thermal exploitation cruising at the optimal v for the ASW-27B, $s_s = 0.52\text{m/s}$.

Table 3.1. The additional maximum allowable distance between M and T provided by v_{opt} as opposed to $v_{\text{L/D}}$ given $\Delta h = 700\text{m}$ and $s_s = 0.52\text{m/s}$.

Climb Rate	Number of Agents				
	2	3	4	5	10
0.5m/s	na*	85 (1.5)	65 (0.8)	45 (0.5)	15 (0.1)
1m/s	205m (4.6%)	130 (1.5)	85 (0.8)	55 (0.5)	15 (0.1)
2m/s	290m (4.3%)	155 (1.5)	90 (0.8)	60 (0.5)	15 (0.1)
3m/s	325m (4.4%)	160 (1.5)	90 (0.7)	60 (0.5)	15 (0.1)
4m/s	340m (4.4%)	165 (1.5)	90 (0.7)	60 (0.5)	15 (0.1)
5m/s	345m (4.3%)	165 (1.5)	95 (0.8)	60 (0.5)	15 (0.1)

* not applicable, $N > 2$ for thermal climb rates of 0.5m/s.

where d_1 , v_1 , and s_1 represent the first leg of the cycle between the target and the first thermal, d_3 , v_3 , and s_3 represent the final leg of the cycle between the second thermal and the target, and d_2 , v_2 , and s_2 represent the leg between the two thermals T_1 and T_2 . The second term in the numerator of Equation 3.12 represents the partial exploitation of thermal T_1 .

3.2.1 Optimal Airspeeds

After differentiating Equation 3.12, the equations for the optimal v_1 and v_3 exhibit the same properties as those in Section 3.1: both equations are identical in form and dependent on each other and, as before, MATLAB's `fmincon` confirms that the optimal v_1 is equivalent to the optimal v_3 , so that $v_1 = v_3 = v_c$:

$$v_c = \frac{-1 + \sqrt{1 + AB}}{A} \quad (3.13)$$

where

$$A = \frac{1}{d_c}(t_{\text{away}} - t_c) \quad (3.14)$$

$$B = \frac{1}{ad_c}(\Delta h - bd_c) + A\frac{c}{a} \quad (3.15)$$

where d_c represents the total cruising distance minus the distance traveled between thermals: $d_c = d_1 + d_3$. In fact, Equation 3.13 is the general form of Equation 3.9 when $d_1 \neq d_3$ and although the terms within t_{away} and t_c differ for different scenarios, this general form for the optimal airspeed remains the same. For instance, if the cycle in Figure 3.1(b) was changed to $M \rightarrow T_1 \rightarrow T_2 \rightarrow T_3 \rightarrow E$, where E is an exploration job, the term " $t_{\text{away}} - t_c$ " would now equal the sum of the cruising times and exploitation times in $T_1 \rightarrow T_2 \rightarrow T_3$, d_c would be the sum of the distances between $M \rightarrow T_1$ and $T_3 \rightarrow E$, and Equation 3.13 determines the new optimal airspeed. Note the difference between d and d_c : d represents the distance between M and T in single-thermal exploitation, whereas d_c represents the sum of the lengths of the first and last legs in multiple-thermal exploitation. If single-thermal exploitation is represented in the multiple-thermal formulation, then $d_c/2 = d$ since the first and last cruise legs are identical.

3.2.2 Inter-Thermal Cruising

Equation 3.12 may also be differentiated with respect to v_2 to determine the optimal cruising speed between thermals:

$$\frac{\partial N}{\partial v_2} = \frac{\partial}{\partial v_2} \left[\frac{\frac{d_1}{v_1} + \frac{s_2 d_2}{v_2 T_1} + \frac{d_2}{v_2} + \frac{\Delta h}{T_2} + \frac{d_3}{v_3}}{s_s^{-1} \left(\Delta h - s_1 \frac{d_1}{v_1} - s_3 \frac{d_3}{v_3} \right)} + 1 \right] = \frac{\frac{\partial}{\partial v_2} \left(\frac{s_2 d_2}{v_2 T_1} + \frac{d_2}{v_2} \right)}{s_s^{-1} \left(\Delta h - s_1 \frac{d_1}{v_1} - s_3 \frac{d_3}{v_3} \right)}$$

Substituting a quadratic fit for s_2 and evaluating the derivative:

$$\frac{\frac{\partial}{\partial v_2} \left(\frac{(av_2^2 + bv_2 + c)d_2}{v_2 T_1} + \frac{d_2}{v_2} \right)}{s_s^{-1} \left(\Delta h - s_1 \frac{d_1}{v_1} - s_3 \frac{d_3}{v_3} \right)} = \frac{\left(a - \frac{c}{v_2^2} \right) \frac{d_2}{T_1} - \frac{d_2}{v_2^2}}{s_s^{-1} \left(\Delta h - s_1 \frac{d_1}{v_1} - s_3 \frac{d_3}{v_3} \right)}$$

Setting to zero, multiplying out the denominator, and expanding:

$$\frac{ad_2}{T_1} - \frac{cd_2}{v_2^2 T_1} - \frac{d_2}{v_2^2} = 0$$

Multiplying by T_1/d_2 and collecting like terms:

$$a - \frac{1}{v_2^2} (c + T_1) = 0$$

which leaves the optimal cruising airspeed from T_1 to T_2 to be

$$v_2 = \sqrt{\frac{c + T_1}{a}} \tag{3.16}$$

Surprisingly, the optimal cruising speed in $T_1 \rightarrow T_2$ is equal to the MacCready speed in reverse, i.e., the MacCready speed for T_1 rather than T_2 . Since $T_1 < T_2$ in scenarios involving multiple-thermal exploitation, the time spent exploiting T_1 should be minimized. The reversed MacCready speed is slower than the normal MacCready speed in $T_1 \rightarrow T_2$ and minimizes the height lost during this phase, which translates to a lower required altitude for reaching T_2 .

The reader is reminded that if the cycle in Figure 3.1(b) is beneficial, i.e., $N_{M \rightarrow T_1 \rightarrow M} > N_{M \rightarrow T_2 \rightarrow M} > N_{M \rightarrow T_1 \rightarrow T_2 \rightarrow M}$, then the cycle $N_{M \rightarrow T_1 \rightarrow T_2 \rightarrow T_1 \rightarrow M}$ should be taken instead of simply $N_{M \rightarrow T_1 \rightarrow T_2 \rightarrow M}$, provided that T_1 is available on the

cruise back. That is, if T_1 decreases the number of agents required for a cycle by acting as a via point between M and T_2 that allows an agent to depart M at a lower altitude, then it must likewise be possible for T_1 to decrease the number of agents by acting as a via point between T_2 and M that allows an agent to arrive at M at a higher altitude.

Indeed, the optimal cruising speed in $T_2 \rightarrow T_1$ is equal in value to the reversed MacCready speed that optimized $T_1 \rightarrow T_2$. However, the difference between the two MacCready speeds is that the segment $T_2 \rightarrow T_1$ is optimized by the forward form of the MacCready speed, $v_{MC} = \sqrt{(c + T_1)a^{-1}}$, instead of the reversed form $v_{MC} = \sqrt{(c + T_2)a^{-1}}$. To reiterate, in its normal form, the MacCready speed optimizes a cruise to a thermal based on the thermal that the aircraft is *traveling to*. In this paper, the MacCready speed is said to be reversed when the thermal that the aircraft is *starting from* is used to optimize an inter-thermal cruise in monitoring scenarios.

3.3 Optimizing Multiple Agents by Maximizing a Free Parameter

The theory behind multiple-agent cycles was developed by considering an alternative way of representing the resources used in a monitoring cycle. It is slightly unintuitive to compare monitoring cycles by a difference in agents, e.g., claiming that one cycle requires half of an agent less than another cycle. This section reformulates the governing equations to include a free resource, specifically, loitering time and exploration distance. The connection to multiple-agent theory lies in the fact that only multiple-agent cycles can possess free resources. Single-agent cycles cannot have free resources because the objective is to minimize the duration that the target is left unmonitored; the free resource is converted into minimizing the ratio of the time spent away from the target to the time spent monitoring the target. This is fundamentally different from the integer optimization treatment of the multiple-agent cycles covered in Section 2.3.

3.3.1 Free Time

Loitering time will be analyzed by considering the following equation:

$$N = \frac{\frac{2d}{v} + \frac{\Delta h}{T} + t_{\text{free}}}{s_s^{-1} (\Delta h - s \frac{2d}{v})} + 1 \quad (3.17)$$

Equation 3.17 is a form of Equation 3.2 with an additional segment of $T \rightarrow L$, where L represents a loitering period t_{free} at the thermal. In this thesis, loitering is restricted to an agent remaining at the altitude ceiling within a thermal. In reality, atmospheric dynamics necessitate the prediction of dissipating thermals. By remaining within a thermal for an extended period, the loitering agent has a better sense of whether or not a thermal is dissipating, which becomes critical in the decision making process for the subsequent agents seeking a thermal. Alternatively, t_{free} , along with d_{free} , can be a way of measuring the margin of error within a cycle.

Equation 3.17 is utilized by solving for t_{free} :

$$t_{\text{free}} = (N - 1) \left(\Delta h - s \frac{2d}{v} \right) \frac{1}{s_s} - \left(\frac{2d}{v} + \frac{\Delta h}{T} \right) \quad (3.18)$$

The way to solve this equation is to first calculate the optimal number of agents without t_{free} , i.e., by solving Equation 3.2 and Equation 3.9, and rounding up to the nearest integer number of agents, $\lceil N \rceil$. Rounding N up to the nearest integer is necessary to account for the additional t_{free} since free time is available only if a cycle has more than enough agents. A difference in agents can now be interpreted as a difference in t_{free} ; this can be seen clearly if Equation 3.17 is rearranged in the following manner:

$$\lceil N \rceil - \left(\frac{\frac{2d}{v} + \frac{\Delta h}{T}}{s_s^{-1} (\Delta h - s \frac{2d}{v})} + 1 \right) = \frac{t_{\text{free}}}{s_s^{-1} (\Delta h - s \frac{2d}{v})} \quad (3.19)$$

where the left-hand side equals the difference between the integer number of agents required in reality and the non-integer number of agents required in theory.

After comparing the values of t_{free} given by v_c to the values of t_{free} given by $v_{L/D}$, it was seen that v_c did not always provide a larger t_{free} than $v_{L/D}$ despite requiring a smaller N for a cycle. This result reinstated that maximizing the endurance of

a coordinated soaring mission is an integer optimization problem; the objective is to optimize the resources available, $\lceil N \rceil$, rather than minimizing the number of resources, N . Thus, the optimal cruising airspeed during real missions involving multiple agents must be derived by differentiating Equation 3.18 with respect to v instead of differentiating Equation 3.2. The new optimal cruising airspeed is given by Equation 3.20.

$$v_{\text{opt}} = \sqrt{\frac{c + s_s(\lceil N \rceil - 1)^{-1}}{a}} \quad (3.20)$$

where the calculation of v_{opt} requires calculating v_c and $\lceil N \rceil$. The value of v_c actually converges to v_{opt} as N approaches an integer value, showing that the two optimization problems are related. In addition, v_{opt} converges to $v_{L/D}$, $\sqrt{c/a}$, as $\lceil N \rceil$ tends to infinity (as was seen in Figure 3.2 of Section 3.1).

A pleasant consequence of Equation 3.20 is that v_{opt} is constant for a given $\lceil N \rceil$, which means that d can be divided into ranges of constant v_{opt} rather than calculating a different optimal airspeed for every value of d , as was done with v_c . The reader must keep in mind the difference between v_c and v_{opt} : v_c is the optimal cruising airspeed in scenarios involving one agent, whereas v_{opt} is the optimal cruising airspeed for multiple-agent scenarios where the monitoring target can be monitored indefinitely in theory. The reference cruising airspeed for any coordinated soaring monitoring mission can equal up to about three or four different values; thermals requiring $\lceil N \rceil \geq 5$ are rarely the best options and v_{opt} changes

Table 3.2. The operating range for v_{opt} in terms of d given six thermal climb rates (m/s) for the ASW-27B, with $\Delta h = 700\text{m}$ and $s_s = 0.52\text{m/s}$.

T	Optimal Airspeed				
	32.8m/s $\lceil N \rceil = 2$	30.2m/s $\lceil N \rceil = 3$	29.3m/s $\lceil N \rceil = 4$	28.9m/s $\lceil N \rceil = 5$	28.6m/s $\lceil N \rceil = 6$
0.5	na*	0 - 5.88	5.89 - 8.69	8.70 - 10.35	10.36 - 11.44
1	0 - 4.64km	4.65 - 8.85	8.86 - 10.89	10.90 - 12.10	12.11 - 12.89
2	0 - 6.98km	6.99 - 10.36	10.37 - 12.00	12.01 - 12.97	12.98 - 13.61
3	0 - 7.77km	7.78 - 10.86	10.87 - 12.36	12.37 - 13.26	13.27 - 13.85
4	0 - 8.16km	8.17 - 11.10	11.11 - 12.55	12.56 - 13.40	13.41 - 13.97
5	0 - 8.39km	8.40 - 11.25	11.26 - 12.65	12.66 - 13.49	13.50 - 14.05

* not applicable, $N > 2$ for thermal climb rates of 0.5m/s.

very slightly beyond that. Table 3.2 lists ranges of d for scenarios involving up to 5 agents given six different thermal climb rates.

3.3.2 Free Distance

Another way of quantifying the advantage of a cycle requiring less agents is through exploration distance, d_{free} . This can be thought of as an alternative to using t_{free} as loitering time. An agent now has the option of cruising slightly off course to explore nearby regions, the advantage of which is a higher likelihood of locating new thermals or identifying areas of sink to be avoided by subsequent agents. Consider Equation 3.21:

$$N = \frac{\frac{2d}{v} + \frac{\Delta h}{T} + \frac{d_{\text{free}}}{v_{\text{free}}}}{s_s^{-1} \left(\Delta h - s \frac{2d}{v} - s_{\text{free}} \frac{d_{\text{free}}}{v_{\text{free}}} \right)} + 1 \quad (3.21)$$

Contrary to t_{free} , d_{free} affects the arrival height at the monitoring target. This is why d_{free} appears in the denominator of N whereas t_{free} does not. Nevertheless, solving for d_{free} and differentiating with respect to v leads to the same optimal airspeed that maximized t_{free} . This is because d_{free} can be thought of as an alternative usage of t_{free} . Or in other words, the optimal airspeed maximizes the free resource regardless of how the resource is used, so long as the integer number of agents is kept constant.

Differentiating for v_{free} shows that v_{free} is equal to the cruising speed that maximizes d_{free} , given by Equation 3.20. This is expected since d_{free} can be thought of as an extension of the cruising segments, which implies that v_{free} and v_c have identical effects on the overall system.

Figure 3.4 and Figure 3.5 show the values of t_{free} and d_{free} , respectively. Solid lines represent the additional times and distances provided by v_{opt} compared to $v_{L/D}$ and belong to the left axis, whereas the dashed lines represent the total times and distances provided by v_{opt} and belong to the right axis; the dashed lines are meant to put the solid lines into perspective. Breaks in the plots denote distances where the number of agents changes; the graphs show distances that require up to five agents. The dashed lines extend past the solid lines in all cases because the values of the additional times and distances were not recorded after the t_{free} from

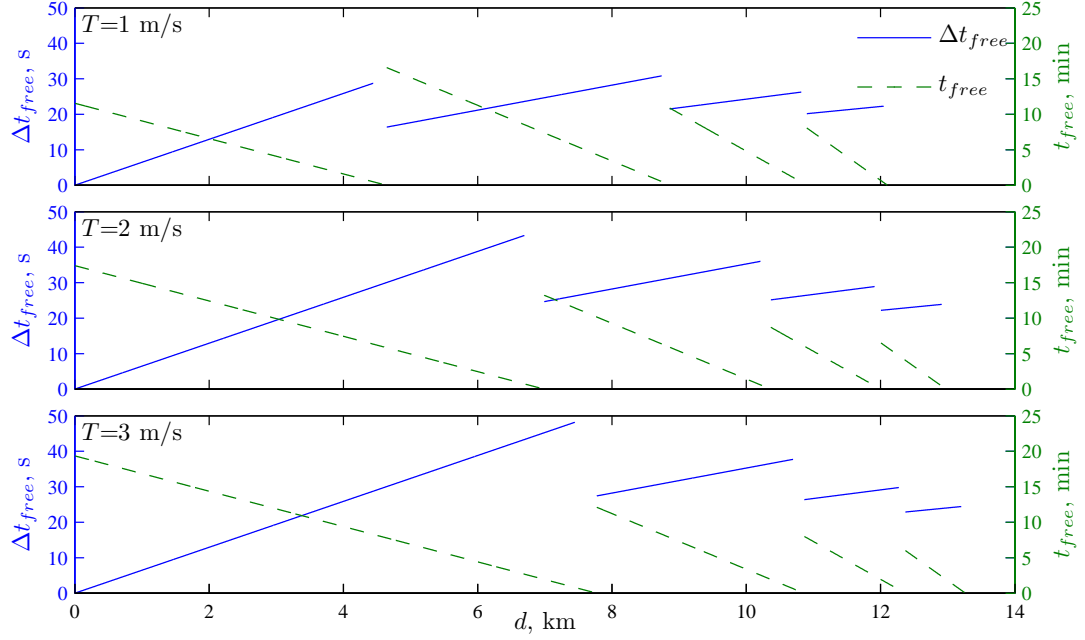


Figure 3.4. The t_{free} gained from cruising at v_{opt} instead of $v_{L/D}$, $\Delta h = 700\text{m}$, $s_s = 0.52\text{m/s}$.

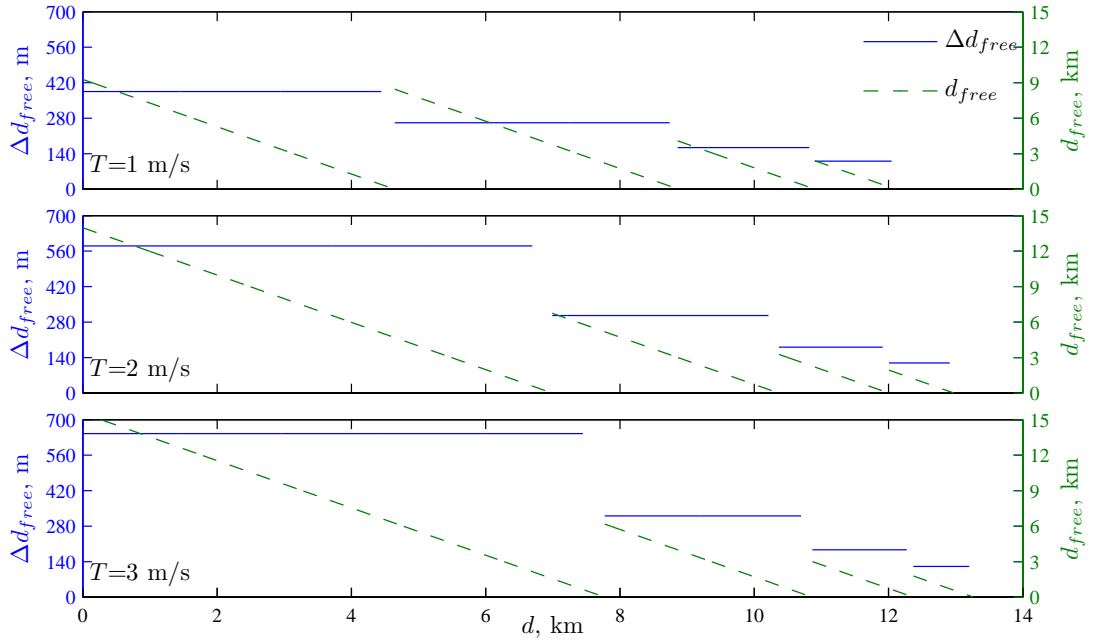


Figure 3.5. The d_{free} gained from cruising at v_{opt} instead of $v_{L/D}$, $\Delta h = 700\text{m}$, $s_s = 0.52\text{m/s}$.

$v_{L/D}$ became negative. In other words, the dashed lines extend past the solid lines because the maximum d using v_{opt} is larger than the maximum d using $v_{L/D}$. The additional distance gained is constant given a certain number of agents since the free time rises at a constant rate given a fixed optimal airspeed. The loitering time gained is less than one minute for all three thermal strengths and the distance gained is less than 700m. These gains become useful when N approaches an integer value, i.e., toward the right sides of the dashed lines, where resources begin to dwindle.

3.3.3 Aggregate Thermal

It is interesting to note that the second term in the numerator of Equation 3.20 represents a rate equal to the available altitude at the target divided by the time spent away from the target:

$$\frac{s_s}{\lceil N \rceil - 1} = \frac{\Delta h - s \frac{2d}{v}}{\frac{2d}{v} + \frac{\Delta h}{T} + t_{free}} \quad (3.22)$$

The right-hand side of Equation 3.22 is a rate that can be thought of as an aggregate thermal and the left-hand side is its relationship with N . The effects of d and Δh are incorporated into the thermal climb rate for a more relevant metric in describing thermals given a particular environmental scenario. Thus, the aggregate thermal is a way of discounting a thermal's strength by the energy required to reach it.

This explains the resemblance of Equation 3.20 to the equation for the MacCready speed. Hence, if a cycle has an aggregate thermal strength of 0.5m/s, the optimal cruising speed is equal to the MacCready speed for a thermal of strength 0.5m/s (32.8m/s for the ASW-27B).

The aggregate thermal concept exists in multiple-thermal cycles as well and is a general way of combining multiple thermals, the distances between them, and the lengths of the first and last legs of the cycle into one rate. The derivation steps are identical to those in the single-thermal cycle: reformulate Equation 3.12 to include a free resource, apply the ceiling operator on N , solve for the free resource, and differentiate with respect to a cruising speed. Here, the derivation is done in

terms of free distance in the cycle $N_{M \rightarrow T_1 \rightarrow T_2 \rightarrow T_1 \rightarrow M}$ and with the knowledge that $v_1 = v_4 = v_c$ ($d_1 + d_4 = d_c$), where v_1 is the crusing speed from $M \rightarrow T_1$, v_4 is the crusing speed from $T_1 \rightarrow M$, and v_2 and v_3 are the inter-thermal crusing speeds:

$$\begin{aligned} [N] &= 1 + \frac{\frac{d_1}{v_1} + \frac{s_2 d_2}{v_2 T_1} + \frac{d_2}{v_2} + \frac{\Delta h}{T_2} + \frac{d_3}{v_3} + \frac{s_3 d_3}{v_3 T_1} + \frac{d_4}{v_4} + \frac{d_{\text{free}}}{v_{\text{free}}}}{s_s^{-1} \left(\Delta h - s_1 \frac{d_1}{v_1} - s_4 \frac{d_4}{v_4} - s_{\text{free}} \frac{d_{\text{free}}}{v_{\text{free}}} \right)} \\ &= 1 + \frac{\frac{d_c}{v_c} + \frac{s_2 d_2}{v_2 T_1} + \frac{d_2}{v_2} + \frac{\Delta h}{T_2} + \frac{d_3}{v_3} + \frac{s_3 d_3}{v_3 T_1} + \frac{d_{\text{free}}}{v_{\text{free}}}}{s_s^{-1} \left(\Delta h - s_c \frac{d_c}{v_c} - s_{\text{free}} \frac{d_{\text{free}}}{v_{\text{free}}} \right)} \end{aligned}$$

Solving for d_{free} :

$$d_{\text{free}} = \frac{v_{\text{free}}}{1 - ([N] - 1)s_s^{-1}s_{\text{free}}} \left[\frac{d_c}{v_c} + \frac{s_2 d_2}{v_2 T_1} + \frac{d_2}{v_2} + \frac{\Delta h}{T_2} + \frac{d_3}{v_3} + \frac{s_3 d_3}{v_3 T_1} - ([N] - 1)s_s^{-1} \left(\Delta h - s_c \frac{d_c}{v_c} \right) \right]$$

Differentiating d_{free} with respect to v_c :

$$\frac{\partial d_{\text{free}}}{\partial v_c} = \frac{v_{\text{free}}}{1 - ([N] - 1)s_s^{-1}s_{\text{free}}} \left[-\frac{d_c}{v_c^2} - ([N] - 1)s_s^{-1} \left(-d_c \left(a - \frac{c}{v_c^2} \right) \right) \right]$$

where a quadratic fit was substituted for s_c . Setting to zero and multiplying both sides by $[1 - ([N] - 1)s_s^{-1}s_{\text{free}}]/v_{\text{free}}$ gives

$$\begin{aligned} 0 &= -\frac{d_c}{v_c^2} - ([N] - 1)s_s^{-1} \left(-d_c \left(a - \frac{c}{v_c^2} \right) \right) \\ &= 1 - ([N] - 1)s_s^{-1}(av_c^2 - c) \end{aligned}$$

Solving for v_c^2 :

$$v_c^2 = \frac{([N] - 1)s_s^{-1}c + 1}{a([N] - 1)s_s^{-1}}$$

and simplifying:

$$v_c = \sqrt{\frac{c + s_s([N] - 1)^{-1}}{a}} \quad (3.23)$$

where the aggregate thermal equals

$$\frac{s_s}{[N] - 1} = \frac{\Delta h - s_c \frac{d_c}{v_c} - s_{\text{free}} \frac{d_{\text{free}}}{v_{\text{free}}}}{\frac{d_c}{v_c} + \frac{s_2 d_2}{v_2 T_1} + \frac{d_2}{v_2} + \frac{\Delta h}{T_2} + \frac{d_3}{v_3} + \frac{s_3 d_3}{v_3 T_1} + \frac{d_{\text{free}}}{v_{\text{free}}}} \quad (3.24)$$

The utility of the aggregate thermal is that instead of thinking in terms of the number of agents required for a particular cycle, one can think in terms of the aggregate thermal for the cycle, avoiding confusion in scenarios where only one agent is available or when the zero-altitude-loss and continuous monitoring constraints do not apply. Equation 3.20 does not directly apply to scenarios with only one agent because maximizing t_{free} is no longer of interest since there is no free time available. Instead, $\lceil N \rceil$ is replaced by the non-integer N in Equation 3.20, where the interest reverts to minimizing the ratio of the time spent away from the target to the time spent at the target. This is precisely the reason why Equation 3.13 gives the same values for the optimal airspeed as Equation 3.20 without the ceiling operator:

$$v_c = \frac{-1 + \sqrt{1 + AB}}{A} = \sqrt{\frac{c + s_s(N - 1)^{-1}}{a}} \quad (3.25)$$

This was a coincidental result that was realized by finding optimal speeds for different conditions, calculating N , plugging N into Equation 3.25, and arriving at the same optimal speed. Equation 3.25 shows that v_c converges to $v_{L/D}$ and v_{MC} as d approaches infinity and zero, respectively. The critical difference between the two equations is that the latter equation, for the continuous monitoring scenario, must be solved iteratively, i.e., v_c depends on N , but N is a function of v_c , and cannot be used to find v_c for single-agent cycles.

In spite of this, there are other scenarios where the optimal cruising speed is known and the aggregate thermal strength can be determined. In any scenario, the formulation of the aggregate thermal involves defining a resource gained in units of distance, normally altitude, and the time it took to gain that resource. Consider a scenario where the goal is to create a thermal map of a region. The available agents explore the region, keeping a memory of thermal locations, strengths, uncertainty, etc., until needing to gain altitude to continue exploration. Each agent can then choose the thermal that benefits them the most by calculating aggregate thermal strengths.

For this case, the aggregate thermal is equal to the estimated height gained from a thermal, relative to an aircraft's current altitude, divided by the estimated time to gain that altitude given the thermal climb rate, the estimated final altitude, the distance between an agent and a thermal, and the cruising speed. The

optimal cruising speed, in this scenario, will reach the final altitude the fastest and this speed is known as the MacCready speed, covered in Section 2.4. Note that if the agent’s next exploration region is established before thermalling, then the MacCready speed will not be optimal. Analogous to v_c maximizing the aggregate thermal, the MacCready speed optimizes the aggregate thermal strength by minimizing the time to reach the final altitude. Knowing that the optimal air-speed in this scenario is independent of N eliminates the circularity discussed in the previous paragraph and allows the aggregate thermal strength to be used as a metric for choosing the “strongest” thermal based on an agents relative position to a thermal with respect to the target location.

3.4 Multiple-Thermal Exploitation

In addition to the theory presented on multiple-thermal exploitation thus far, a better intuitive understanding is sought as to when multiple-thermal exploitation is preferred over single-thermal exploitation. It has been noted that, at the least, multiple-thermal exploitation involves exploiting a weaker, but closer, T_1 as a via point to a stronger, yet farther, T_2 . However, the importance of the location of T_1 with respect to T_2 and M , the disparity between climb rate and distance, and the benefit of multiple-thermal exploitation remains to be explored. For simplicity, multiple-thermal exploitation cycles are limited to the partial cycle: $M \rightarrow T_1 \rightarrow T_2 \rightarrow M$, or equivalently, $M \rightarrow T_2 \rightarrow T_1 \rightarrow M$; and the full cycle $M \rightarrow T_1 \rightarrow T_2 \rightarrow T_1 \rightarrow M$. As mentioned previously, though the full cycle is preferred over the partial cycle, atmospheric dynamics will at times present the partial cycle as the best option due to thermal creation and dissipation.

Figure 3.6 shows polar maps of regions indicating whether single-thermal exploitation is preferred over multiple-thermal exploitation. The location of T_2 and M is constant in each map, where M is located at the origin and T_2 is located along the 90° line at radius equal to d_3 and is represented by a star; the value d_3 is indicated at the top of each map. Given T_1 , T_2 , d_3 , these maps were created by choosing a location for T_1 , thus setting d_1 , d_2 , and calculating N for the cycles $M \rightarrow T_1 \rightarrow M$, $M \rightarrow T_2 \rightarrow M$, and $M \rightarrow T_1 \rightarrow T_2 \rightarrow T_1 \rightarrow M$, represented by N_{T_1} , N_{T_2} , and $N_{T_1+T_2+T_1}$, respectively. If the location of T_1 re-

sulted in $N_{T_2} > N_{T_1} < N_{T_1+T_2+T_1}$, where single-thermal exploitation of T_1 requires the least N , then the location was given a red marker. If the location of T_1 resulted in $N_{T_1} > N_{T_2} < N_{T_1+T_2+T_1}$, where single-thermal exploitation of T_2 requires the least N , then the location was given a blue marker. Similarly, if the location of T_1 resulted in $N_{T_1} > N_{T_1+T_2+T_1} < N_{T_2}$, where the full cycle, $M \rightarrow T_1 \rightarrow T_2 \rightarrow T_1 \rightarrow M$, requires the least N , then the location was given a black marker. Finally, regions of white within the radius d_3 represent locations where the zero-altitude-loss constraint could not be satisfied. In this manner, the maps were populated by choosing all possible locations of T_1 within d_3 and assigning the appropriate marker. Distance d_3 increases from left to right and top to bottom.

As expected, it becomes less beneficial to exploit T_2 as d_3 increases. The maps show that at close distances, $d_3 < 1350\text{m}$, exclusively exploiting T_2 is desired over multiple-thermal exploitation; note that there are no red or black points in the first map, dummy points were plotted solely to produce a complete legend. The next map to the right shows a developing circular red region around the origin. With the development of the red region, a developing black region begins slightly within the red circle and extends to the location of T_2 . As d_3 increases, the circular red region grows while the blue and black regions shrink, where the black region always “connects” the red region to T_2 . Thus, exploiting T_1 as a via point is a maneuver that is present at larger distances of d_3 and d_1 and is beneficial even if T_2 can be “easily” reached.

The third row of maps extend to distances where exploiting T_2 alone would result in a loss of altitude within a cycle. The map to the left shows a region where multiple-thermal exploitation would be beneficial if T_1 was sufficiently far away from the origin, whereas the map to the right no longer has this region because d_3 has become too large. These observations imply that if the zero-altitude-loss constraint cannot be satisfied for a thermal T_2 , then multiple-thermal exploitation with T_1 is not worth considering because T_1 would also need to be very far away and the uncertainty in thermal dynamics during the cruising time would be too risky; it would probably be more practical to explore the region for a better option.

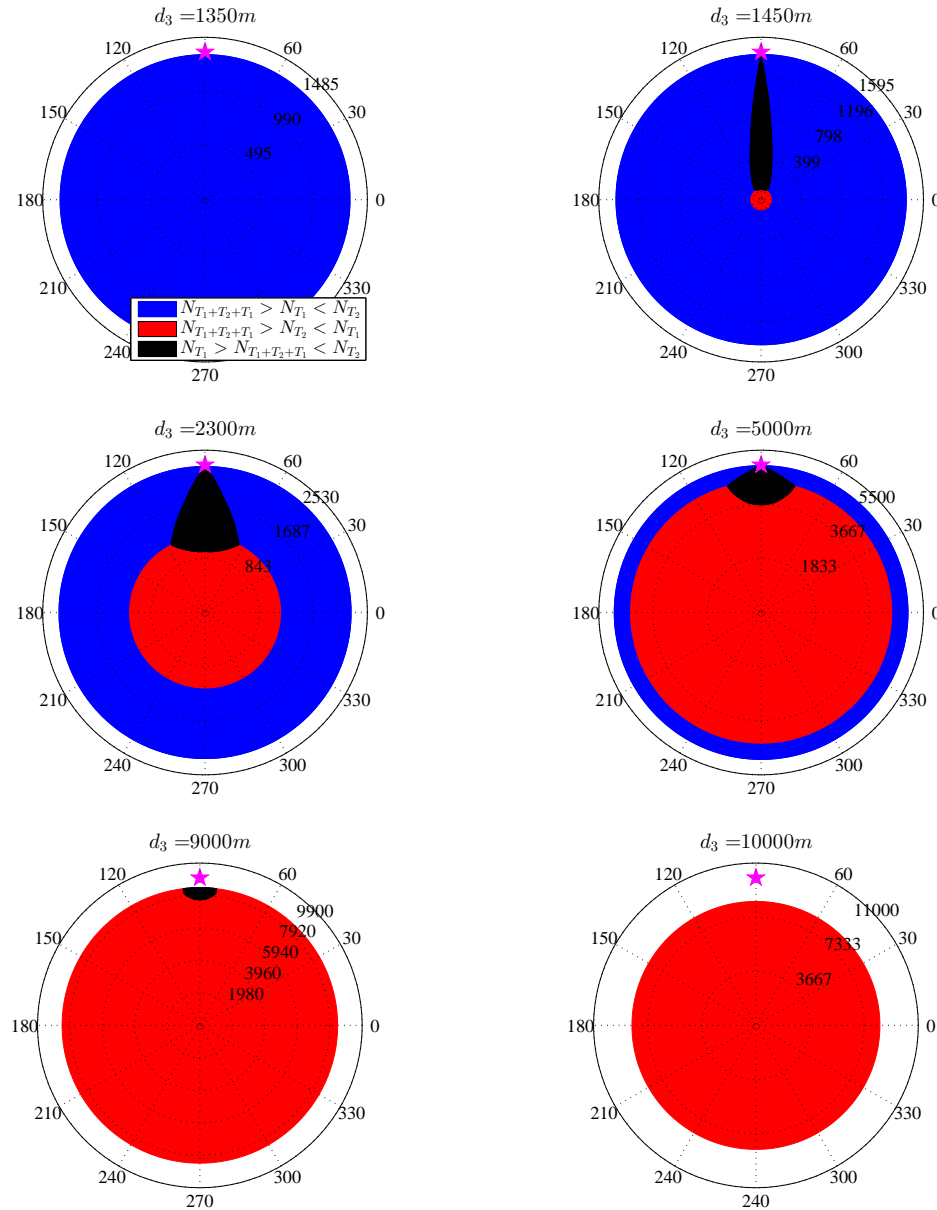


Figure 3.6. The polar maps of multiple-thermal exploitation for $\Delta h = 350\text{m}$, $s_s = 0.52\text{m/s}$, $T_1 = 1.5\text{m/s}$, and $T_2 = 3\text{m/s}$.

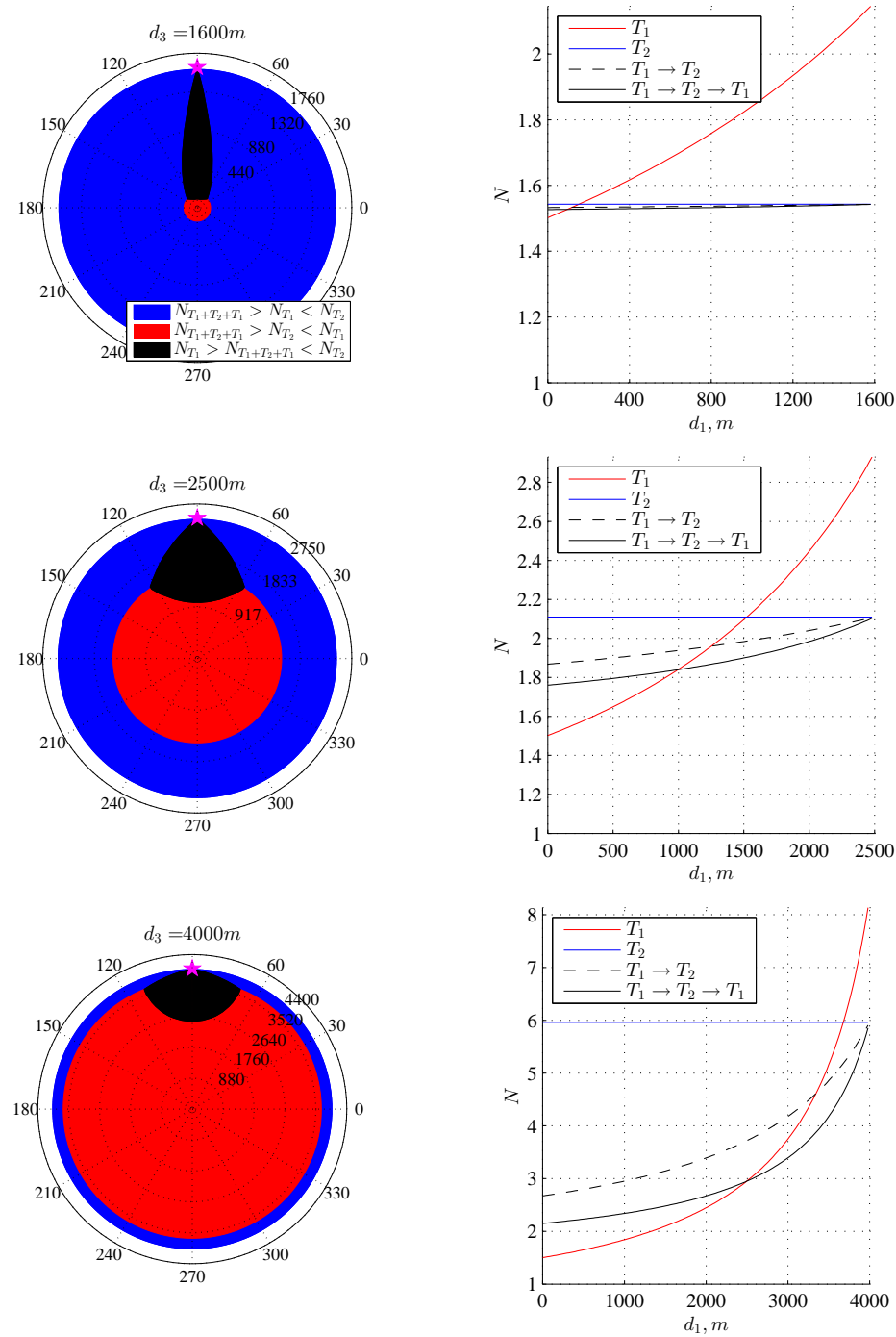


Figure 3.7. The polar maps of multiple-thermal exploitation for $\Delta h = 200\text{m}$, $T_1 = 1\text{m/s}$, and $T_2 = 4.5\text{m/s}$ and the corresponding d_3 annotated along the 90° line.

Another interesting observation is that the maximum angular range of the black region for all maps, not only the maps pictured in Figure 3.6, between $d_3 = 0\text{m}$ and $d_3 = 10,000\text{m}$ is approximately 75° . The largest angular range for other conditions was roughly equal to 95° , where the maximum range occurs very close to the origin in all maps. As a general rule, multiple-thermal exploitation is potentially beneficial if T_1 is located within a 75° region on the path to T_2 , or 37.5° to both sides of T_2 .

Figure 3.7 shows the scenario described by $\Delta h = 200\text{m}$, $T_1 = 1\text{m/s}$, and $T_2 = 4.5\text{m/s}$ for three different values of d_3 . The graphs on the right correspond to the polar plots on the left and plot N as a function of d_1 , where d_1 is the distance between M and T_1 along the 90° line. The solid blue lines represent the exploitation of T_2 and are horizontal because d_3 is constant in each scenario. The solid red lines represent the exploitation of T_1 , the dashed black lines represent the partial cycle, and the solid black lines represent the full cycle. The important message in this figure is that there will be scenarios where full-cycle exploitation will significantly change the number of agents required for a cycle: the scenario in the second row, starting from $d_1 \approx 1650\text{m}$ and ending at $d_1 \approx 2050\text{m}$, would require two agents ($\lceil N \rceil$) for full-cycle multiple-thermal exploitation, whereas the other cycles would require three agents.

Replacing the full cycle in Figure 3.6 with a partial cycle affects the polar maps by changing only the black region. The effect is a flattening of the bottom rounded region, resulting in a relatively straight line between the two endpoints of the previously circular curve. As examples, the black region of the fourth polar map in Figure 3.6 would be roughly half as long due to the flattening of the circular curve and the black region of the fifth polar plot would disappear entirely. Thus, a partial cycle decreases the area where multiple-thermal exploitation is optimal and enlarges the area where single-thermal exploitation of T_1 is optimal.

3.5 Transitional Altitude Changes

Transitional changes in altitude occur when an agent transitions between jobs. The transition involves a change in airspeed and, since the topic is on soaring gliders, this change involves a conversion to or from potential energy. The transitional

altitude change decreases in significance as the size of the glider decreases, since smaller gliders have smaller cruising airspeeds. Comparing a 5m/s change in the lower range of airspeeds for the ASW-27B vs. the same change in the SB-XC:

$$\Delta h_{\text{ASW}} = \frac{v_1^2 - v_2^2}{2g} = \frac{35^2 - 30^2}{2g} = 16.6\text{m}$$

$$\Delta h_{\text{SBXC}} = \frac{v_1^2 - v_2^2}{2g} = \frac{18^2 - 13^2}{2g} = 7.9\text{m}$$

The behavior controller must take these changes into account so that the minimum allowable altitude constraint is not violated. Because the agents are lowest when arriving at thermals, a potential violation exists if the controller does not include the two transitional changes within $M \rightarrow T_1$ (and $T_1 \rightarrow T_2$ during multiple-thermal exploitation) in calculating the departing altitude from M (and T_1 during multiple-thermal exploitation).

The following equations employ new variables: g is the acceleration due to gravity, v_s and v_T are the monitoring and thermalling airspeeds respectively, δh_S and δh_T are the transitional changes in altitude at the monitoring and thermalling locations respectively, and an underbar and overbar represent the bottom and top of the location, respectively. Thus, $\delta h_{\underline{S}}$ is the transitional change in altitude at the bottom of the monitoring target, which is the change in altitude due to a difference between the monitoring airspeed v_s and the cruising airspeed v_1 toward the thermal. $\delta h_{\underline{T}}$ is the change at the bottom of the thermal, which is due to the difference between the cruising airspeed v_1 and the thermalling airspeed v_T . Whereas $\delta h_{\overline{T}}$ is the change due to the difference between v_T and v_2 .

If $v_1 \geq v_T$:

$$N = 1 + \frac{\frac{d_1}{v_1} + \frac{d_2}{v_2} + \left(\Delta h - \underbrace{\frac{v_1^2 - v_T^2}{2g}}_{\delta h_{\overline{T}}} \right) T^{-1}}{\left[\Delta h - \frac{d_1}{v_1} s_1 - \frac{d_2}{v_2} s_2 + \left(\underbrace{y_2'' - y_s''}_{\delta h_{\overline{S}}} + \underbrace{y_s'' - v_1^2}_{\delta h_{\underline{S}}} + \underbrace{v_T^2 - y_2''}_{\delta h_{\overline{T}}} \right) / 2g \right] s_s^{-1}} \quad (3.26)$$

$$= 1 + \frac{\frac{d}{v_1} + \frac{d}{v_2} + \left(\Delta h - \frac{v_1^2 - v_T^2}{2g} \right) T^{-1}}{\left[\Delta h - s_1 \frac{d}{v_1} - s_2 \frac{d}{v_2} + (v_T^2 - v_1^2) / 2g \right] s_s^{-1}}$$

where $\delta h_{\bar{T}}$ affects (decreases) t_T but not the departing altitude at M.

If $v_1 < v_T$:

$$\begin{aligned} N &= 1 + \frac{\frac{d_1}{v_1} + \frac{d_2}{v_2} + \Delta h/T}{\left[\Delta h - \frac{d_1}{v_1} s_1 - \frac{d_2}{v_2} s_2 + (\underbrace{y_2^z - y_s^z}_{\delta h_{\bar{S}}} + \underbrace{y_s^z - y_1^z}_{\delta h_S} + \underbrace{y_T^z - y_2^z}_{\delta h_{\bar{T}}} + \underbrace{y_1^z - y_T^z}_{\delta h_T} < 0})/2g \right] s_s^{-1}} \\ &= 1 + \frac{\frac{d}{v_1} + \frac{d}{v_2} + \Delta h/T}{\left(\Delta h - s_1 \frac{d}{v_1} - s_2 \frac{d}{v_2} \right) s_s^{-1}} \end{aligned} \quad (3.27)$$

where $\delta h_{\bar{T}}$ now affects (raises) the departing altitude at M but not t_T .

Equation 3.27 reduces to Equation 3.2 and the optimal airspeed for v_1 and v_2 is given by Equation 3.25. Unfortunately, the optimal airspeed toward the thermal will almost always be larger than the airspeed within the thermal and thus the optimal airspeed must be found from Equation 3.26. Differentiating with respect to v_2 gives an optimal airspeed equivalent to Equation 3.25, whereas differentiating with respect to v_1 no longer results in a quadratic function:

$$\begin{aligned} v_1^4 \left(\frac{a}{2gT} \right) + v_1^3 \left(\frac{b}{gT} + \frac{d_2 s_2}{d_1 g T v_2} + \frac{d_2}{d_1 g v_2} \right) + \\ v_1^2 \left(\frac{3c}{2gT} + \frac{3}{2g} + \frac{ad_2}{v_2} + \frac{a\Delta h}{T} + \frac{av_T^2}{2gT} \right) + v_1 (2ad_1) + Z = 0 \end{aligned} \quad (3.28)$$

where $Z = -\Delta h + bd_1 + s_2 d_2 / v_2 - v_T^2 / 2g - cd_2 / v_2 - c\Delta h / T - cv_T^2 / 2gT$. The optimal airspeed for v_1 becomes cumbersome to solve for in closed-form and may instead be solved for by a constrained optimization function such as `fmincon` and the result can then be approximated by a quadratic fit. Appendix B.4 plots the effect of these altitude changes on the optimal airspeed and the estimated number of agents for the ASW-27B and SB-XC.

3.6 A Comment on Assumptions

This section discusses lifting the assumptions listed in Chapter 2.

Winds can be treated in the same way as in MacCready theory. Tailwind speeds

are subtracted from the reference cruising airspeed, whereas headwind speeds are added to the reference cruising airspeed. The speeds of sinking air masses are added to the c -term in Equations 3.20 and 3.25, where sink speeds are positive and increase the reference cruising airspeed. In relation to Equation 3.12, the speed of a sinking air mass is added to the c -term in B :

$$B = \frac{1}{ad_c} (\Delta h - bd_c) + A \frac{c + s_{am}}{a} \quad (3.29)$$

where s_{am} is the speed of the sinking air mass. This was derived by adding s_{am} to s_1 and s_3 in Equation 3.12.

Assumptions 2 and 3 may be lifted as long as these quantities can be estimated; all that is required to calculate the optimal airspeed is to estimate the time of a circuit and the resulting altitude left over for monitoring, i.e., the ratio between the resource gained and the time it took to gain it.

To simplify calculations in this thesis, the maximum allowable altitude is set to the altitude where the thermal strength begins dissipating. Exploitation into the dissipation (altitudes closer to the actual inversion layer) may be included in the N calculations with an estimated function for the thermal strength as a function altitude. The question arises of how far up an glider should exploit the dissipating region of a thermal. The answer is found by applying a fact from MacCready theory to the aggregate thermal theory: the MacCready setting (expected thermal strength in cross-country soaring) is the minimum rate of climb a glider is willing to exploit. Thus, if a cross-country soaring glider is thermalling and expects the next encountered thermal to have a strength of 3m/s, then the glider should depart the current thermal when the climb rate is lower than 3m/s. Likewise, in scenarios where the aggregate thermal is applicable, a glider should depart a thermal once the climb rate is lower than the aggregate thermal strength of the cycle, regardless of whether this occurs above the maximum allowable altitude or not. This can be deduced from an analyses provided in Appendix B and leads to the following conclusion: with the goal of maximizing a free resource during multiple-agent scenarios, a glider should at least exploit a thermal to an altitude where the rate of climb is equal to the monitoring sink rate of the glider.

Assumption 4, homogeneous agents, may be lifted by keeping track of the sink

polar fit coefficients and monitoring/thermalling sink rates for each agent in a system of inhomogeneous agents.

Dealing with assumption 5, atmospheric dynamics, is an obstacle for any real-world scenario, irrespective of the cruising airspeed. Traveling at $v_{L/D}$ to a dissipating thermal will leave an agent just as stranded as if the agent had traveled at v_{opt} . The difference between the two cases is that traveling at $v_{L/D}$ lessens the altitude loss during cruise, hence, more time at the monitoring target. This, however, comes at the cost of flying slowly toward a thermal that may be dissipating, increasing the chances of arriving at a dead thermal. Should an aircraft arrive at a dead thermal or be stuck midway up the working altitude due to thermal dissipation, a new minimum allowable altitude should be established and the aggregate thermal metric should be used to choose the next thermal.

The effects of the duration of transient maneuvers and the changes in altitude during transient maneuvers will be discussed further in Chapter 4. As a supplement, Reichmann presents an important graphical analysis of the losses due to an incorrect expected climb rate in a thermal; he notes that the cruise speed will not be significantly affected until rather large errors are made and that the zero setting, for which the airspeed is $v_{L/D}$, should be avoided whenever possible [34].

3.7 Summary

This chapter put forth the equations for the number of agents and the optimal airspeeds for the different persistent monitoring scenarios: single-agent single-thermal, single-agent multiple-thermal, and multiple-agent. The chapter began with a simple proof showing that the number of agents in a monitoring cycle is minimized when the working altitude is maximized, meaning that it is suboptimal to both depart the thermal lower than the altitude ceiling and to depart the monitoring target higher than the minimum altitude required for reaching the first thermal. Following this, it was found that the optimal airspeeds toward the thermal and toward the target for the single-agent single-thermal scenario were equivalent and formulated in terms of two auxiliary variables A and B . Additionally, for the single-agent multiple-thermal scenario, the inter-thermal airspeed from $T_1 \rightarrow T_2$ was found to equal the reversed MacCready airspeed, i.e., the MacCready airspeed

toward T_2 is dependent on T_1 and independent of T_2 . And the optimal airspeed from $T_2 \rightarrow T_1$ on the path back toward the monitoring target reverts back to the normal MacCready speed, i.e., the MacCready speed is calculated based on T_1 .

The aggregate thermal was derived by maximizing a free resource (loitering time and exploration distance) for when multiple agents are available. This approach is preferred over minimizing the number of agents because the real-life number of agents will always be an integer number; including a free resource allows the agents to convert an extra non-integer number of agents into a usable resource. The airspeed that maximizes the free resources in a monitoring cycle was found to be given by the MacCready speed for the aggregate thermal, where the aggregate thermal is essentially a discounted thermal strength that can also condense multiple thermals into one rate. It was noted that the optimal airspeed in single-agent scenarios is equivalent to the MacCready speed for the aggregate thermal without the ceiling operator acting on the number of agents.

The formulation of the aggregate thermal allows one to regard the monitoring cycle more intuitively. Two cycles differing by a certain number of agents can instead be expressed by a difference in their aggregate thermal strengths. In general, the aggregate strength is way of quantifying the rate at which a resource is gained relative to the location where the resource is used, e.g., for persistent monitoring, the aggregate thermal is equivalent to the ratio between the workable altitude at the monitoring target and the time needed to gain that workable altitude, where workable altitude is dependent on the proximity of the thermal or thermals.

Equations for the number of agents required in a cycle where transitional changes in altitude are included show that the optimal airspeed toward the thermal is no longer equal to the optimal airspeed toward the monitoring target. While the optimal airspeed toward the target is equal to the aggregate MacCready speed, the optimal airspeed toward the thermal is too complicated to solve in closed-form and must be approximated by a lower order function after being solved for by a constrained optimization routine. Finally, even if these transitional changes in altitude are negligible, they must be accounted for by the behavior controller in calculating the departure altitude from the target, as well as the departure altitude from the first thermal in multiple-thermal exploitation, if the minimum allowable altitude constraint is considered inviolable.

A comment on lifting the theoretical assumptions concluded the chapter. Adjusting the optimal airspeed in the presence of headwinds, tailwinds, and sinking air masses parallels the adjustments made in MacCready theory. Environmental quantities like Δh and T need not be constant and systems of inhomogeneous agents are possible but require stricter bookkeeping of sink polar fit coefficients and monitoring/thermalling sink rates.

Chapter 4

Simulation Results

CHAPTER 4 presents flight simulation results for single-agent single-thermal persistent monitoring. The purpose of this chapter is to both assess the accuracy of the governing equations covered in Chapter 3 and to append these equations to better match flight results, where unmodeled dynamics and simplifying assumptions are potential sources of error.

The Schleicher ASW-27B ($m = 320\text{kg}$, $S = 9\text{m}^2$), representative of large UAVs, and the RnR Products SB-XC glider ($m = 10\text{kg}$, $S = 1\text{m}^2$, representative of small UAVs, are flown under four fixed exploitation scenarios. Each scenario is simulated multiple times with the airspeed set at the optimal cruising airspeed, v_c , and with the airspeed set at the best L/D airspeed, $v_{L/D}$. The number of agents required in flight is found graphically by noting the durations of the monitoring, cruising, and thermalling stages in the cycle.

It will be shown that, under most conditions, cruising at the optimal airspeed provides only a modest improvement to the monitoring cycle. However, depending on the importance of the minimum allowable altitude for the agents, these improvements are potentially critical for cycles requiring a slightly non-integer ($N \geq \lceil N \rceil$) number of agents when flown at $v_{L/D}$, where a small improvement translates into saving an entire additional agent. Simulations show that the thermalling/monitoring departure controller and an accurate estimate of the working altitude at the monitoring target are vital in predicting these potentially critical improvements in flight.

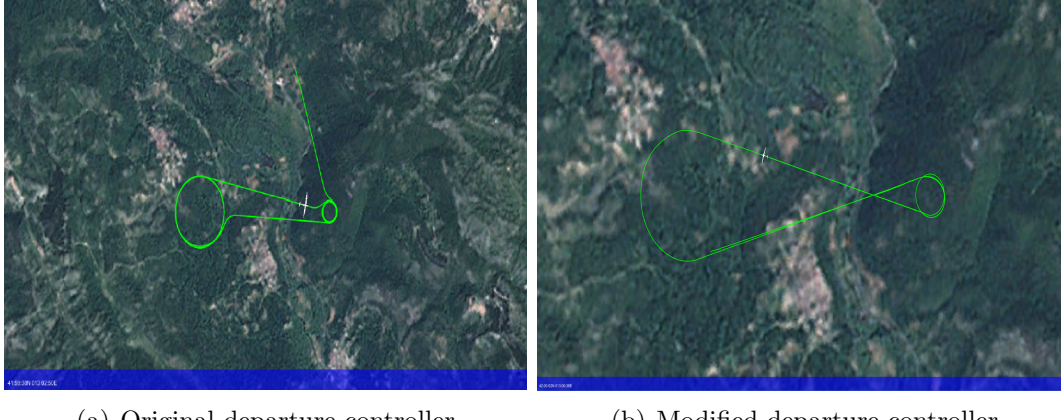


Figure 4.1. Silent Wings simulation flight paths during single-thermal exploitation with an ASW-27B glider.

4.1 Simulation Setup

The four chosen scenarios are summarized in Table 4.1. The interface with Silent Wings was established via MATLAB’s Simulink, where UDP was used to receive aircraft states and to autonomously send control commands to the glider. The Simulink model and the Silent Wings Simulator were run from separate computers to facilitate the addition of agents in future simulations involving multiple agents.

In each simulation, the environment was set to be windless except for one fixed thermal set at a known GPS position with a chosen climb rate and an inversion layer set at 2070 meters above sea level. The altitude ceiling for the glider was chosen to be 2000 meters above sea level, where the interaction with the inversion layer began at 1980 meters, i.e., 20 meters were allotted for “realizing” the dissipation before exiting the thermal.

The glider’s initial behavior was set to cruise to the thermal and climb to the altitude ceiling, where the altitude ceiling was chosen as the starting location for the cycles in the results. Upon reaching the ceiling, the glider began to roll and change airspeed before cruising with the proper heading and airspeed toward the monitoring target, which was assigned a GPS position to match the distance specified by the scenario. The glider would then monitor the target until sinking to the departure altitude and cruising back to the thermal to repeat the cycle. Silent Wings screenshots show an example flight path in Figure 4.1.

The thermalling and monitoring controllers were simple radius hold controllers, for which the circling radius within the thermal and monitoring target was 150 meters and 500 meters, respectively. The respective commanded airspeeds for the ASW-27B were 31m/s and 27.78m/s, where $v_{L/D} = 27.78\text{m/s}$, and the respective commanded airspeeds for the SB-XC were both equal to $v_{L/D} = 13.14\text{m/s}$. The radii at these two locations were taken into account in the distance setting, thus, the 2km separation setting corresponded to a separation of 2.65km with the circling radii included. A switch-case block was used for gain scheduling in the airspeed controller, where the gains were determined through trial and error. The polar fit coefficients required for calculating the optimal airspeeds were found by flying the glider in Silent Wings at the operating altitudes instead of consulting a documented source. The gliders were flown with flaps fully retracted and the polar fit coefficients were $a = 0.001559$, $b = -0.06475$, and $c = 1.174055$, for the ASW-27B and $a = 0.020057$, $b = -0.4831$, and $c = 3.3843$ for the SB-XC, with sink rate taken as positive with units of m/s, depicted in Figure 4.2. Black circles represent the flight data obtained from the simulator, red filled circles represent the points chosen for the quadratic fit sink polars, and the red curves represent the quadratic fit sink polars. Three points, as opposed to a least squares fit, were chosen so that the lower range of estimated airspeeds had lower errors compared to the higher range of airspeeds, since the environmental conditions in simulation required lower airspeeds.

4.2 Initial Simulation Results for the ASW-27B

Figure 4.3 represents key information from a representative simulation. The top graph shows the actual height of the glider during simulation and the expected height, whereas the bottom graph shows the response of the airspeed controller. Red lines represent expected altitude and commanded airspeed in the first and second graph, respectively, and blue lines represent the actual values during simulation. Shaded green regions represent the transitions and cruise within $T \rightarrow M$ and shaded yellow regions represent transitions and cruise within $M \rightarrow T$. This figure represents the scenario $\Delta h = 350\text{m}$, $d = 1\text{km}$, and $T = 4\text{m/s}$, which had the strongest theoretical aggregate thermal of 2.14m/s given the optimal airspeed

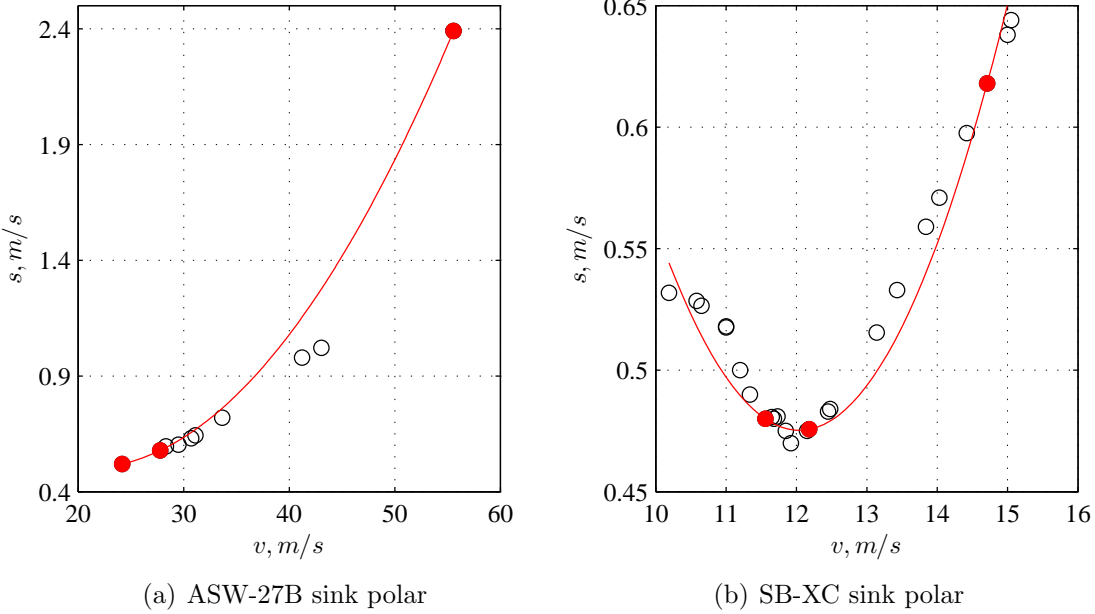


Figure 4.2. Polar fits for the ASW-27B and the SB-XC.

obtained from Equation 3.13, 46.35m/s. These graphs were generated for all 24 simulations and were used to obtain the information presented in Table 4.2 (discussed later in this section). It is important to understand that the actual and commanded airspeeds correspond in time with the actual height of the agent and not the expected height.

The stages illustrated in the height plot will now be explained from left to right. The shaded green region contains three stages. First, the glider starts at the top of the thermal at 2000 meters and enters a transition to begin cruising at v_c . This transition consists of rolling into the proper heading while simultaneously losing altitude to reach the desired airspeed, i.e., converting potential energy to kinetic energy. The glider then cruises at v_c until reaching the monitoring target, where it again enters a transition to reach the desired circling airspeed, this time trading kinetic energy for potential. Thus, the three stages in the green region are the two transitions with the one cruising stage in between them. Following the green region, the white region represents the monitoring stage where the glider holds a fixed radius and airspeed around the target. The glider eventually losses too much altitude and cruises back to the thermal, represented by the yellow region.

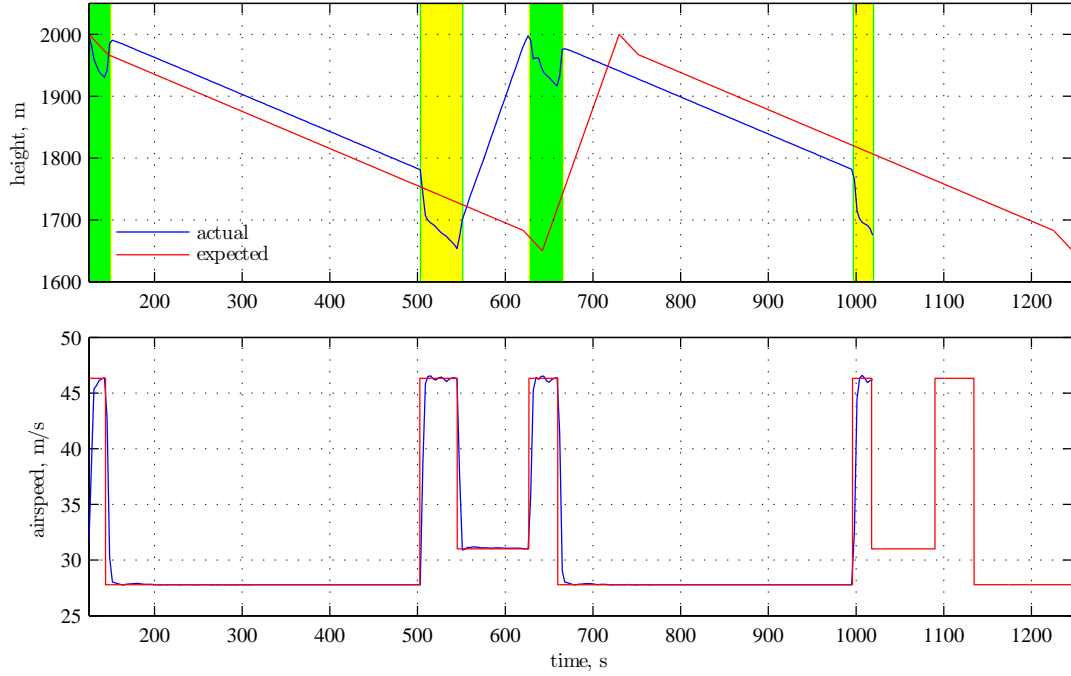


Figure 4.3. Simulation plot of the scenario $\Delta h = 350\text{m}$, $d = 1\text{km}$, and $T = 4\text{m/s}$, whose theoretical aggregate thermal strength is 2.14m/s .

Similar to the previous transition, the glider trades altitude for speed, cruises to the thermal, and trades speed for altitude before reaching the thermal. The cruising stage is seen clearly here as the straight line with a slope a bit less than -1 and lasting for approximately 45 seconds. Finally, the glider regains altitude at a relatively constant rate until repeating the cycle. The final, right-most point shown in the graph represents the bottom of the thermal of the second cycle, 1650 meters above sea level, where the actual arrival time is sooner than the expected arrival time. Note that the final yellow region does not include the second transition experienced just before starting the thermalling stage.

A couple of subtle points remain to be discussed. Starting from the first green region, one sees that the height lost during the initial transition is approximately entirely regained during the second transition. However, the same cannot be said of the two transitions in the first yellow region, where the height gained is about half of the height lost. This imbalance has to do with the characteristic region of sinking air surrounding all thermals. The reason why only half of the height is regained is because the glider enters a region of sinking air that was not encountered

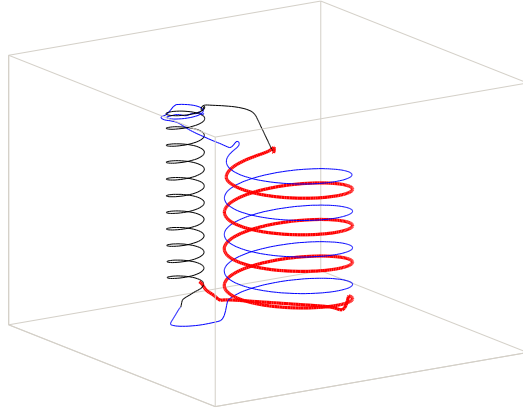


Figure 4.4. Simulation flight path for run 1 of case 3 with v_c .

at the initial transition in the yellow region. In the green region, the reason why roughly all of the height is regained is because the glider spends extra time within the thermal during the initial transition, i.e., the glider engages in a banked turn while still within the region of lift. In addition, a small amount of the imbalance in the yellow region is attributed to the difference in airspeeds: the initial transition loses the altitude required to reach v_c from a speed of 27.78m/s, whereas the final transition gains the altitude required to reach 31m/s from v_c .

The final point to note is the difference in cruise durations: the first and final cruises required about half of the time required for the middle two cruises. Consider the flight path shown in Figure 4.1a where the glider exits the thermal and monitoring target already in the direction of travel. Most of the simulations did not work out as fortuitously, i.e., the glider engaged in a banked turn in order to reach the proper heading. The banked turns lasted up to ten seconds and would manifest as circular curves stemming off from the reference radius at either the thermal or the monitoring target. This acted as an extension of the cruising segment and is the main cause for the difference in transit times. Figure 4.4 and Figure 4.5 illustrate these cruise extensions and are discussed after the next few paragraphs.

Table 4.1 describes the scenario settings for each of the four simulated cases and is used in conjunction to Table 4.2. Table 4.2 lists the N for each of the 24 simulated cycles, half with v_c (values without parenthesis) and half with $v_{L/D}$

Table 4.1. The case descriptions of the four different scenarios tested in simulation.

Case	Scenario Description					
	Δh , m	d , km	T , m/s	v_c , m/s	N	\bar{N}
1	350	1	4	46.35	1.28 (1.31)	1.35 (1.30)*
2	350	2	4	39.76	1.47 (1.52)	1.53 (1.50)*
3	350	1	1	35.08	1.81 (1.82)	1.84 (1.80)*
4	350	2	1	33.28	2.08 (2.11)	2.12 (2.07)*

* $v_{L/D}$ outperforms v_c

Table 4.2. This table lists the number of agents required in 24 simulations.

Case	Number of Agents from Simulations			
	N_1	N_2	N_3	N_4
1	1.36 (1.38)	1.40 (1.41)	1.41 (1.44)	1.43 (1.42)*
1	1.41 (1.37)*	1.42 (1.39)*	1.43 (1.43)	1.41 (1.43)
1	1.39 (1.37)*	1.39 (1.41)	1.38 (1.46)	1.39 (1.39)
2	1.61 (1.53)*	1.59 (1.51)*	1.61 (1.54)*	1.56 (1.52)*
2	1.63 (1.53)*	1.66 (1.52)*	1.72 (1.55)*	1.67 (1.53)*
2	1.57 (1.51)*	1.58 (1.51)*	1.59 (1.51)*	1.58 (1.52)*
3	1.90 (1.93)	1.94 (1.94)	2.01 (2.03)	2.00 (1.98)*
3	1.89 (1.93)	1.91 (1.95)	1.95 (2.04)	1.93 (1.98)
3	1.89 (1.92)	1.93 (1.96)	1.99 (1.94)*	1.97 (1.93)*
4	2.36 (2.11)*	2.31 (2.10)*	2.24 (2.10)*	2.23 (2.10)*
4	2.23 (2.12)*	2.21 (2.12)*	2.21 (2.12)*	2.22 (2.11)*
4	2.32 (2.11)*	2.29 (2.13)*	2.24 (2.12)*	2.23 (2.11)*

* $v_{L/D}$ outperforms v_c

(values within parenthesis). The four values of N in Table 4.2 correspond to four different starting points for a cycle calculation: N_1 is for the cycle starting and ending at the altitude ceiling, N_2 is for the cycle starting and ending at the top of M, N_3 is for starting and ending at the bottom of M, and N_4 is for starting and ending at the altitude floor. These N should be compared to the N predicted by theory, shown in Table 4.1, to get a sense of the accuracy of the theoretical model. Note that the expected values of N in Table 4.1 were calculated with $s_s = 0.6\text{m/s}$. Equation 3.22 may be used to convert these values to aggregate thermal strengths. Lastly, asterisks were placed wherever $v_{L/D}$ outperformed v_c . Note that the values within parenthesis have no relation to the values without parenthesis, except for case number, due to the random starting altitude and location in each simulation run. This means that, for example, the first row of values within parenthesis (or without) may be switched with the second row, which may lead to the asterisks being omitted or located at different locations. Thus, the asterisks simply provide a “first-glance” comparison in performance between v_c and $v_{L/D}$. Instead, *all* of the values without parenthesis should be compared with *all* of the values with parenthesis within a given case.

A new variable, \bar{N} , was introduced to quantify the effect of an asymmetric transition in the cycles involving v_c , where the cruising airspeed is larger than the reference airspeed at either T or M. The altitude lost during the transition when entering M is balanced by the transition when leaving M, i.e., the gain in potential energy upon entering M is lost upon exiting M. Unfortunately, the same cannot be said for the transitions around T. Entering T results in an altitude gain that shortens the exploitation time of the thermal. This effect is not canceled because the transitional loss of potential energy at the altitude ceiling does not necessarily mean that the exploitation time is extended. For the exploitation time to increase, the glider would need to continue thermalling until the transitional loss has been regained, i.e., the transition would need to occur within the thermal. Nevertheless, this may have been inadvertently accounted for since the glider does, at times, remain within the thermal during its transition trajectory. In any case, \bar{N} introduces a transitional correction factor by decreasing the working altitude by an amount equal to the transitional altitude loss from exiting T. The implicit assumption here is that the transitional altitude loss is not at all regained at the

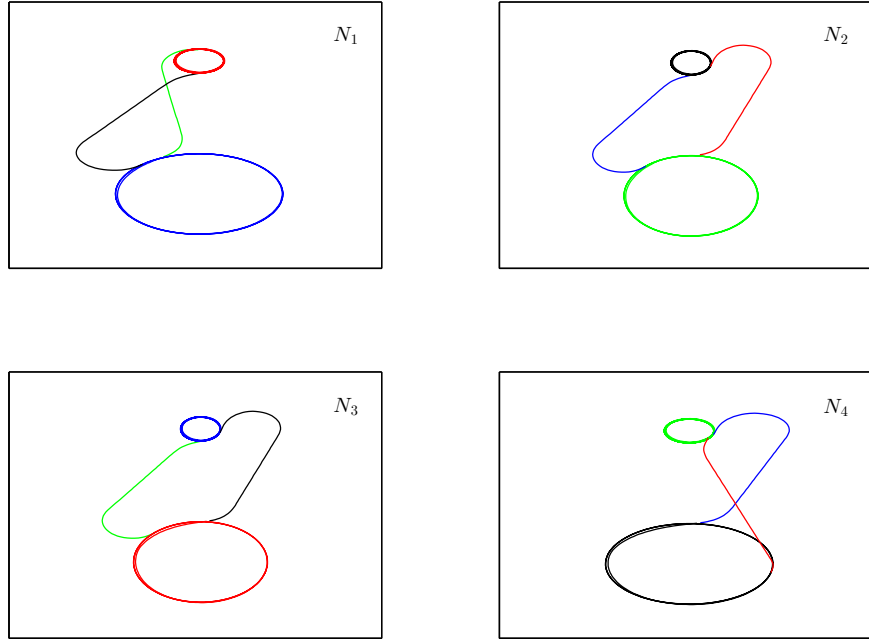


Figure 4.5. Simulation flight path for run 1 of case 3 for v_c divided into the individual N_1 through N_4 .

top of T. This correction factor appears to decently match the simulation results, presumably because of the surrounding area of sinking air around the thermals adding to the negative effect of shortening the monitoring time.

Figures 4.4 and 4.5 suggest an important change to the departure controller is necessary. Both of these figures show run 1 of case 3 cruising at v_c . Figure 4.4 shows the flight path for the entire simulation, whereas Figure 4.5 divides the simulation run into the four segments tabulated in Table 4.2. In Figure 4.4, the thermalling stage is shown in black with the smaller radius and the monitoring stages are shown in blue and a thick red. The monitoring stage in blue preceded the monitoring stage in red, meaning that the monitoring in blue came before thermalling and the monitoring in red came after the thermalling (recall that the simulations started at the thermal inversion layer). The different departure trajectories depicted in Figure 4.5 account for a large portion of the error and variation seen in Table 4.2.

The colors represent the task order within the calculations of N_1 through N_4 . Green, blue, black, and red correspond to orders one, two, three and four. In the plot showing N_1 , the agent began by departing the thermal at the inversion layer

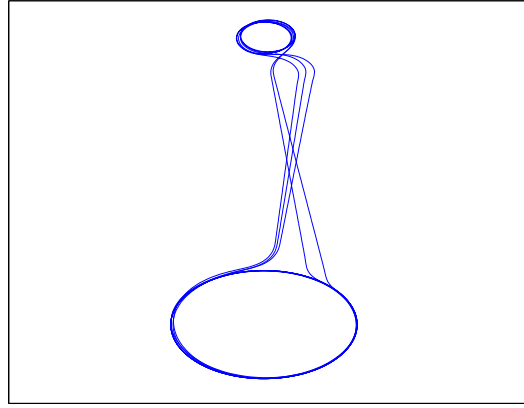


Figure 4.6. Simulation flight path for run 3 of case 2 for $v_{L/D}$ with the superposition of N_1 through N_4 .

and cruising to the monitoring target. From there on, the agent monitored the target, departed the target and arrived at the thermal, and finished at the top of the thermal. In the plot showing N_2 , the agent began by monitoring the target and finished by cruising back to the top of the monitoring target. The important distinction between N_1 and N_2 in this run is the departure angle from the thermal. In N_1 , the agent departs in a shorter trajectory while being near the outer region of lift. In N_2 , the agent departs the thermal in a much longer trajectory in addition to being away from the region of lift. This is presumed to be exactly why N_1 is less than N_2 in run 1 of case 3. In N_3 , the agent now must suffer the consequences introduced in N_2 by monitoring from a lower starting altitude, hence the lower red segment in Figure 4.4. This compounding of error is presumably why N_3 and N_4 perform even worse than N_2 . The modified departure controller would either delay or prematurely end the thermalling or monitoring stages to minimize the length of the departing trajectory. Such a controller would cause the trajectories to be similar to those seen in run 3 of case 2 flown at $v_{L/D}$, shown in Figure 4.6. These trajectories are near perfect and have nearly identical values for N_1 through N_4 that agree with the predicted N for $v_{L/D}$.

4.3 ASW-27B Simulations with Transitional Altitude Changes

The simulations presented in this section are based on the theory discussed in Section 3.5 and were conducted prior to implementing a new departure controller.

As discussed in Section 3.5, accounting for the transitional changes in altitude results in $v_1 \neq v_2$ due to the asymmetric effect that the cruising stage toward the thermal has on the system. v_2 remains equal to v_c , whereas v_1 must be solved for by a constrained optimization routine such as MATLAB's `fmincon`. Generally, v_1 is significantly slower than v_2 because, with slower airspeeds toward the thermal, less altitude is lost during the transition at the bottom of the monitoring target and less altitude is gained during the transition at the bottom of the thermal. Thus, a slower v_1 extends the monitoring duration and also utilizes more of the thermal.

Simulation results are listed in Table 4.4, with Table 4.3 listing the associated scenario conditions, where values within parenthesis correspond to $v_{L/D}$ simulations (copied from Table 4.1). It is observed that, for the most part, including the transitional changes has a positive impact on the cycle, as expected due to the more accurate optimal airspeeds. The inclusion provides a 4.2% average improvement to the results in Table 4.2, but the error relative to the expected N is still 4.1% on average, down from 8.8% in the previous simulations.

Despite the considerable improvement, the variance in the results remains unsatisfactory. Less varied results are desired for better predictability in flight and the necessary changes are implemented into the SB-XC simulations of the next section.

4.4 SB-XC Simulations with a Modified Departure Controller

The modified departure controller changes the glider flight paths from the paths seen in Figures 4.1a and 4.5 to the minimum distance path constrained by a minimum turn constraint [37], seen in Figure 4.1b. Thermalling departure is triggered

Table 4.3. Case descriptions for the simulation results with transitional altitude changes included in the airspeed calculation.

Scenario Description						
Case	Δh , m	d , km	T , m/s	v_{c1} , m/s	v_{c2} , m/s	N
1	350	1	4	32.27	46.35	1.28 (1.31)
2	350	2	4	31.00	39.76	1.47 (1.52)
3	350	1	1	31.00	35.08	1.81 (1.82)
4	350	2	1	31.00	33.28	2.08 (2.11)

Table 4.4. Simulation results with transitional altitude changes included in the airspeed calculation.

Number of Agents from Simulations				
Case	N_1	N_2	N_3	N_4
1	1.37 (1.38)	1.38 (1.41)	1.39 (1.44)	1.35 (1.42)
1	1.33 (1.37)	1.31 (1.39)	1.29 (1.43)	1.35 (1.43)
1	1.34 (1.37)	1.32 (1.41)	1.31 (1.46)	1.35 (1.39)
2	1.47 (1.53)	1.45 (1.51)	1.47 (1.54)	1.50 (1.52)
2	1.53 (1.53)	1.50 (1.52)	1.51 (1.55)	1.53 (1.53)
2	1.49 (1.51)	1.50 (1.51)	1.51 (1.51)	1.53 (1.52)*
3	1.92 (1.93)	1.93 (1.94)	1.96 (2.03)	1.94 (1.98)
3	1.93 (1.93)	1.92 (1.95)	1.91 (2.04)	1.92 (1.98)
3	1.96 (1.92)*	1.94 (1.96)	1.96 (1.94)*	1.95 (1.93)*
4	1.94 (2.11)	2.15 (2.10)*	2.15 (2.10)*	2.15 (2.10)*
4	2.16 (2.12)*	2.16 (2.12)*	2.16 (2.12)*	2.18 (2.11)*
4	2.15 (2.11)*	2.14 (2.13)*	2.14 (2.12)*	2.14 (2.11)*

* $v_{L/D}$ outperforms v_c

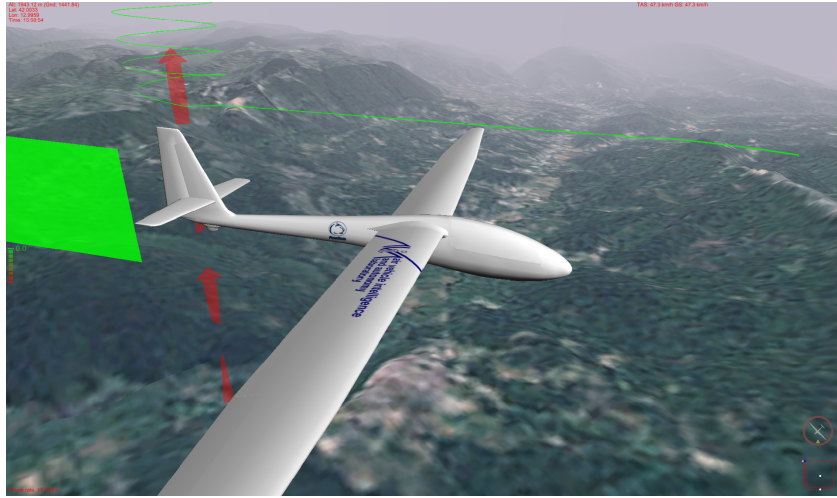


Figure 4.7. Silent Wings SB-XC screenshot.

when the glider is within a set of GPS coordinates and above the inversion layer altitude. This way the glider continues exploiting the thermal until reaching a viable departure point instead of banking away from the thermal and as in the previous simulations. Monitoring departure functions the similarly except the controller must check whether or not the glider can circle the target without violating the minimum altitude constraint when arriving at the thermal. Departure is triggered when the glider arrives within the set of viable departure coordinates and an additional circle cannot be completed.

A level of complexity is added with the variance decrease in flight paths. The working altitude is no longer equal to the inversion layer minus the minimum allowable altitude because the agents will most likely never reach the minimum altitude due to the early departure from the monitoring target. At a 500 meter monitoring radius, the ASW-27B and the SB-XC lose 68 and 128 meters, respectively, every time they complete one full circle around the monitoring target (estimated to within 3.8% by $2\pi R_s/v_s$: 65.44m and 123.25m respectively). Therefore, a considerable price is paid with the departure controller implemented in this thesis, in terms of not fully utilizing the available working altitude. A more appropriate controller may allow for the glider to depart the monitoring target by turning into the monitoring zone instead of departing tangent to it, allowing the agent to depart from any point around the monitoring target.

In any case, the working altitude was found graphically after running a few trial

simulations with the desired airspeeds by noting the thermal arrival and departure altitudes, which remained constant within each case. The starting GPS position for each simulation from here on in was kept constant with the exception of the starting altitude, which also varied only between cases. The length of the cruising stages are now equal to the actual distances traveled by the glider, 1.530km and 2.585km, instead of the separation between target and thermal minus the circling radii. Calculating Δh and d_c in this way lowers the discrepancy between simulation results and expected results but simultaneously complicates physical implementation due to the level of estimation involved. Considering the purpose of this thesis, accurately setting Δh and d_c assists in pinpointing the sources of error in the governing equations.

Initial simulation results are shown in Table 4.6 and described in Table 4.5. The important observations are that cases 3 and 4 have an error of approximately 3%, whereas case 1 has an error of approximately 6% and case 2 is completely off from the expected result. Case 2 can be explained by a poorly predicted monitoring cycle in that the glider remained in the thermal for less time than expected. Recall that simulation calculations begin at the top of the thermal. Thus, before the calculations begin, the glider enters the thermal at some altitude and exploits it until reaching a departure point from which the N calculations begin. If the arrival altitude is different the next time the glider exploits the thermal, then the thermalling durations may differ and the departure altitude may change. Because of the high thermal strength in case 2, circling the thermal an extra time around translates to a large gain in departure altitude. This has a positive effect on the system in terms of reducing N , but a negative effect on accurately predicting N . The next set of simulations change the initial thermal arrival altitude in case 2 so that Δh is equal for both halves of the simulations.

The error in case 1, on the other hand, is explained by the strong area of sink around the 4m/s thermal in the simulation. This sink translated to an approximate 20m altitude loss upon entering the thermal. This was found by noting the monitoring departure altitude, subtracting from it the altitude lost during cruise given v_c and s_c , and noting the actual arrival altitude at the thermal. The difference between the expected thermal arrival and the actual thermal arrival is the altitude loss due to the surrounding area of sink. To reduce error, the variable

Table 4.5. Case descriptions for the initial SB-XC simulations with a modified departure controller.

Scenario Description						
Case	Δh , m	d , km	T , m/s	v_c , m/s	$\delta h_{\underline{T}}$, m	N
1	350	1.530	4.00	14.36	0	1.69
2	300	2.585	4.00	13.41	0	3.32
3	325	1.530	1.05	13.71	0	2.33
4	275	2.585	1.05	13.22	0	5.30

Table 4.6. Initial SB-XC simulations with a modified departure controller.

Number of Agents from Simulations				
Case	N_1	N_2	N_3	N_4
1	1.82	1.82	1.81	1.81
1	1.83	1.82	1.81	1.81
1	1.83	1.83	1.83	1.83
2	4.40	4.41	2.29	2.30
2	4.70	4.88	2.30	2.30
2	4.43	4.44	2.30	2.30
3	2.39	2.37	2.39	2.39
3	2.39	2.40	2.40	2.40
3	2.39	2.39	2.39	2.39
4	5.44	5.41	5.44	5.44
4	5.48	5.49	5.47	5.47
4	5.48	5.48	5.27	5.27

Table 4.7. Case descriptions for the SB-XC simulation results with a modified departure controller and δh_T compensation.

Case	Scenario Description					
	Δh , m	d , km	T , m/s	v_c , m/s	$\delta h_{\underline{T}}$, m	N
1	350 (344)	1.530	4.00	14.22	20	1.75 (1.79 1.77)
2	300 (308)	2.585	4.00	13.33	20	3.88 (3.85 4.13)
3	325 (319)	1.530	1.05	13.71	0	2.33 (2.37 2.34)
4	275 (274)	2.585	1.05	13.22	0	5.30 (5.35 5.30)

Table 4.8. SB-XC simulations with a modified departure controller and δh_T compensation.

Case	Number of Agents from Simulations			
	N_1	N_2	N_3	N_4
1	1.84 (1.88)	1.84 (1.90)	1.84 (1.91)	1.84 (1.91)
1	1.84 (1.90)	1.84 (1.90)	1.84 (1.90)	1.84 (1.90)
1	1.83 (1.90)	1.83 (1.90)	1.83 (1.90)	1.83 (1.90)
2	3.93 (4.06)	3.92 (3.99)	3.92 (3.97)	3.92 (3.97)
2	3.96 (4.05)	3.93 (4.02)	3.91 (4.02)	3.90 (4.03)
2	3.93 (4.03)	3.91 (4.03)	3.91 (4.03)	3.91 (4.03)
3	2.39 (2.44)	2.37 (2.44)	2.39 (2.44)	2.39 (2.44)
3	2.39 (2.43)	2.40 (2.43)	2.40 (2.43)	2.40 (2.43)
3	2.39 (2.44)	2.39 (2.44)	2.39 (2.44)	2.39 (2.44)
4	5.44 (5.47)	5.41 (5.48)	5.44 (5.54)	5.44 (5.54)
4	5.48 (5.47)*	5.49 (5.48)	5.47 (5.51)	5.47 (5.50)
4	5.48 (5.49)	5.48 (5.47)	5.27 (5.47)	5.27 (5.47)

$\delta h_{\underline{T}}$ was included in the calculations and represents this expected altitude loss. The derivation for v_c is included in Appendix B.2 and amounts to subtracting a $\delta h_{\underline{T}}$ -term in the auxiliary variable B in Equation 3.13. The new calculations and simulations are shown in Tables 4.7 and 4.8.

The average error improved to 2.8% for all of the cases flown at v_c . Average error in cases flown with $v_{L/D}$ (values within parenthesis) is slightly higher at 4.0% due to the actual $\delta h_{\underline{T}}$ being a couple of meters larger than the $\delta h_{\underline{T}}$ values in Table 4.7; a glider remains in the region of sink for a longer period of time when flying at a slower airspeed. A more sophisticated controller would hold a higher speed through the region of sink, with the speed adjustment discussed in Section 2.4.

The reader must note that the decrease in error is due to a better estimate of N and not better performance from v_c . In fact, the updated v_c (slightly slower) performed either equally or worse than the v_c in Table 4.6. This observation points to an unfavorable quadratic fit of the sink polar, seen in Fig. 4.2b. A more favorable polar fit would be shaped so that slightly faster speeds are given in the calculation of v_c .

One final note is made on the sensitivity of N with respect to Δh . If Δh were 25m smaller in case 4, N would jump to 7.1 ($v_c = 13.15\text{m/s}$) from 5.3. And if Δh dropped to 291m from 350m in case 1, N would equal 2 ($v_c = 13.95\text{m/s}$) instead of 1.75; $N = 3$ ($v_c = 13.47\text{m/s}$) if Δh drops to 209m. The conclusion is that N is highly sensitive to Δh in weaker cycles of $N > 4$.

4.5 ASW-27B Simulations with a Modified Departure Controller

Updated ASW-27B simulations with the new departure controller are shown in Tables 4.9 and 4.10. The average error for the v_c cases is 1.2% and 1.8% for the $v_{L/D}$ (values within parenthesis), again marginally higher presumably due to $\delta h_{\underline{T}}$ being slightly larger when cruising at slower airspeeds through the area of sink surrounding a thermal. The lower average error relative to the SB-XC simulation results in Table 4.8 is assumed to be the result of a more favorable sink polar fit;

Table 4.9. Case descriptions for the ASW-27B simulation results with a modified departure controller and δh_T compensation.

Scenario Description						
Case	Δh , m	d , km	T , m/s	v_c , m/s	$\delta h_{\underline{T}}$, m	N
1	358 (322)	1.530	4.00	42.20	10	1.36 (1.44 1.41)
2	300 (365)	2.585	4.00	35.21	10	1.76 (1.65 1.83)
3	315 (323)	1.530	1.05	34.00	0	1.92 (1.93 1.95)
4	280 (297)	2.585	1.05	31.67	0	2.48 (2.43 2.52)

Table 4.10. ASW-27B simulations with a modified departure controller and δh_T compensation.

Number of Agents from Simulations				
Case	N_1	N_2	N_3	N_4
1	1.40 (1.45)	1.38 (1.46)	1.38 (1.45)	1.38 (1.45)
1	1.38 (1.45)	1.38 (1.45)	1.38 (1.45)	1.38 (1.45)
1	1.38 (1.45)	1.38 (1.45)	1.38 (1.36) [†]	1.38 (1.35) [†]
2	1.77 (1.64) [†]	1.77 (1.64) [†]	1.77 (1.64) [†]	1.77 (1.64) [†]
2	1.77 (1.64) [†]	1.77 (1.64) [†]	1.77 (1.64) [†]	1.77 (1.64) [†]
2	1.77 (1.64) [†]	1.77 (1.64) [†]	1.76 (1.64) [†]	1.76 (1.64) [†]
3	1.93 (1.97)	1.93 (1.97)	1.93 (1.97)	1.93 (1.97)
3	1.93 (1.97)	1.93 (1.97)	1.93 (1.97)	1.93 (1.97)
3	1.93 (1.97)	1.93 (1.97)	1.93 (1.97)	1.93 (1.97)
4	2.53 (2.61)	2.53 (2.61)	2.54 (2.60)	2.54 (2.58)
4	2.53 (2.60)*	2.53 (2.60)*	2.54 (2.59)	2.54 (2.58)
4	2.53 (2.60)	2.53 (2.60)*	2.54 (2.59)	2.54 (2.58)

[†] $v_{L/D}$ outperforms v_c due to an additional $\Delta h > 35m$

a slightly different fit may have produced larger errors.

The $v_{L/D}$ results for the second half of run 3 of case 1 reflects the same issue discussed in Section 4.4, namely that of a difference in thermal arrival altitudes amounting to a difference in exploitation duration. The second half of this run experienced $\Delta h = 393\text{m}$, for which N is expected to equal 1.38.

A final note on the sensitivity of N with respect to Δh . If Δh were 60m smaller in case 4, N would increase from 2.48 to 3 ($v_c = 30.60\text{m/s}$). And if Δh dropped to 137m from 358m in case 1, N would equal 2 ($v_c = 33.50\text{m/s}$) instead of 1.36; $N = 3$ ($v_c = 30.60\text{m/s}$) if Δh drops to 100m. These observations support the conclusion made in Section 4.4: N is highly sensitive to Δh only in weaker cycles (approximately $N > 3$ for the ASW).

4.6 Summary

This chapter presented Silent Wings flight simulation results for single-agent single-thermal persistent monitoring with the ASW-27B, representative of medium to large sized gliders, and the SB-XC, representative of small sized gliders. The aim of these simulations was to assess the accuracy of the equations given in Chapter 3 and compare performance to the best L/D airspeed by having the glider cruise between monitoring and thermalling jobs given various fixed environmental settings.

Initial flight results with the ASW-27B shed light on the importance of a sophisticated departure controller in minimizing the cruise distances and lowering the variance of the required number of agents to ensure uninterrupted monitoring of a target. The initial simulations triggered monitoring departure upon hitting the minimum altitude required for reaching the fixed thermal above the minimum allowable altitude constraint for the system; thermalling departure was triggered upon reaching the thermal inversion layer, where this “inversion layer” was 70m below the actual inversion layer and provided the glider with approximately 20m of altitude for realizing thermal dissipation. The bearing of the glider relative to the subsequent target location was neglected, often resulting in a suboptimal trajectory that nearly doubled cruise duration and unnecessarily separated the glider from the previous target by banking away instead of into the target. The average

error for these simulations dropped from 8.8% to 4.1% when transitional altitude changes were included in calculating the optimal airspeeds.

The modified departure controller was first tested on the SB-XC. Cruise durations were minimized and the variance in the required number of agents decreased significantly but an added degree of difficulty was introduced in cycle consistency: it was now possible for the glider to circle the thermal or monitoring target an extra time around because of the limited number of viable departure points in the controller. The glider departed within a very small range of GPS coordinates that aligned the glider with the arrival GPS coordinates of the subsequent job. It was seen that the first completed cycle could require two fewer agents than the next completed cycle. Thus, if such a departure controller were implemented, unnecessary attention would be required in predicting the number of agents to assign to monitoring cycles. Additional departure points must be made available by allowing agents to bank into their current targets instead of departing strictly tangential to them. This provides fuller utilization of the working altitude at the cost of slightly increasing variance from cycle to cycle. Additional improvements exist in increasing the airspeed when the glider flies through regions of sink around a thermal and exiting the dissipating thermal at the optimal altitude (Appendix B.1).

The shortcomings in the controller did not compromise the goal of assessing accuracy and predictability. The initial SB-XC simulations also showed that the simulations flown with $T = 4\text{m/s}$ were about half as accurate than those with $T = 1\text{m/s}$. This was concluded to be caused by the stronger area of sink around the 4m/s thermal and thus an additional term, δh_T (Appendix B.2), was added to compensate for this loss. The consequent airspeeds differed slightly but the estimated N better matched simulation results and the error dropped to 2.8% for the SB-XC and 1.2% for the ASW-27B. It was noted that sensitivity to the predicted working altitude was high for $N > 4$ for the SB-XC and $N > 3$ for the ASW-27B.

Chapter 5

Conclusion

5.1 Summary of Contributions

Mission endurance is a primary challenge for flocks of cooperating small unmanned aerial vehicles. The exploitation of atmospheric thermal columns is one way of extending mission endurance and involves each agent alternating between energy expenditure at a mission target (weather monitoring, forest fire detection, load transport, etc.) and energy gain at a thermal.

Given a map of thermal strengths and locations, a flock can coordinate itself into a cycle that ensures a mission target remain occupied at all times by at least one agent. As the agent nears a predefined minimum allowable altitude, it departs the target to cruise to the best available thermal while the next agent in the cycle arrives upon its departure. In this way, mission endurance persists so long as a populated thermal map exists and a sufficient number of agents is available for the set of environmental conditions at hand.

The challenges in implementing such a system are numerous and include path planning, thermal detection, thermal centering, and optimal job allocation. This thesis focused on the challenge of optimizing monitoring cycles with respect to the number of agents required for continuous monitoring of a ground target. The agents considered in this thesis were soaring gliders which contained no onboard sources of propulsion energy. A set of assumptions simplified the environmental conditions and led to a fully defined and constrained system from which a simple equation for the number of required agents was formulated. Gradually, this equa-

tion was manipulated and appended to handle a variety of scenarios and this led to the discovery of optimal cruising airspeeds, optimal thermal departure altitudes, an increased understanding of multiple-thermal exploitation, and the aggregate thermal concept.

The scenarios considered involved either a single agent or multiple agents exploiting either a single thermal or multiple thermals. Equations for the number of agents were differentiated with respect to the cruising airspeeds and resulted in closed-form equations for the optimal airspeeds toward the monitoring target, toward the thermal, and during inter-thermal cruise. Inter-thermal cruises were optimized by the forward and reversed MacCready speeds, where the reversed MacCready speed was defined as the MacCready speed calculated based on the initial thermal instead of the final thermal. The optimal cruising airspeed toward a thermal was found to equal the optimal cruising airspeed toward the monitoring target and both were functions of thermalling duration, polar fit coefficients, and separation between thermal and target. Both airspeeds were equivalent unless transitional changes in altitude were included in the calculation for the number of agents. In that case, the form for the airspeed toward the target remained unchanged and the airspeed toward the thermal became a fourth order polynomial for which a numerical solution was required.

A short proof showed that the number of agents required for a persistent monitoring cycle is minimized when the exploitable altitude range in a thermal is maximized. A supplementary proof showed that the optimal thermal departure altitude has a thermal climb rate equal to the aggregate thermal strength of the cycle, regardless of how the thermal decay is modeled. This implied that, for monitoring cycles with multiple agents seeking to maximize a free resource, the minimum optimal thermal departure altitude has a thermal climb rate equal to the monitoring sink rate of a glider.

The aggregate thermal concept was discovered via the maximization of a free resource in multiple-agent scenarios. Optimal airspeeds were of the same form as MacCready airspeeds with the thermal climb rate replaced by a rate equal to the altitude available at the monitoring target divided by the time required to gain that altitude given the thermal climb rate and distance away from the target. The aggregate thermal can be thought of as a general way of discounting energy sources

by their accessibility and proximity relative to a target of interest. It was found that minimizing the number of agents in a cycle was equivalent to maximizing the aggregate thermal strength of the cycle and that it was trivial to convert between the two quantities.

Multiple-thermal exploitation was briefly covered by polar map plots of regions where multiple-thermal exploitation was preferred over single-thermal exploitation. Multiple-thermal exploitation was potentially beneficial if the two thermals were positioned roughly within 37.5° to both sides of the monitoring target. Analytical results showed that the number of agents can be decreased significantly in cycles requiring a high number of agents ($N \geq 4$). However, the risk of performing such maneuvers under uncertain atmospheric conditions remains to be analyzed.

Silent Wings flight simulation results were run with a single agent and a single fixed thermal in an environment absent of wind gusts. The Schleicher ASW-27B and the RnR Products SB-XC were chosen to represent large and small scale UAVs, respectively, and repeatedly cruised between a thermal at fixed GPS coordinates and an arbitrary fixed point away from the thermal which represented the monitoring target. The progression of simulation results showed that a sophisticated monitoring departure controller was required for maximal utilization of the working altitude and minimal variance in error, where the error refers to the difference between analytic results and simulation results. Additionally, it was observed that cycles involved with strong thermal climb rates had approximately double the error relative to cycles with weaker thermals. This was concluded to be caused by the area of sink around a thermal and an additional term was included in the calculation of the number of agents to account for this loss.

Final simulation results contained average errors of 2.8% for the SB-XC and 1.2% for the ASW-27B, down from average initial errors of 8.8% for the ASW-27B. The error was highly sensitive to the working altitude at the monitoring target for cycles with $N > 3$. Simulation results supported analytical results in that optimal airspeeds provided a meager improvement over the best L/D airspeed and added a considerable amount of complexity in terms of the amount of estimation required in calculations. Nevertheless, these improvements are capable of salvaging an entire agent from a cycle when cruising at the best L/D airspeed requires a slightly non-integer ($N \geq \lceil N \rceil$) number of agents.

5.2 Recommendations for Future Work

5.2.1 Increased Complexity in Simulations

Additional areas of complexity remain to be added to flight simulations including wind gusts, non-stationary thermals, and thermals with limited lifetimes. Knowledge of the effect that each of these has on the estimate for the required number of agents would be helpful in assessing the risk of misallocating a sufficient number of agents to a monitoring cycle. A behavior controller that handles unexpected dissipating thermals and unexpectedly strong thermals encountered during cruise is absolutely crucial in minimizing the resources required for a cycle.

Multiple-agent simulations are needed for understanding the added complexity of properly coordinating the agents. Once a system of multiple-agents is controlled properly, the monitoring group of agents must be coupled with the exploring group of agents so that the entire system remains self-sufficient. The hiring of additional agents into either one of the job groups should create an interesting dynamic and a complex behavioral control problem.

5.2.2 Multiple-Thermal Exploitation

A deeper analysis of multiple-thermal exploitation is desired. Possible examinations include the completion rate of full multiple-thermal exploitation cycles and the relationship between the thermal separations and the angular range for which multiple-thermal exploitation is beneficial.

5.2.3 Novel Thermalling Controller

Departure from a thermal involves transitioning to a cruising airspeed from a slower thermalling airspeed, resulting in a loss of altitude. The free resources in a cycle may be increased if this loss of altitude is forced to occur before departure, i.e., if a glider accelerates to the cruising airspeed before departing the thermal. The benefit and difficulty of this remains to be studied. The equations for the number of agents for such a controller are included in Appendix B.3.

5.2.4 Departure and Arrival Controllers

Further treatment of departure and arrival controllers is another area of future work. The degree of effects from cruising faster through the areas of sink around strong thermals and departing lower or higher than the optimal departure altitude should be studied.

Appendix

A

Vehicle Properties

Table A.1. Properties of the Schleicher ASW-27B glider [2].

Parameter	Value
Span including winglets	15m (49.22ft)
Wing area	9m ² (96.88ft ²)
Aspect ratio	25
Fuselage length	6.55m (21.49ft)
Cockpit height	0.80m (2.62ft)
Cockpit width	0.64m (2.10ft)
Height at tail unit	1.30m (4.27ft)
Wing airfoils	DU 89-134/14 and DU 92-131/14MOD
Empty mass	235kg (518lb)
Flight mass max.	500kg (1102lb)
Mass of one wing	58kg (128lb)
Wing loading max.	55.56kg/m ² (11.38lb/ft ²)
Wing loading min.	32.80kg/m ² (6.7lb/ft ²)
Water ballast max.	165L (43.59US Gal)
Useful load max.	130kg (287lb)
Useful load in pilot seat	115kg (254lb)
For m=320kg:	
Max. speed	285km/h (154kts)
Max. maneuver speed	215km/h (116kts)
Min. speed	70km/h (37.8kts)
Min. sink	0.52m/s (102ft/min)
Best L/D	28 at 100km/h (54kts)

Table A.2. Properties of the RnR Products SB-XC glider [3].

Parameter	Value
Span	170.0in
Flying weight	158oz
Wing area	1656in ²
Aspect ratio	19.8
Stab span	36.5in
Stab area	135in ²
Wing loading	13.6oz/ft ²
Wing Airfoil	SD-2048

Supplementary Material

B.1 Exploitation During Dissipation

This section derives the optimal departure altitude for a glider exploiting a dissipating thermal, referred to in Section 3.6. Section 3.1.1 provided a proof showing that, given the assumptions in Section 2.2, a monitoring cycle is optimized when the working altitude Δh is maximized. In reality, however, thermal dissipation exists and the question arises of when it is optimal to leave a thermal whose strength is decreasing.

Here, the answer is found by appending Equation 3.17 to include the time spent in the dissipating lift and the altitude reached by exploiting this lift. The appending may be done by assuming a region of constant lift that endures for $\Delta h/T$ seconds, followed by the region of dissipation for which the climb rate is a function of altitude. This climb rate function is approximated and it is shown that the optimal thermal departure altitude, independent of the approximated climb rate function, has a climb rate equal to the aggregate thermal strength of the cycle. It follows that the minimum thermal departure altitude for gliders in multiple-agent scenarios is the altitude where the climb rate equals the monitoring sink rate, since the maximum aggregate thermal strength equals $s_s/(\lceil N \rceil - 1) = s_s/(2 - 1) = s_s$.

Start with a linear decay model for a thermal with a climb rate of 4m/s that decays to 0m/s after 75m beyond the altitude of constant lift :

$$T_d(h) = 4 - \frac{4}{75}h \quad (\text{B.1})$$

where T_d is the climb rate in the dissipating thermal and h is the altitude above the region of constant lift. The total time spent exploiting a thermal is then

$$t_t = \frac{\Delta h}{T} + \int_0^{h_d} T_d^{-1} dh \quad (\text{B.2})$$

where Δh is the working altitude and T is the constant thermal climb rate of a glider. The optimal departure altitude for single-agent scenarios is found by differentiating N with respect to h_d , whereas the optimal departure altitude for multiple-agent scenarios is found by differentiating a free resource with respect to h_d .

The derivation below works with t_{free} because the math is less tedious and the answer is in the form of the aggregate thermal. The aggregate thermal result can then be applied to single-agent scenarios by omitting the ceiling operator on N . The validity of this was covered by Equation 3.25, where the aggregate thermal strength without the ceiling operator on N determines the optimal airspeed in single-agent scenarios. It is expected that differentiating N with respect to h_d will produce a less elegant result, but that this result is necessary if h_d is to be found non-iteratively.

Appending N to include the exploitation of a dissipating thermal region above a certain altitude:

$$N = \frac{\frac{d_c}{v_c} + \frac{\Delta h}{T} + \int_0^{h_d} T_d^{-1} dh + t_{\text{free}}}{s_s^{-1} \left(\Delta h + h_d - s_c \frac{d_c}{v_c} \right)} + 1 \quad (\text{B.3})$$

Solving for t_{free} :

$$t_{\text{free}} = (\lceil N \rceil - 1) \left(\Delta h + h_d - s_c \frac{d_c}{v_c} \right) \frac{1}{s_s} - \left[\frac{d_c}{v_c} + \frac{\Delta h}{T} + \int_0^{h_d} \left(4 - \frac{4}{75} h \right)^{-1} dh \right] \quad (\text{B.4})$$

Differentiating with respect to h_d :

$$\frac{\partial t_{\text{free}}}{\partial h_d} = (\lceil N \rceil - 1) \frac{1}{s_s} - \left(4 - \frac{4}{75} h_d \right)^{-1} \quad (\text{B.5})$$

Setting to zero and solving for h_d gives

$$h_d = -\frac{75}{4}(\lceil N \rceil - 1)^{-1}s_s + 75 \quad (\text{B.6})$$

Evaluating Equation B.6 for $s_s = 0.5\text{m/s}$ and $\lceil N \rceil = 2$ gives $h_d = 65.625\text{m}$. Plugging this back into Equation B.1 gives $T_d(h) = 0.5\text{m/s}$.

In general, given a linear decay model, the optimal departure altitude is

$$h_d = -\frac{1}{m}(\lceil N \rceil - 1)^{-1}s_s + a \quad (\text{B.7})$$

where m is the slope of the linear decay, a is the x -intercept, and $(N - 1)^{-1}s_s$ is the aggregate thermal. The corresponding linear climb rate decay function is

$$T_d(h) = m(a - h) \quad (\text{B.8})$$

Plugging the former equation into the latter produces

$$T_d(h) = m \left(a - \frac{1}{m}(\lceil N \rceil - 1)^{-1}s_s + a \right) = (\lceil N \rceil - 1)^{-1}s_s \quad (\text{B.9})$$

which proves that the optimal departure altitude has a climb rate equal to the aggregate thermal strength of the cycle regardless of m and a , i.e., regardless of the thermal model.

If an exponential decay model is used, then:

$$T_d(h) = N_0 e^{-\lambda h} \quad (\text{B.10})$$

$$t_{\text{free}} = (\lceil N \rceil - 1) \left(\Delta h + h_d - s_c \frac{d_c}{v_c} \right) \frac{1}{s_s} - \left[\frac{d_c}{v_c} + \frac{\Delta h}{T} + \int_0^{h_d} (N_0 e^{-\lambda h})^{-1} dh \right] \quad (\text{B.11})$$

$$\frac{\partial t_{\text{free}}}{\partial h_d} = (\lceil N \rceil - 1) \frac{1}{s_s} - (N_0 e^{-\lambda h_d})^{-1} \quad (\text{B.12})$$

$$h_d = -\frac{1}{\lambda} \ln \left(\frac{1}{N_0} (\lceil N \rceil - 1)^{-1} s_s \right) \quad (\text{B.13})$$

$$T_d(h) = N_0 e^{-\lambda \left[-\frac{1}{\lambda} \ln \left(\frac{1}{N_0} (\lceil N \rceil - 1)^{-1} s_s \right) \right]} = (\lceil N \rceil - 1)^{-1} s_s \quad (\text{B.14})$$

The same result is reached here and it is deduced that the optimal departure

altitude in all one-to-one thermal decay functions has a climb rate equal to the aggregate thermal strength for that cycle. This is the more general form than that seen in MacCready theory for cross-country soaring, which states that a thermal should be departed when the climb rate drops below the next MacCready setting.

B.2 Accounting for the Area of Sink Around a Thermal

Given below is the derivation for including an expected altitude loss due to the surrounding area of sink around a thermal, $\delta h_{\underline{T}}$, in the optimal cruising airspeed calculation, v_c . $\delta t_{\underline{T}}$ is included for completeness and represents the duration of $\delta h_{\underline{T}}$. Note that this quantity was set to zero in the simulations presented in Chapter 4 because it is contained within the quantity $s_c d_c / v_c$. The derivation is given in the context of multiple-thermal exploitation, for which $\delta h_{\underline{T}}$ occurs when T_1 is entered while cruising away from M. The derivation steps are identical to those in Chapter 3 and result in subtracting a $\delta h_{\underline{T}}$ -term in the auxiliary variable B :

$$\begin{aligned} \frac{\partial N}{\partial v_c} &= \frac{\partial}{\partial v_c} \left[\frac{\frac{d_c}{v_c} + \frac{s_2 d_2}{T_1 v_2} + \frac{d_2}{v_2} + \frac{\Delta h}{T_2} + \frac{d_3}{v_3} + \frac{s_3 d_3}{T_1 v_3} + \delta t_{\underline{T}}}{s_s^{-1} (\Delta h - s_c \frac{d_c}{v_c} - \delta h_{\underline{T}})} + 1 \right] = \\ &\quad \frac{\frac{\partial}{\partial v_c} \left(\frac{d_c}{v_c} + \frac{s_2 d_2}{T_1 v_2} + \frac{\Delta h}{T_2} + \frac{\Delta h}{T_2} + \frac{d_3}{v_3} + \frac{s_3 d_3}{T_1 v_3} + \delta t_{\underline{T}} \right)}{s_s^{-1} (\Delta h - s_c \frac{d_c}{v_c} - \delta h_{\underline{T}})} + \\ &\quad \left(\frac{d_c}{v_c} + \frac{s_2 d_2}{T_1 v_2} + \frac{d_2}{v_2} + \frac{\Delta h}{T_2} + \frac{d_3}{v_3} + \frac{s_3 d_3}{T_1 v_3} + \delta t_{\underline{T}} \right) \frac{\partial}{\partial v_c} \left[s_s^{+1} \left(\Delta h - s_c \frac{d_c}{v_c} - \delta h_{\underline{T}} \right)^{-1} \right] = \\ &\quad \frac{-d_c/v_c^2}{s_s^{-1} (\Delta h - s_c \frac{d_c}{v_c} - \delta h_{\underline{T}})} + \frac{\left(\frac{d_c}{v_c} + \frac{s_2 d_2}{T_1 v_2} + \frac{d_2}{v_2} + \frac{\Delta h}{T_2} + \frac{d_3}{v_3} + \frac{s_3 d_3}{T_1 v_3} + \delta t_{\underline{T}} \right) (a - \frac{c}{v_c^2}) (d_c)}{s_s^{-1} (\Delta h - s_c \frac{d_c}{v_c} - \delta h_{\underline{T}})^2} \end{aligned}$$

Simplifying and setting to zero:

$$\frac{\partial N}{\partial v_c} = 1 - \frac{\left(\frac{d_c}{v_c} + \frac{s_2 d_2}{T_1 v_2} + \frac{d_2}{v_2} + \frac{\Delta h}{T_2} + \frac{d_3}{v_3} + \frac{s_3 d_3}{T_1 v_3} + \delta t_{\underline{T}} \right) (a v_c^2 - c)}{\Delta h - s_c \frac{d_c}{v_c} - \delta h_{\underline{T}}} =$$

$$\begin{aligned}
\Delta h - d_c \left(av_c + b + \frac{c}{v_c} \right) - \delta h_{\underline{T}} - av_c d_c + \frac{cd_c}{v_c} - (t_{\text{away}} - t_c)av_c^2 + (t_{\text{away}} - t_c)c = \\
[\Delta h - bd_c + (t_{\text{away}} - t_c)c - \delta h_{\underline{T}}] - (2ad_c)v_c - (t_{\text{away}} - t_c)av_c^2 = \\
\frac{1}{ad_c} [\Delta h - bd_c + (t_{\text{away}} - t_c)c - \delta h_{\underline{T}}] + 2v_c + \frac{1}{d_c}(t_{\text{away}} - t_c)v_c^2 = \\
Av_c^2 + 2v_c - B = 0
\end{aligned}$$

and applying the quadratic formula:

$$v_c = \frac{-1 + \sqrt{1 + AB}}{A} \quad (\text{B.15})$$

where

$$t_{\text{away}} - t_c = \frac{s_2 d_2}{T_1 v_2} + \frac{d_2}{v_2} + \frac{\Delta h}{T_2} + \frac{d_3}{v_3} + \frac{s_3 d_3}{T_1 v_3} + \delta t_{\underline{T}} \quad (\text{B.16})$$

$$A = \frac{1}{d_c}(t_{\text{away}} - t_c) \quad (\text{B.17})$$

$$B = \frac{1}{ad_c} [\Delta h - bd_c + (t_{\text{away}} - t_c)c - \delta h_{\underline{T}}] \quad (\text{B.18})$$

B.3 Novel Thermalling Controller Equations

Section 3.5 presented equations that include the transitional altitude changes arising from job transitions, where changes in airspeed result in changes in altitude. This section presents similar equations but for the novel thermalling controller mentioned in Chapter 5.

If $v_1 \geq v_T$ and $v_2 \leq v_T$:

$$N = 1 + \frac{\overbrace{\frac{d_1}{v_1} + \frac{d_2}{v_2} + \left(H - \frac{v_1^2 - v_T^2}{2g} \right) T^{-1}}^{\delta h_{\underline{T}} \geq 0}}{\left[H - \frac{d_1}{v_1} s_1 - \frac{d_2}{v_2} s_2 + \underbrace{(y_2^* - y_s^*)}_{\delta h_{\underline{S}}} + \underbrace{(y_s^* - v_1^2)}_{\delta h_{\underline{S}}} + \underbrace{(v_T^2 - y_2^*)}_{\delta h_{\overline{T}}} / 2g \right] s_s^{-1}} \quad (\text{B.19})$$

where $\delta h_{\underline{T}}$ affects (decreases) the thermal exploitation duration but not the departure altitude at the monitoring target; and where $\delta h_{\overline{T}}$ affects (raises) the arrival altitude at the monitoring target but not the thermal exploitation duration.

If $v_1 \geq v_T$ and $v_2 > v_T$:

$$N = 1 + \frac{\frac{d_1}{v_1} + \frac{d_2}{v_2} + \left(H - \frac{v_1^2 - v_{\bar{T}}^2}{2g} \right) T^{-1} - \frac{v_{\bar{T}}^2 - v_2^2}{2g} (T - s_{\bar{T}})^{-1}}{\left[H - \frac{d_1}{v_1} s_1 - \frac{d_2}{v_2} s_2 + \underbrace{(v_2^2 - y_s^2)}_{\delta h_{\bar{S}}} + \underbrace{y_s^2 - v_1^2}_{\delta h_{\underline{S}}} + \underbrace{v_{\bar{T}}^2 - v_2^2}_{\delta h_{\bar{T}} = 0} + \underbrace{v_1^2 - v_{\bar{T}}^2}_{\delta h_{\underline{T}} = 0} \right] s_s^{-1}} \quad (\text{B.20})$$

where $\delta h_{\underline{T}}$ affects (decreases) the thermal exploitation duration but not the departure altitude at the monitoring target; where $\delta h_{\bar{T}}$ affects (increases) the thermal exploitation duration but not the arrival altitude at the monitoring target; and where $v_{\bar{T}}$ and $s_{\bar{T}}$ are the final increased thermalling airspeed and sink rate, respectively.

If $v_1 < v_T$ and $v_2 \leq v_T$:

$$N = 1 + \frac{\frac{d_1}{v_1} + \frac{d_2}{v_2} + H/T}{\left[H - \frac{d_1}{v_1} s_1 - \frac{d_2}{v_2} s_2 + \underbrace{(y_2^2 - y_s^2)}_{\delta h_{\bar{S}}} + \underbrace{y_s^2 - y_1^2}_{\delta h_{\underline{S}}} + \underbrace{y_{\bar{T}}^2 - y_2^2}_{\delta h_{\bar{T}} \geq 0} + \underbrace{y_1^2 - y_{\bar{T}}^2}_{\delta h_{\underline{T}} \leq 0} \right] s_s^{-1}} \quad (\text{B.21})$$

where the thermal exploitation duration is unaffected and $\delta h_{\underline{T}}$ and $\delta h_{\bar{T}}$ both decrease the monitoring duration.

If $v_1 < v_T$ and $v_2 > v_T$:

$$N = 1 + \frac{\frac{d_1}{v_1} + \frac{d_2}{v_2} + H/T - \frac{v_{\bar{T}}^2 - v_2^2}{2g} (T - s_{\bar{T}})^{-1}}{\left[H - \frac{d_1}{v_1} s_1 - \frac{d_2}{v_2} s_2 + \underbrace{(v_2^2 - y_s^2)}_{\delta h_{\bar{S}}} + \underbrace{y_s^2 - y_1^2}_{\delta h_{\underline{S}}} + \underbrace{v_{\bar{T}}^2 - v_2^2}_{\delta h_{\bar{T}} = 0} + \underbrace{v_1^2 - v_{\bar{T}}^2}_{\delta h_{\underline{T}} \leq 0} \right] s_s^{-1}} \quad (\text{B.22})$$

where $\delta h_{\bar{T}}$ affects (increases) the thermal exploitation duration but not the arrival altitude at the monitoring target; where $\delta h_{\underline{T}}$ raises the departure altitude at the monitoring target; and where $v_{\bar{T}}$ and $s_{\bar{T}}$ are the final increased thermalling airspeed and sink rate, respectively.

B.4 Effect of Transitional Altitude Changes

The figures on the next few pages show the effect of including transitional altitude changes in the calculation of the optimal airspeed and number of agents for a cycle, covered in Section 3.5. Solid blue represents values derived from ignoring the transitional altitude changes, solid green represents values derived from including transitional altitude changes, and dashed red represents values derived from the novel thermalling controller discussed in Section B.3 and briefly in Chapter 5. The graphs in the left column of both figures represent cruising airspeeds toward thermals, whereas the right column in both figures represents cruising airspeeds toward the monitoring target.

As expected, transitional altitude changes are much less significant for the SB-XC due to the lower operating airspeeds, seen when comparing Figure B.1 to Figure B.2. As discussed in Section 3.5, including transitional changes modifies the equation for the cruising airspeed toward the thermal and not the cruising airspeed toward the monitoring target, which is seen in the second column in both figures. The estimated and transitionally-derived airspeeds toward the thermals differ strongly for the ASW-27B and slightly for the SB-XC but both exhibit the same pattern: increasing airspeed with increasing thermal strengths, where the estimated airspeeds act as a strict upper bound for the transitionally-derived airspeeds and the thermalling airspeed acting as the loose lower bound until the thermalling airspeed merges with the estimated airspeeds. Note that the red curves represent the airspeeds derived from the novel thermalling controller equations; the thermalling airspeed is the airspeed held while exploiting a thermal and was set to 27.78m/s for the ASW-27B and 14m/s for the SB-XC in each respective plot; monitoring airspeeds were 27.78m/s and 12m/s respectively; the working altitude was 350m. Including the thermalling controller has a significant impact on the airspeeds toward the monitoring target and closely matches the transitionally-derived airspeed toward the thermal.

Figures B.3 and B.4 show that none of the airspeeds present a significant advantage over the best L/D airspeed, especially for the SB-XC, which agrees with the simulation results in Chapter 4.

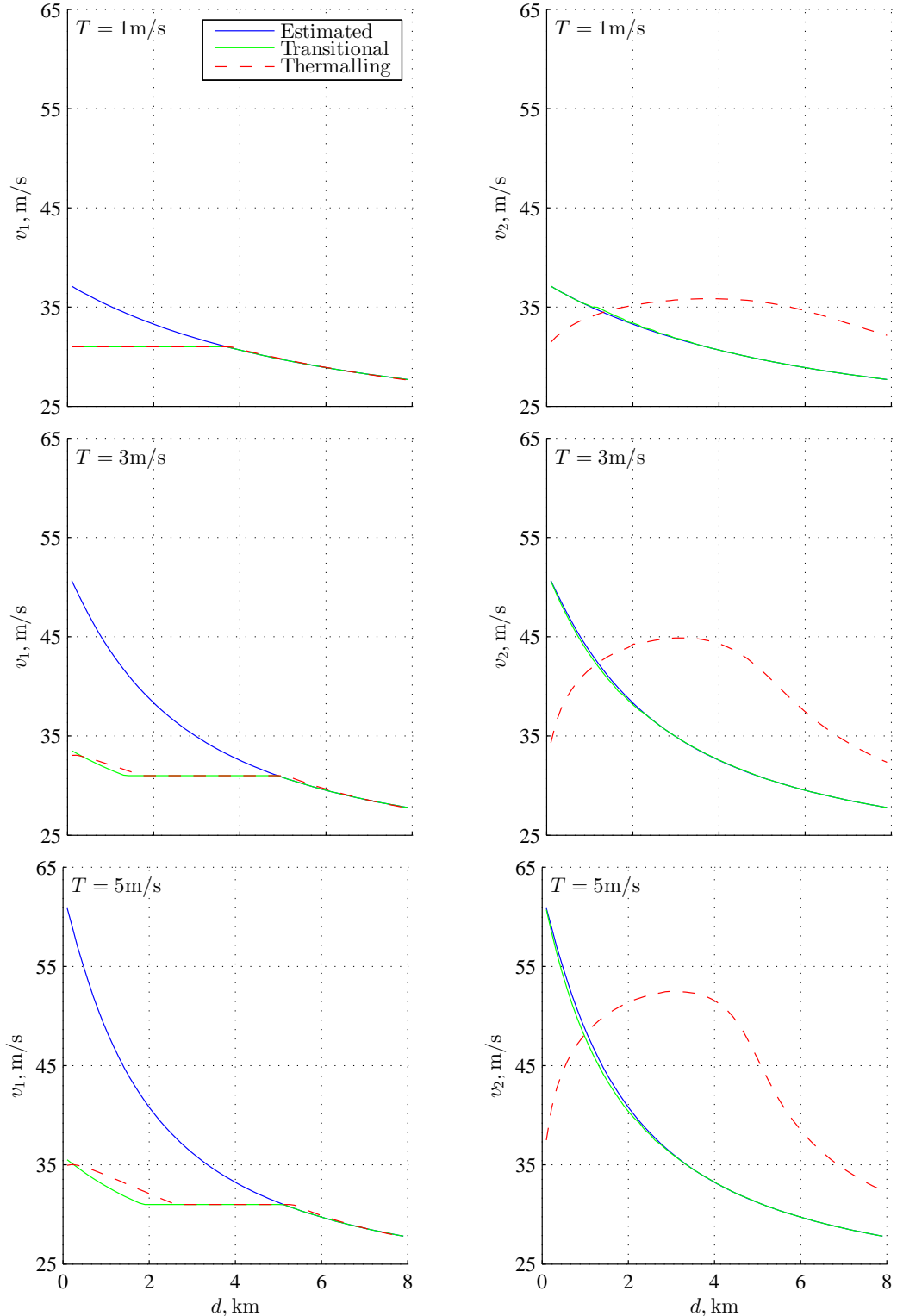


Figure B.1. A comparison of the estimated, transitionally-derived, and novel thermalling controller-derived cruising airspeeds for the ASW-27B.

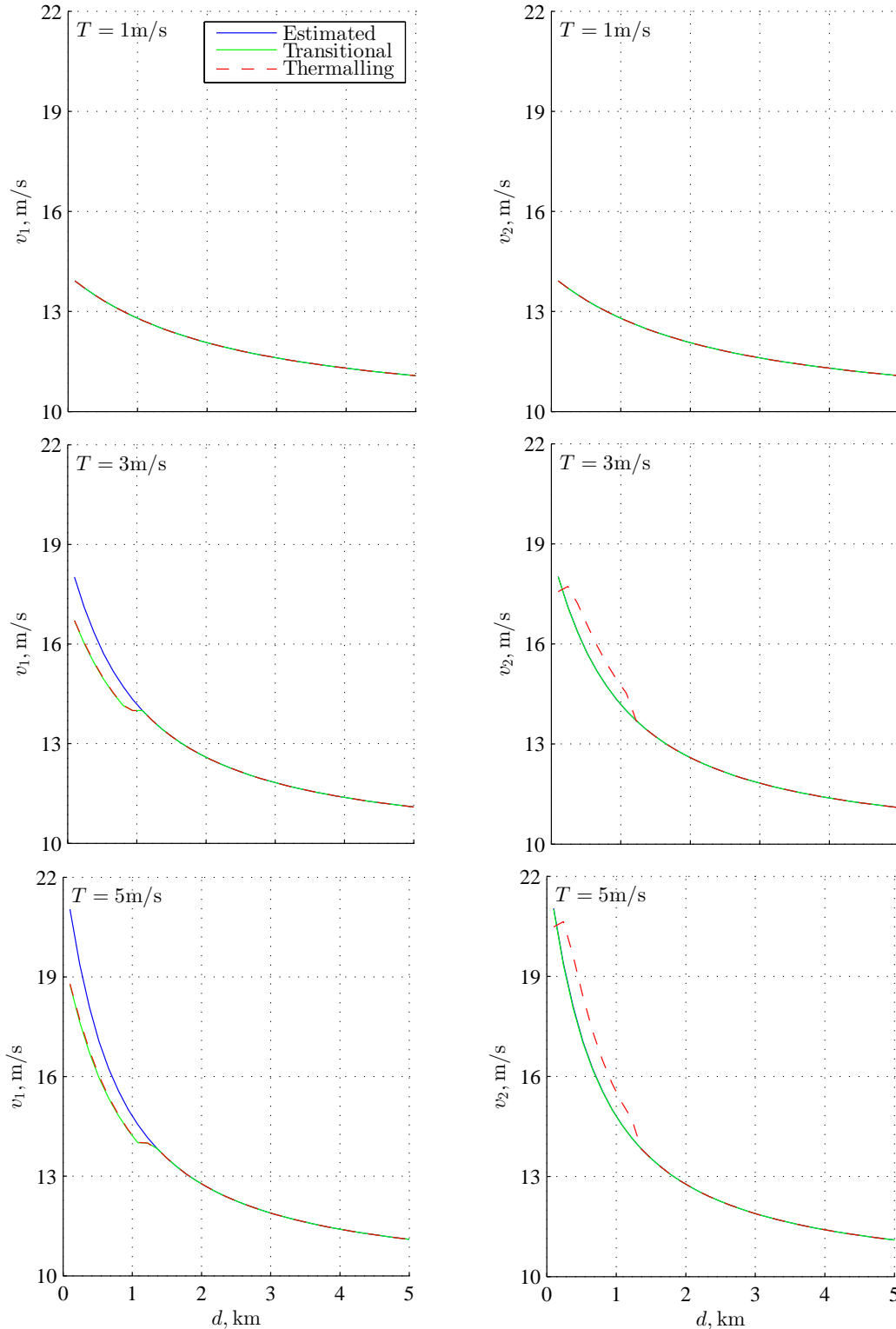


Figure B.2. A comparison of the estimated, transitionally-derived, and novel thermalling controller-derived cruising airspeeds for the SB-XC.

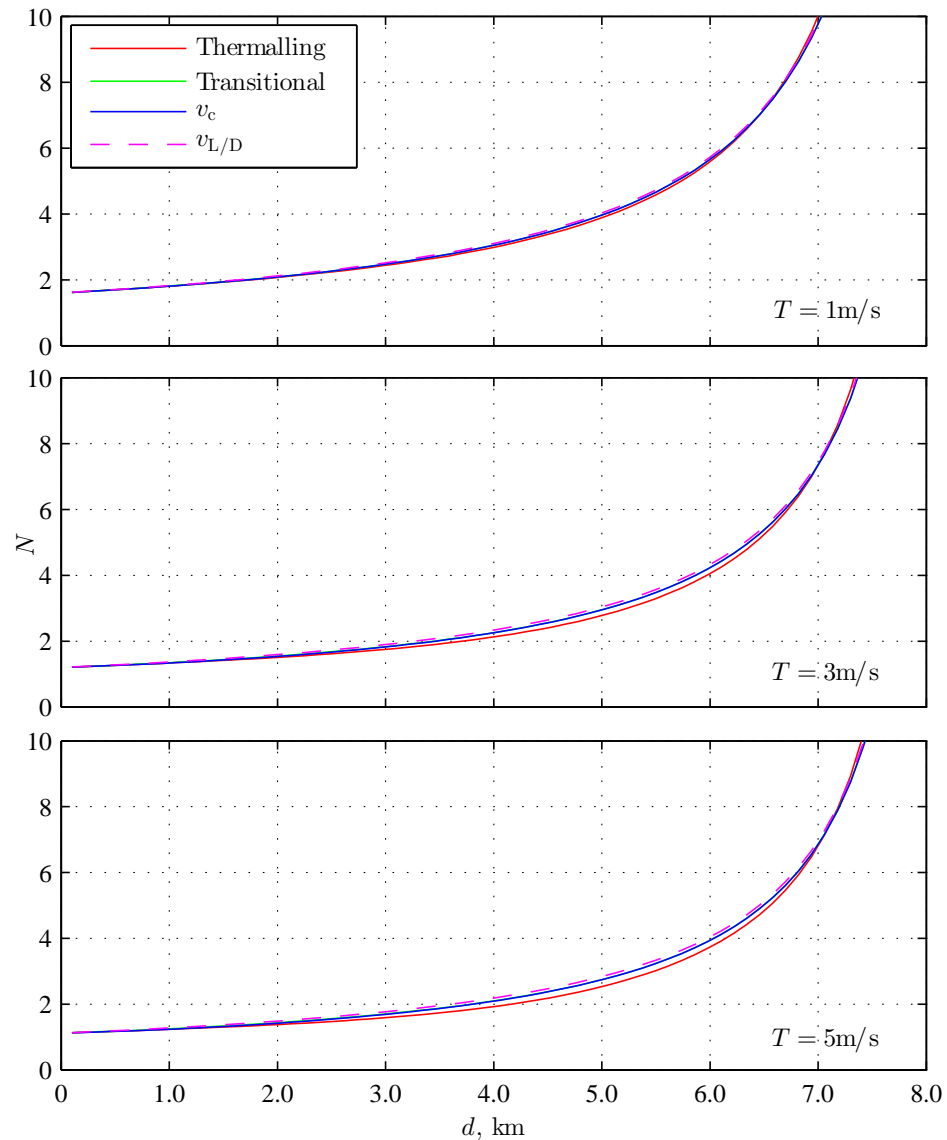


Figure B.3. The number of required agents with the estimated, transitionally-derived, and novel thermalling controller-derived, and best L/D cruising airspeeds for the ASW-27B.

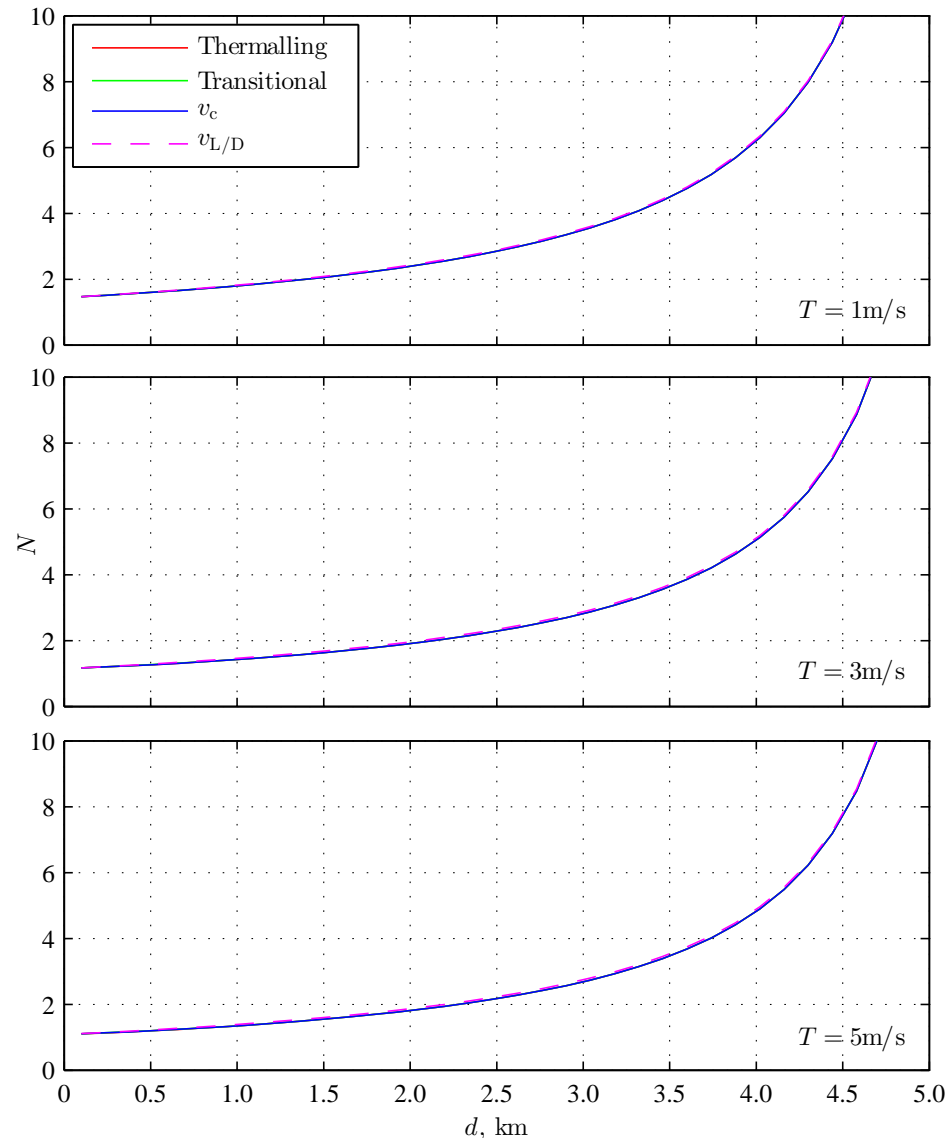


Figure B.4. The number of required agents with the estimated, transitionally-derived, and novel thermalling controller-derived, and best L/D cruising airspeeds for the SB-XC.

Bibliography

- [1] FEDERAL AVIATION ADMINISTRATION (2007), “Thermal Soaring,” .
URL http://www.aviationweather.ws/095_Thermal_Soaring.php
- [2] EASTERN SAILPLANE STAFF (2012), “ASW 27B,” .
URL <http://www.easternsailplane.com/eastern/eastern.php/Schleicher/ASW27B>
- [3] ELIAS, J., “Performance Testing of RnRs SBXC Using GPS,” .
URL <http://www.xcsoaring.com/techPicts/%20Ellias%20performance%20test.pdf>
- [4] SUJIT, P., D. KINGSTON, and R. BEARD (2007) “Cooperative Forest Fire Monitoring Using Multiple UAVs,” in *46th IEEE Conference on Decision and Control*, Institute of Electrical and Electronics Engineers, New Orleans, Louisiana.
- [5] ZHU, H. C. and H. H. LIU (2014) “Indoor Simulation Platform for Forest Fire Detection and Surveillance,” in *AIAA Guidance, Navigation, and Control Conference*, AIAA Paper 2014-0264, American Institute of Aeronautics and Astronautics, National Harbor, Maryland.
- [6] ELSTON, J. S., J. ROADMAN, M. STACHURA, and B. ARGROW (2011) “The Tempest Unmanned Aircraft System for In Situ Observations of Tornadic Supercells: Design and VORTEX2 Flight Results,” *Journal of Field Robotics*, pp. 461–483.
- [7] LIN, P.-H. (2006) “The First Successful Typhoon Eyewall-Penetration Reconnaissance Flight Mission Conducted by the Unmanned Aerial Vehicle, Aerosonde,” *Bulletin of the American Meteorological Society*, pp. 1481–1483.
- [8] MAZA, I., K. KONDAK, M. BERNARD, and A. OLLERO (2010) “Multi-UAV Cooperation and Control for Load Transportation and Deployment,” *Journal of Intelligent and Robotic Systems*, **57**, pp. 417–449.

- [9] LI, Z., J. F. HORN, and J. W. LANGELAAN (2014) “Coordinated Transport of a Slung Load by a Team of Autonomous Rotorcraft,” in *AIAA Guidance, Navigation, and Control Conference*, AIAA Paper 2014-0968, American Institute of Aeronautics and Astronautics, National Harbor, Maryland.
- [10] COLOZZA, A. and J. L. DOLCE (2005) *High-Altitude, Long-Endurance Airships for Coastal Surveillance, Tech. Rep. NASA/TM2005-213427*, NASA.
- [11] WHARINGTON, J. (1998) *Autonomous Control of Soaring Aircraft by Reinforcement Learning*, Ph.D. thesis, Royal Melbourne Institute of Technology, Melbourne, Australia.
- [12] WHARINGTON, J. and I. HERZBERG (1998) “Control of a High Endurance Unmanned Air Vehicle,” in *21st Congress of International Council of the Aeronautical Sciences*, ICAS-98-3.7.1, ICAS and AIAA, Melbourne, Australia.
- [13] KLAS ANDERSSON, V. D. V. C., ISAAC KAMINER (2012) “Thermal Centering Control for Autonomous Soaring; Stability Analysis and Flight Test Results,” *Journal of Guidance, Control, and Dynamics*, **35**, pp. 963–975.
- [14] DAUGHERTY, S. C. and J. W. LANGELAAN (2014) “Improving Autonomous Soaring via Energy State Estimation and Extremum Seeking Control,” in *AIAA Guidance, Navigation, and Control Conference*, AIAA Paper 2014-0260, American Institute of Aeronautics and Astronautics, National Harbor, Maryland.
- [15] BIRD, J. and J. W. LANGELAAN (2012) “Spline Mapping to Maximize Energy Exploitation of Non-uniform Thermals,” Proceedings of the XXXI OSTIV Congress, Uvalde, Texas.
- [16] CHAKRABARTY, A. and J. W. LANGELAAN (2011) “Energy-Based Long-Range Path Planning for Soaring-Capable Unmanned Aerial Vehicles,” *Journal of Guidance, Control, and Dynamics*, **34**, pp. 1002–1015.
- [17] METZGER, D. E. and K. J. HEDRICK (1975) “Optimal Flight Paths for Soaring Flight,” *Journal of Aircraft*, **12**, pp. 867–871.
- [18] CHUNG, J. J., M. ANGEL, T. SOTO, and S. SUKKARIEH (2012) “A new utility function for smooth transition between exploration and exploitation of a wind energy field,” in *Intelligent Robots and Systems (IROS), 2012 IEEE/RSJ International Conference on*, pp. 4999–5005.
- [19] LAWRENCE, N. R. and S. SUKKARIEH (2011) “Autonomous Exploration of a Wind Field with a Gliding Aircraft,” *Journal of Guidance, Control, and Dynamics*, **34**, pp. 719–733.

- [20] OKE, T. R. (1987) *Boundary Layer Climates*, 2nd ed., Methuen, London, pp. 72–73.
- [21] KERLINGER, P. (1989) *Boundary Layer Climates*, University of Chicago Press, Chicago, pp. 78–100.
- [22] THOMAS, C. (2005), “NASA Dryden Aerospace Engineer Michael Allen Hand-Launches a Model Motorized Sailplane During a Study Validating the use of Heat Thermals to Extend Flight Time,” .
URL http://www.dfrc.nasa.gov/Gallery/Photo/Autonomous_Soaring/HTML/EC05-0198-11.html
- [23] AERONAUTICS SYSTEMS STAFF (2007), “Orbiter UAV,” .
URL http://www.aeronautics-sys.com/orbiter_mini_uav_muas
- [24] ALLEN, M. J. (10-13 Jan. 2005) “Autonomous Soaring for Improved Endurance of a Small Uninhabited Air Vehicle,” in *AIAA Aerospace Sciences Meeting and Exhibit*, Reno, NV.
- [25] DEPENBUSCH, N. and J. W. LANGELAAN (2011) “Coordinated Mapping and Exploration for Autonomous Soaring,” in *Infotech@Aerospace Conference*, AIAA Paper 2011-1436, St. Louis, MO.
- [26] BETHKE, B., J. HOW, and J. VIAN (2008) “Group Health Management of UAV Teams With Applications to Persistent Surveillance,” in *American Control Conference*, pp. 3145–3150.
- [27] ——— (2009) “Multi-UAV Persistent Surveillance With Communication Constraints and Health Management,” in *AIAA Guidance, Navigation, and Control Conference*, Chicago, Illinois.
- [28] BETHKE, B., J. REDDING, J. HOW, M. VAVRINA, and J. VIAN (2010) “Agent Capability in Persistent Mission Planning using Approximate dynamic programming,” in *American Control Conference*.
- [29] CUTLER, M. J., T. W. McLAIN, R. W. BEARD, and B. CAPOZZI (2010) “Energy Harvesting and Mission Effectiveness for Small Unmanned Aircraft,” in *AIAA Guidance, Navigation, and Control Conference*, AIAA Paper 2010-8037, American Institute of Aeronautics and Astronautics, Toronto, Ontario.
- [30] PATEL, C. K. and I. KROO (2006) “Control Law Design for Improving UAV Performance Using Wind Turbulence,” in *44th AIAA Aerospace Sciences Meeting and Exhibit*, AIAA Paper 2006-231, American Institute of Aeronautics and Astronautics, Reno, Nevada.

- [31] PIPPIN, C. E., H. CHRISTENSEN, and L. WEISS (2013) “Dynamic, Cooperative Multi-Robot Patrolling with a Team of UAVs,” in *Society of Photo-Optical Instrumentation Engineers (SPIE) Conference Series*, vol. 8741 of *Society of Photo-Optical Instrumentation Engineers (SPIE) Conference Series*.
- [32] NIGAM, N., S. BIENIAWSKI, I. KROO, and J. VIAN (2012) “Control of Multiple UAVs for Persistent Surveillance: Algorithm and Flight Test Results,” *Control Systems Technology, IEEE Transactions on*, **20**(5), pp. 1236–1251.
- [33] DEPENBUSCH, N. and J. W. LANGELAAN (2013) “Minimum Risk Planning for Teams of Unmanned Air Vehicles,” in *AIAA Infotech*, AIAA Paper 2013-4808, American Institute of Aeronautics and Astronautics, Boston, Massachusetts.
- [34] REICHMANN, H. (1993) *Cross-Country Soaring*, Soaring Society of America, Chicago, pp. 114–124.
- [35] BURCH, J. D. (2000), “Performance Airspeeds for the Soaring Challenged,” URL <http://www.5c1.net/Glider%20Performance%20Airspeeds.htm>
- [36] COCHRANE, J. H. (1999) “MacCready Theory with Uncertain Lift and Limited Altitude,” *Technical Soaring*, **23**(3), pp. 88–96.
- [37] DUBINS, L. E. (1957) “On Curves of Minimal Length with a Constraint on Average Curvature, and with Prescribed Initial and Terminal Positions and Tangents,” *American Journal of Mathematics*, **79**(3), pp. 497–516.
URL <http://www.jstor.org/stable/2372560>